Impact of MIMO and Carrier Aggregation in LTE-Advanced

João de Quintanilha Meleiro de Araújo Martins

Thesis to obtain the Master of Science Degree in

Electrical and Computer Engineering

Examination Committee

Chairperson: Prof. Fernando Duarte Nunes

Supervisor: Prof. Luís Manuel de Jesus Sousa Correia

Member of Committee: Prof. António José Castelo Branco Rodrigues

Member of Committee: Eng. Rui Paulo Ferreira

October 2013

To the Ones I love

Acknowledgements

First of all, I would like to thank Professor Luís M. Correia for giving me the opportunity to work on this thesis. His supervision and advice proved to be as inspiring and motivational as useful, being reflected on the final outcome. I would also like to thank him for the opportunity of working and meeting with the GROW team, as well as with Optimus, which helped me getting a closer insight into the reality of the topics related to my work.

I would like to thank Optimus, namely Eng. Luís Santo, Eng. Rui Ferreira, Eng. Pompeu Costa, Eng. Pedro Claro and Eng. João Seco for all the constructive critics, technical support, suggestions and advices. Being able to conduct measurements in a live LTE-A cluster brought great added value to this thesis.

To Michał Maćkowiak for all the patience and effort spent reviewing my work, as well as helping me with positive criticism and knowledge sharing. This was vital to the development and completion of this thesis.

To all my friends who followed me during this journey in IST. The ones I made before and after the first day, through the very last, sharing good friendship moments and teaching me how to take the most out of life.

Last, but not least, I would like to thank to my family for everything that I am today.

Abstract

The main purpose of this thesis was to study the impact of MIMO and Carrier Aggregation in LTE-Advanced networks, concerning capacity, QoS and interference. A model for the evaluation of network downlink performance was developed and implemented in a multi-user simulator. Results were obtained after simulating the new improvements in a replicated urban network in Lisbon. Moreover, field measurements, using CA, were also included, enabling the comparison with low-load simulated results. Inter-band aggregation of two component carriers, with 10 MHz each, resulted in the approximate sum of capacities from each component, achieving 140 Mbit/s per sector. MIMO 4×4 and 8×8 configurations enabled peak user performances of 187 Mbit/s and 300 Mbit/s, respectively, representing gains of 34% and 115%, compared to the similar MIMO 2×2 scenario. In high-load conditions, average cell capacity increases linearly with bandwidth, up to 60 MHz of aggregated bandwidth, and reaches 4 times the cell capacity of a 20 MHz carrier when using 100 MHz, instead. MIMO 4×4 and 8×8 high-load results show average network capacity gains of 24% and 74%, respectively, compared to MIMO 2×2 scenarios.

Keywords

LTE-Advanced, MIMO, Carrier Aggregation, Capacity, Performance, Interference.

Resumo

O principal objectivo desta tese foi o estudo de impacto do MIMO e da agregação de portadoras em redes LTE-*Advanced*, no que diz respeito a capacidade, qualidade de serviço e interferência. Foi desenvolvido um modelo para avaliação do desempenho da rede, no canal descendente, e este foi por sua vez implementado num simulador, para ambientes multi-utilizador. Foram obtidos resultados da aplicação das novas melhorias numa rede urbana em Lisboa. Por sua vez, também foram incluídas medidas reais na rede, com agregação de portadoras, permitindo a comparação com simulações de reduzida carga na rede. A agregação inter-banda de duas componentes portadoras, cada uma com 10 MHz de largura de banda, resultou na soma aproximada das capacidades de cada uma das componentes separadas, atingindo 140 Mbit/s, por sector. As configurações MIMO 4×4 e 8×8 permitiram taxas máximas de débito por utilizador de 187 Mbit/s e 300 Mbit/s, respectivamente, a que correspondem ganhos de 34% e115%, comparadas com o cenário análogo de MIMO 2×2. Em condições de carga elevada na rede, a capacidade média das células aumenta linearmente com a largura de banda, até atingir 60 MHz de largura de banda agregada, e depois atinge 4 vezes a capacidade de uma portadora de 20 MHz, ao agregar 100 MHz. Resultados dos cenários MIMO 4×4 e 8×8, com a rede carregada, indicam ganhos na capacidade da rede de 24% e de 74%, respectivamente, quando comparadas com o cenário de MIMO 2×2.

Palavras-chave

LTE-Advanced, MIMO, Agregação de Portadoras, Capacidade, Desempenho, Interferência.

Table of Contents

List of Figures

List of Tables

List of Acronyms

3GPP	3rd Generation Partnership Project
ACI	Adjacent Channel Interference
ACLR	Adjacent Channel Leakage Ratio
AMBR	Aggregated Maximum Bit Rate
AMC	Adaptive Modulation and Coding
ANACOM	Autoridade Nacional de Comunicações
ARP	Allocation and Retention Priority
BS	Base Station
CA	Carrier Aggregation
CBR	Constant Bit Rate
CC	Component Carrier
CCI	Co-Channel Interference
CDF	Cumulative Distribution Function
CDMA2000	Code Division Multiple Access 2000
CP	Cyclic Prefix
C-plane	Control Plane
CS	Circuit Switched
CSE	Cell Spectral Efficiency
CSI	Channel State Information
CV	Coefficient of Variation
DL	Downlink
DMB-H	Digital Multimedia Broadcast – Handheld
DRM	Data Rate Model
DRX	Discontinuous Reception
DVB-H	Digital Video Broadcast – Handheld
E-MBMS	Evolved Multimedia Broadcast Multicast Service
eNB	Evolved NodeB
EPA	Extended Pedestrian A
EPC	Evolved Packet Core
EPS	Evolved Packet System
ETU	Extended Typical Urban
E-UTRA	Evolved UMTS Radio Access
E-UTRAN	Evolved UMTS Terrestrial Radio Access Network
EVA	Extended Vehicular A

FDD	Frequency Division Duplex
FDMA	Frequency Division Multiple Access
FF	Fast Fading
FRS	Frequency Reuse Scheme
FTP	File Transfer Protocol
GBR	Guaranteed Bit Rate
GBSB	Geometrically Based Single Bounce
GPRS	General Packet Radio System
GSM	Global System for Mobile Communications
HSPA	High Speed Packet Access
HSS	Home Subscriber Service
IA	Interference Aware
ICI	Inter-Cell Algorithm
IMT-A	International Mobile Telecommunications – Advanced
IP	Internet Protocol
ITU-R	International Telecommunication Union – Radiocommunication Sector
LTE	Long Term Evolution
LTE-A	LTE-Advanced
MCS	Modulation and Coding Scheme
MH	Mobile Hashing
MIMO	Multiple Input Multiple Output
MM	Mobility Management
MME	Mobility Management Entity
MMS	Multimedia Messaging Service
MT	Mobile Terminal
MU-MIMO	Multi-User MIMO
OFDM	Orthogonal Frequency Division Multiplexing
OFDMA	Orthogonal Frequency Division Multiple Access
PAPR	Peak-to-Average Power Ratio
PBCH	Physical Broadcast Channel
PCEF	Policy and Charging Enforcement Function
PCRF	Policy and Charging Rules Function
PDCCH	Physical Downlink Control Channel
PDF	Probability Density Function
PDN	Packet Data Network
PDP	Power Delay Profile
PDSCH	Physical Downlink Shared Channel
PF	Proportional Fair
P-GW	Packet Data Network Gateway
PHICH	Physical Hybrid-ARQ Indicator Channel

PMI	Precoding Matrix Index
PRACH	Physical Random Access Channel
PS	Packet Switched
PS	Packet Scheduling
PUCCH	Physical Uplink Control Channel
PUSCH	Physical Uplink Shared Channel
QAM	Quadrature Amplitude Modulation
QCI	QoS Class Identifier
QoE	Quality of Experience
QoS	Quality of Service
QPSK	Quadrature Phase-Shift Keying
RB	Resource Block
RE	Resource Element
RLB	Radio Link Budget
RLC	Radio Link Control
RMG	Relative MIMO Gain
RN	Relay Node
ROA	Region Of Analysis
RR	Round Robin
RRM	Radio Resource Management
RS	Reference Signal
RSRP	Received Signal Received Power
Rx	Receiver
SAE	System Architecture Evolution
SC-FDMA	Single Carrier Frequency Division Multiple Access
SFBC	Space-Frequency Block Code
S-GW	Serving Gateway
SINR	Signal-to-Interference-plus-Noise Ratio
SMS	Short Message Service
SNR	Signal-to-Noise Ratio
SS	Synchronisation Signal
SU-MIMO	Single User MIMO
TDD	Time Division Duplex
TM	Transmission Mode
TTI	Transmission Time Interval
Tx	Transmitter
UE	User Equipment
UL	Uplink
UMTS	Universal Mobile Telecommunications System
U-plane	User Plane

USE	User Spectral Efficiency
VoIP	Voice over IP

List of Symbols

Δh_b	Difference between the height of the BS and the height of the buildings
Δh_m	Difference between the buildings height and the height of the MT
$\Delta\rho$	Difference between SNR and SINR levels.
$\Delta \mathrm{f}$	Signal bandwidth
$\eta_{overhead}^{APP/PHY}$	Overhead loss up to the application layer
μ_{RMG}	Average RMG depending on the cell type and antenna configuration
μ_X	Mean value of variable X
ρ_{IN}	Signal-to-interference-plus-noise ratio
ρ_N	Signal-to-noise ratio
ρ_N^{ref}	Average required SINR associated with specific reference throughput
σ_{RMG}	Standard deviation of RMG depending on the cell type and antenna configuration
σ_X	Standard deviation of variable X
π	Pi
φ	Street orientation angle
$a_{0,max}$	Maximum value for coefficient a_0
a_0	DRM throughput coefficient
a_1	DRM throughput coefficient
a_2	DRM coefficient
$a_{3,max}$	Maximum value for coefficient a_3
a_3	DRM coefficient
a_4	DRM coefficient
b	Buildings separation distance
C_{MIMO}	Capacity (bit rate) of a MIMO scheme
C_{SISO}	Capacity (bit rate) of a SISO scheme
d	Horizontal distance between the BS and the MT
f_c	Frequency carrier of the signal
F_N	Noise figure
$G_{M/S}$	Relative gain of a MIMO scheme, in relation to a SISO scheme
G_{MIMO}	Maximum achievable capacity/throughput gain associated to the use of MIMO
$G_{RMG}^{4\times4}$	RMG for a MIMO 4×4 scheme
$G_{RMG}^{8\times8}$	RMG for a MIMO 8×8 scheme

G_r	Gain of the Rx antenna
G_t	Gain of the Tx antenna
I	Interference power
I_i	Interference power coming from the ith Tx
k_a	Increase of path loss for the BS antennas below the roof tops of the adjacent buildings
k_d	Average power decay
k_d	Dependence of the multi-screen diffraction loss versus distance
k_f	Dependence of the multi-screen diffraction loss versus frequency
L_0	Free-space propagation path loss
L_{bsh}	Loss due to the height difference between the rooftop and the antennas
L_c	Losses in the cable between the transmitter and the antenna
L_{msd}	Loss between the BS and the last rooftop
L_{ori}	Street orientation correction factor
L_p	Path loss
$L_p^{COST\ 231\ WI}$	Path loss from the COST 231-Walfish-Ikegami model
L_p^{LoS}	Path loss for LoS propagation
L_p^{NLoS}	Path loss for NLoS propagation
$L_p^{environment}$	Path loss due to the user specific environment
L_{rts}	Loss between the last rooftop and the MT
L_u	Losses in the UE
M_I	Implementation margin
M_{SF}	Slow fading margin
N	Noise power
N_{RB}	Number of used resource blocks
$N_{RB_I}^{CC_j}$	Number of interfered RBs assigned in the jth CC
N_{BS}	Number of BSs
N_{CC}^{Y}	Number of CCs in frequency band Y
N_I	Number of interfering signals reaching the receiver
N_R	Number of Rx antennas
$N_{RB}^{CC_j}$	Number of used RBs assigned in the jth CC
$n_{RB\ i}^{CC_j}$	Number of used RBs assigned in the jth CC, allocated by BS i
N_{RB}^{I}	Number of interfered RBs
N_{RB}^{Y}	Number of used RBs assigned in frequency band Y
N_T	Number of Tx antennas
N_X	Number of samples of variable X
N_b^{sym}	Number of bits per symbol
N_{sub}^{RB}	Number of subcarriers per resource block

N_{sym}^{sub}	Number of symbols per subcarrier
N_u^{BS}	Number of users served by the BS
n_{CRS}	Number of cell-specific Reference Signals multiplexed with PDSCH per RB
n_{PDCCH}	Number of allocated symbols for PDCCH
n_{RB}	total number of RBs for the deployed bandwidth
$n_{ant,DL}$	Number of configured antenna ports
$P_I^{CC_j}$	Percentage of interfered RBs in the jth CC
P_I	Percentage of interfered RBs
P_{Rx}	Power at the receiver
P_{Tx}	Transmitter output power
P_r	Power at the Rx antenna
P_r^{DL}	Power at the Rx antenna, in DL
P_r^{ref}	Rx antenna sensitivity for specific reference service
P_t	Power fed to the Tx antenna
P_t^{DL}	Power fed to the Tx antenna, in DL
R^{LoS}	Cell radius, considering LoS propagation
R^{NLoS}	Cell radius, considering NLoS propagation
R_b	Data rate (throughput at the physical layer)
$R_b^{CC_j}$	Throughput served over the jth CC
$R_b^{RB_c}$	Throughput per RB obtained in the reference frequency assigned to the user
$R_b^{RB_i}$	Throughput obtained for the ith RB
$R_b^{4\times4}$	Throughput of a MIMO 4×4 scheme
$R_b^{8\times8}$	Throughput of a MIMO 8×8 scheme
R_b^{APP}	Application layer throughput
R_b^{BS}	BS served throughput
R_{b_k}	Throughput in the kth RB
R_b^i	Throughput of the ith user served by the BS
T_{RB}	Resource block slot duration
u	Random value with uniform distribution
w	Width of the streets
$\bar{X}$	Mean value of variable X
X_i	Value of sample i of variable X

List of Software

Embarcadero RAD Studio	C++ Integrated Development Environment software
GENEX Probe & Assistant	Wireless network testing and post-processing tool
Map Basic	Programming software and language to create additional tools and functionalities for the MapInfo
MapInfo	Geographic Information System software
Microsoft Excel	Calculation and Graphing software
Microsoft Word	Text editor software

Chapter 1

Introduction

This chapter introduces the subject of this thesis, and presents the contextual and motivational framework that lead to this study. Furthermore, it establishes the scope of the work and describes the contents that compose its structure.

1.1 Overview

Mobile communication networks are living times of great expansion and development, especially in what regards technology and efficiency. This goes in line with the massive growth in the number of user connected devices and of traffic volume, and increasingly wide range of applications with varying requirements and characteristics. Future wireless communication systems need to address these challenges, in order to enable truly networked societies, where information can be accessed and data shared anywhere and anytime, by anyone and anything [Eric13a]. As a result, intense activity has been going on by many contributing companies and standardisation bodies, such as the 3rd Generation Partnership Project (3GPP), in order to develop latest generation mobile communication technologies.

Mobile communication systems are often divided into generations. The first generation started with the analogue mobile radio systems of the 1980s. Then, came the second generation of mobile networks (2G), introducing digital mobile systems for voice services, such as Global System for Mobile Communications (GSM). Later on, data services were included in 2G networks, yet voice was still dominating network traffic. 3G networks were the first to handle broadband data services, boosting data traffic in such a way that changed mobile networks from voice to packet data dominated networks. Long Term Evolution (LTE) is responsible for the introduction of fourth generation networks (4G), although many also claim that LTE Release 10, also referred to as LTE-Advanced (LTE-A), is the true 4G evolution step, with first releases of LTE (Release 8 and Release 9) being labelled as "3.9G". Figure 1.1 shows a timeline of the 3GPP specifications schedule and corresponding commercial deployments, since third generation Wideband Code Division Multiple Access (WCDMA) technology was introduced, in 1999, up to the release of LTE-A, in 2010.

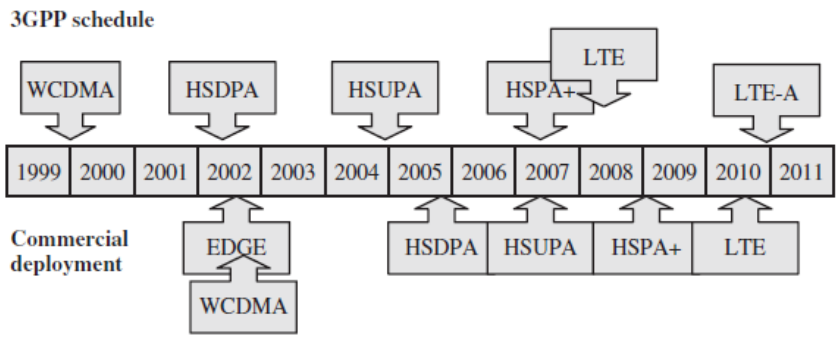

Figure 1.1 – Schedule of 3GPP standard and their commercial deployments (extracted from [HoTo11]).

The evolution of 3G networks into 4G has been driven by the appearance and development of new massified services for mobile devices, and enabled by the advancement of the technology available for mobile systems. There has also been an evolution of the environment in which mobile systems are deployed and operated, especially in terms of competition between mobile operators, challenges from other mobile technologies, new regulation of spectrum use and market aspects of mobile systems [DaPS11]. Operators have been forced to find new forms of creating and extracting value from their

networks, and still provide the best service to users, improving both performance and efficiency.

LTE and LTE-A were both designed to provide high data rates (multimegabit bandwidth), efficient use of the radio network and spectrum resources, lower transport and distribution costs, reduced latency and improved mobility. This combination, together with backwards compatibility with legacy technologies, provides the all-IP converged architecture, aiming to enhance users' interaction with the network and further accelerate the demand for mobile multimedia services, and adding to the already existing and improved voice/data services. With high-speed wireless broadband, users can readily access their Internet services, such as online television, video streaming, blogging, social networking and interactive gaming, from their ever growing variety of mobile devices. Figure 1.2 presents the evolution of the number of mobile subscriptions for different types of devices with cellular connection. Two-and-half-fold increases are predicted, from 2013 to 2018, reaching 4.5 billion of smartphone subscriptions.

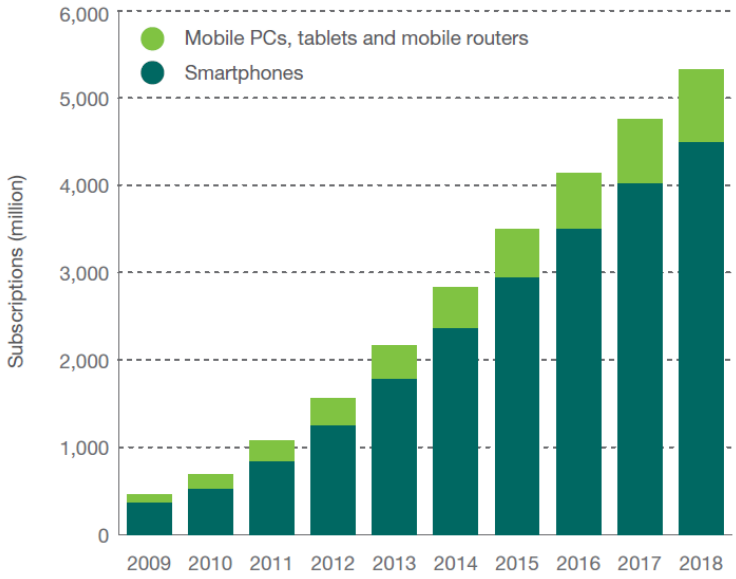

Figure 1.2 – Smartphone, PC, mobile routers and tablet subscriptions with cellular connection, from 2009 to 2018 (extracted from [Eric13b]).

Data services, which already became popular among legacy networks (2G and 3G), include Short Messaging Service (SMS) and Multimedia Messaging Service (MMS), web browsing, file transfer (*i.e.*, FTP) and e-mail. The growing demand for higher bit rates and traffic volume in mobile packet data services is convoyed with the increase in users' expectations, regarding the offered Quality of Experience (QoE). Moreover, due to its highly increased peak data rates and much lower latencies, fourth generation networks enable a whole range of real-time multimedia services, such as high quality video conferencing, multi-user online gaming over IP, high definition video-audio streaming (Mobile Live TV) and other interactive applications, requiring huge amounts of data transferred within small periods of time. This is has driven mobile equipment manufacturers and operators, pushing them to offer technologies and services that match the expectations from consumers at lower costs, in order to remain profitable and fight the tendency for decoupling between revenues and traffic, illustrated in Figure 1.3.

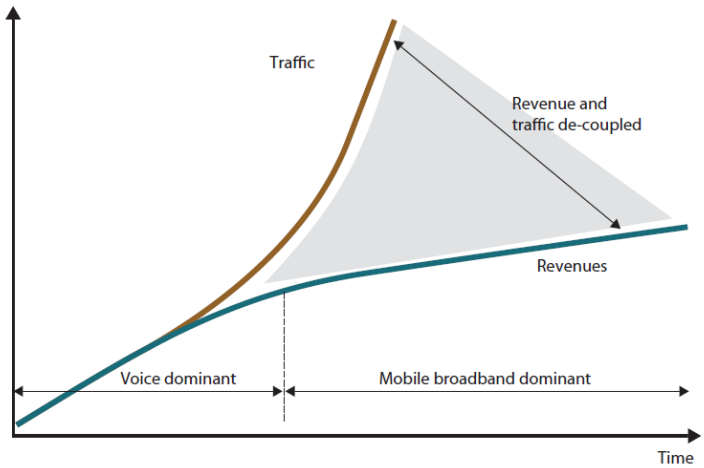

Figure 1.3 –Decoupling between mobile operators' revenues and traffic volumes (extracted from [Eric13c].

LTE Releases 8 and 9 only satisfy to some extent the requirements set by the International Telecommunication Union – Radiocommunication Sector (ITU-R) for 4G networks, in the International Mobile Telecommunications – Advanced (IMT-A) specifications, defined in [ITUR08a]. On the other hand, 3GPP Release 10 and beyond not only fully satisfy the requirements, but also bring further enhancements, exceeding the specifications in several aspects where 3GPP has set more demanding performance targets than those of ITU-R. The main focus goes to the access part of the network which, according to [3GPP12a], should accomplish the following key requirements:

- Peak data rates of 1 Gbit/s for the DL and 500 Mbit/s for the UL;
- Maximum bandwidth of 100 MHz;
- Reduced latency compared to previous releases (Releases 8 and 9), which already satisfy IMT-Advanced requirements;
- Enhanced peak spectrum efficiency, up to 30 bit/s/Hz for DL (8×8 MIMO) and 15 bit/s/Hz for UL (4×4 MIMO), as well as average and cell edge improved spectral efficiencies;
- Support for higher speeds mobility.

In addition to backwards compatibility with previous releases, LTE-A introduces new features, such as enhanced multi-antenna support, to enable higher bitrate throughput, Carrier Aggregation (CA), to increase transmission bandwidth, and Relay Nodes (RNs), to increase coverage and cell edge throughput. These enhancements aim to target the discussed key challenges, handling the overall data traffic growth in an affordable and sustainable way.

1.2 Motivations and Contents

The main scope of this thesis is to study the impact of MIMO and CA in LTE-A networks, in terms of capacity, QoS and interference. This is done by developing a model and implementing it into a

multi-user simulator, in order to extract approximated results of the replicated system conditions. Moreover, field measurements were performed on a real deployed LTE-A cell, providing validation and realistic insights into the actual single-user performance achieved. The main results of the model are presented in the form of key metrics regarding user performance and network capacity, for low-load and high-load conditions. These were chosen accordingly, to enable the comparison between simulated and measured scenarios.

The current work was done in cooperation with Optimus, a mobile operator with an already deployed LTE network in Portugal, putting together a mix of academic and industry concerns for evaluation. The need to evaluate impacts of introducing technological changes in the network, through cost-efficient investments, is one of the main motivations for Optimus. This work is expected to help on the decision regarding in which direction should evolve the existing LTE network. Besides providing all the information concerning the installed network in the city of Lisbon, Optimus played a crucial role by discussing several technical details and technology insights, as well as supporting the performed field measurements' campaign.

This thesis is composed of 5 chapters, including the present one, plus a group of annexes. Chapter 2 provides an overview of LTE and LTE-A, covering network architecture, radio interface, main performance aspects, and services and applications. Particular focus is given to the main technical aspects concerning Multiple Input Multiple Output (MIMO) and CA, presenting, at the end of the chapter, the state of the art with relevant work being done on this topic.

Chapter 3 describes the developed models used in the implementation of the multi-user simulator. It starts with the main assumptions and metrics considered, following a description of the most relevant algorithms implemented. Afterwards, an overview of the simulator is provided, providing additional explanations that were not included in the description of the models, regarding its setup and operation. This chapter ends with an assessment of the simulator, in order to validate the results in the next chapter.

In Chapter 4, simulation and field measurements results are presented. The first section describes the default scenario and configuration parameters that were considered in the simulations. Then, results are presented and discussed in two different sections: one dedicated to the low-load simulations and single-user field measurements, and the other dedicated to the high-load simulations. These sections provide extensive analysis of the results, including the comparison with an established reference scenario. Moreover, some conclusions are already presented in this section, in order to be compiled for the last chapter.

Chapter 5 finalises the present dissertation, compiling the main conclusions of the results obtained in previous chapters. A critical analysis of the work done is provided, including suggestions for future work. A set of annexes closes the present document, containing support information and additional results.

Chapter 2

Fundamental Concepts and State of the Art

This chapter provides an overview of LTE/LTE-A, focusing on MIMO and Carrier Aggregation techniques. The overall network architecture is presented, following the main technical features of the radio interface. Performance aspects with more relevance to this thesis are then examined in Section 2.3, while services and applications are discussed in Section 2.4. Some of the published work in this subject is presented at the end of this chapter, in Section 2.5.

2.1 Network Architecture

The evolution of the overall network architecture from the previous technologies (*e.g.*, GSM, UMTS) to LTE and LTE-A is referred to as System Architecture Evolution (SAE). The main goal of SAE was to provide seamless Internet Protocol (IP) connectivity between the User Equipment (UE) and the Packet Data Network (PDN) using a flat network architecture with reduced latencies and improved performance, as well as being fully optimised for packet-switched services. The result was the Evolved Packet System (EPS), represented in Figure 2.1.

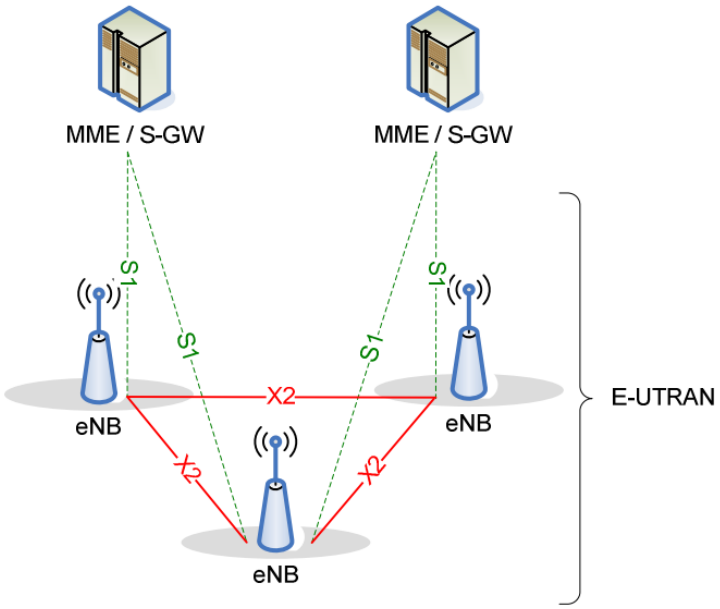

Figure 2.1 – Overall EPS architecture (extracted from [3GPP13b]).

The high-level architecture of EPS consists of three main components, namely the UE, the Evolved UMTS Terrestrial Radio Access Network (E-UTRAN) and the Evolved Packet Core (EPC).

The E-UTRAN corresponds to the access part of the network, handling all radio communications between the UE and the EPC. It has just one component, the Evolved NodeB (eNB), without any separate control node and using an X2 interface to communicate with other eNBs, and an S1 interface to communicate with the EPC. This has the advantage of shorter Transmission Time Interval (TTI), and more flexibility and speed in access during handovers.

The main functions performed by the eNB can be briefly summarised by:

- Securing and optimising radio interface delivery, performing ciphering/deciphering of the User Plane (UP) data and IP header compression/decompression, to avoid repeatedly sending the same or sequential data in the IP header;
- Radio Resource Management (RRM), to control the usage of the radio interface, by allocating resources based on requests, prioritising and scheduling traffic according to required Quality of Service (QoS) and constant monitoring of the resources utilisation.
- Mobility Management (MM), as the eNB controls and analyses radio signal level

measurements carried out by the UE and makes similar measurements itself for decision making.

The EPC is responsible for the overall control of the UE and establishment of the bearers. It consists of three main logical nodes:

- Mobility Management Entity (MME);
- Serving Gateway (S-GW);
- Packet Data Network Gateway (P-GW).

The MME controls the high-level operation of the UE by sending it signalling messages, *e.g.,* for security purposes or the management of data streams. It thus corresponds to the Control Plane (CP) node of the EPC.

The S-GW is the UP node connecting the EPC to the E-UTRAN. It is responsible for forwarding data between the eNBs and the P-GW and it also acts as a mobility anchor when terminals move between eNBs, as well as for other 3GPP technologies (GSM and UMTS).

The P-GW is the EPC's point of contact with the external networks. For instance, it is responsible for the allocation of the IP address for a specific terminal, as well as for the QoS enforcement according to specific policies. Moreover, the P-GW also serves as the mobility anchor for non-3GPP radio-access technologies (*e.g.*, CDMA2000) connected to the EPC.

In addition, the EPC also contains the Policy and Charging Rules Function (PCRF), responsible for QoS handling and charging, and the Home Subscriber Service (HSS), a database containing subscriber information. The Policy and Charging Enforcement Function (PCEF) is included in the P-GW, and it performs gating and filtering functions, as required by the PCRF, for the UE and the services.

2.2 Radio Interface

In LTE, the Downlink (DL) multiple access is based on Orthogonal Frequency Division Multiple Access (OFDMA) and the Uplink (UL) on Single Access Frequency Division Multiple Access (SC-FDMA). The Frequency Division Multiple Access (FDMA) principle allows different users to access the system simultaneously using different frequency bands (*i.e.*, carriers or subcarriers). OFDMA is then achieved by modulating the information onto a multitude of mutual orthogonal narrowband subcarriers (multi-carrier transmission scheme), which can be shared among multiple users. On the other hand, in SC-FDMA, the information is modulated onto only one carrier (single carrier transmission scheme).

The main motivation behind the adoption of OFDMA in LTE is to obtain good performance in frequency selective channels, low complexity of base-band receiver, good spectral efficiency, handling of multiple bandwidths, link adaptation, frequency domain scheduling and compatibility with advanced

MIMO techniques. In addition, the OFDMA orthogonality principle together with fixed frequency domain spacing between subcarriers of 15 kHz substantially mitigates the Adjacent Channel Interference (ACI).

The Cyclic Prefix (CP) insertion, used in both OFDMA and SC-FDMA, avoids Inter Symbol Interference (ISI) while introducing some small overhead in transmission. It consists of copying part of the Orthogonal Frequency Division Multiplexing (OFDM) symbol over an interval larger than the span of the time dispersion in the channel, and adding it to the beginning of the symbol.

The OFDMA scheme offers high flexibility in the time-frequency domain using a resource grid. The basic unit of this grid is a Resource Element (RE), which spans one OFDM symbol onto one subcarrier. A maximum of 2, 4 or 6 physical channel bits are carried per symbol, depending on the modulation scheme used being QPSK, 16-QAM or 64-QAM, respectively, for a coding rate of 1. Resource elements are grouped into Resource Blocks (RBs), each of which correspond to units of 12 subcarriers, with a total occupation of 180 kHz, and a 0.5 ms slot. Each of these time slots comprises 7 OFDM symbols, in the case of the normal CP length, or 6 if the extended CP configuration is used. Two 0.5 ms slots form a 1 ms subframe, which corresponds to the LTE TTI. Subframes can then be grouped into a 10 ms radio frame (10 subframes or 20 slots), the largest unit of time used.

LTE eNBs perform frequency scheduling in the DL by allocating symbols and subcarriers within each subframe into units of RBs. Since each RB corresponds to 84 REs, using the normal CP length, or 72 REs, in the case of extended CP, it is possible to reserve sets of REs for different specific purposes, such as user data transmission, synchronisation signals, reference signals, control signalling and critical broadcast system information. The basic LTE DL physical resource can be seen as a time-frequency grid, as illustrated in Figure 2.2, where one RB, using normal CP length, is highlighted.

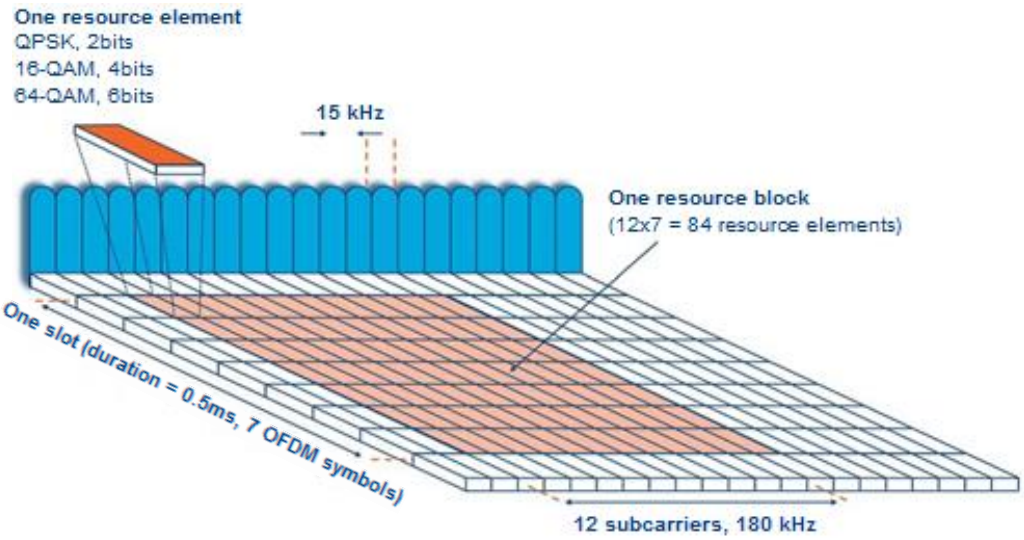

Figure 2.2 – LTE DL physical resource based on OFDMA (extracted from [Eric11]).

OFDMA carries some limitations as well, making it a less favourable option for UL. The transmitted signal shows a high Peak-to-Average Power Ratio (PAPR), which requires high linearity in the

transmitter (Tx) and, consequently, high power and cost requirements that are not suitable for UL transmission and mobile terminals. In LTE, this was solved by using SC-FDMA for UL connections. This multiple-access technology has much in common with OFDMA, in particular the flexibility in the frequency domain, and at the same time it has a significantly low PAPR, resolving to some extent the dilemma of how the LTE UL can benefit from the advantages of multicarrier technology, while avoiding excessive cost and low power efficiency for the mobile terminals.

Similarly to OFDMA, SC-FDMA divides the transmission bandwidth into multiple parallel subcarriers, with the orthogonality principle being maintained in frequency selective channels and using CPs to prevent ISI between information blocks. However, unlike OFDMA, where the subcarriers are independently modulated by data symbols, in SC-FDMA the signal modulated onto a given subcarrier is a linear combination of all the data symbols transmitted at the same time instant. This approach results in a significantly lower PAPR compared to OFDMA schemes. QPSK, 16-QAM and 64-QAM can also be used by this scheme to modulate data streams for UL transmission. A certain user occupies a contiguous part of the spectrum with a 1 ms resolution in the time domain, the frequency band allocation being expressed on 180 kHz RBs, corresponding to 12 subcarriers, as shown in Figure 2.3.

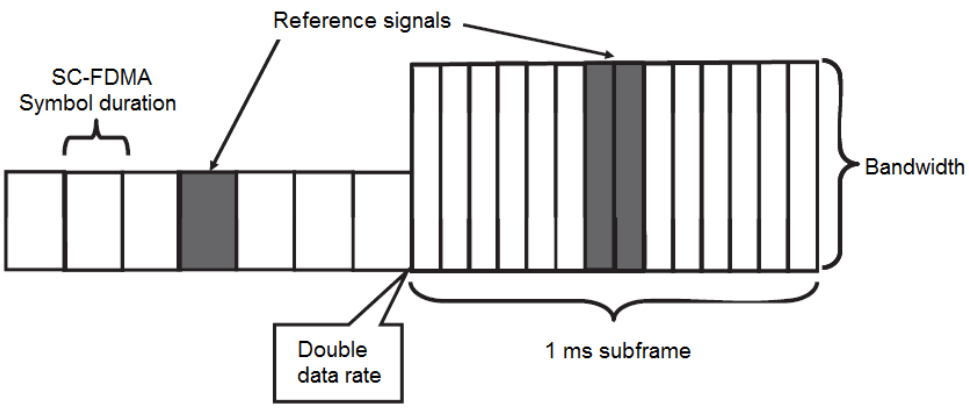

Figure 2.3 – SC-FDMA symbols sequence (extracted from [HoTo11]).

One of the main requirements for LTE in terms of spectrum flexibility is the possibility to deploy radio access in both paired and unpaired spectra, which means that LTE should support both Frequency Division Duplex (FDD) and Time Division Duplex (TDD) modes. The channel bandwidth, in LTE Release 8 and 9, can be selected between 1.4 MHz and 20 MHz depending on the available spectrum. In LTE-A Release 10, the maximum bandwidth allocation was extended to 100 MHz. Table 2.1 shows the corresponding transmission bandwidth configuration for each possible channel, giving the maximum number of RBs that can be allocated.

Concerning the physical layer, physical channels correspond to a number of REs carrying the modulated information. In addition, there are also other sets of REs that do not carry information, corresponding to synchronisation and reference signals. The most relevant physical channels are the Physical Downlink Shared Channel (PDSCH) and the Physical Uplink Shared Channel (PUSCH), both being the main channels for unicast data transmission and some paging and control information in DL and UL, respectively. There is also the Physical Broadcast Channel (PBCH), carrying part of the

system information required by the UE when accessing the network, the Physical Downlink Control Channel (PDCCH), which carries control information and scheduling assignments in DL, the Physical Uplink Control Channel (PUCCH), which is the UL counterpart of the PDCCH, and the Physical Random Access Channel (PRACH), carrying random access information.

Table 2.1 – Channel bandwidth and correspondent transmission bandwidth configuration (adapted from [3GPP13d]).

Channel bandwidth [MHz]	1.4	3	5	10	15	20	40	60	80	100
Transmission bandwidth configuration [RBs]	6	15	25	50	75	100	200	300	400	500

3GPP LTE Release 8 initially defined 17 FDD and 8 TDD operating bands for the Evolved UMTS Radio Access (E-UTRA). Later, in LTE Releases 9 and 10, these were extended to 22 bands for FDD and 9 bands for TDD. Not all of them are available in each of the world's regions, and according to [HoTo11], the most relevant FDD bands adopted in Europe are the 800 MHz, 900 MHz, 1.8 GHz and 2.6 GHz ones. In November 2011, ANACOM, the Portuguese National Authority for Telecommunications, promoted an auction for the allocation of rights of use of frequencies in the 450, 800, 900, 1800, 2100 and 2600 MHz bands.

Another fundamental enhancement included in LTE radio interface specifications is the use of multiple antenna techniques, which is of crucial relevance to this thesis. They were introduced to achieve improved system performance, both in capacity and coverage, as well as in service provisioning, for instance, providing higher user data rates. Multiple Input Multiple Output (MIMO) is the most common technique, where multiple antennas are used simultaneously for transmission and reception, all over a radio channel. Besides MIMO, there are three additional types of transmission schemes, which are SISO, MISO and SIMO. Each of these schemes allows to take advantage from different types of diversity gains, namely, spatial multiplexing and transmit diversity.

Spatial multiplexing consists of sending signals from two or more different antennas with different data streams and, by means of signal processing in the receiver (Rx), separate the data streams, increasing the peak data rates by a factor of 2 or more, depending on the used configuration (*i.e.*, number of antennas). Transmit diversity uses some precoding in signals transmitted from different antennas with the same data stream, thus exploiting the gains from the independent fading among the antennas to achieve higher Signal-to-Noise Ratios (SNRs) and increase the robustness of data transmission. These MIMO technologies usually rely on the transmission of reference signals/symbols to allow the receivers to differentiate the data streams coming from different antennas and to estimate radio channel conditions.

In spatial multiplexing MIMO transmission, the transmitted data streams can be directed to one single user or to multiple different ones, introducing the Single User MIMO (SU-MIMO) and Multi-User MIMO (MU-MIMO) modes. While SU-MIMO increases the data rate of just one user, MU-MIMO allows one to

increase the overall capacity. The number of different data streams transmitted over the same time-frequency resource is referred to as the number of layers, corresponding to the rank of transmission. Figure 2.4 illustrates the operation of a spatial multiplexing MIMO system. The transmitted symbols are mapped onto independent data streams (layers), which in turn are subject to an adaptive antenna mapping, implemented by the precoding step. The receiver then measures the channel elements and estimates the Rank Indication (RI) and the Precoding Matrix Indicator (PMI), feeding them back to the transmitter, and inverts the process to recover the transmitted bits.

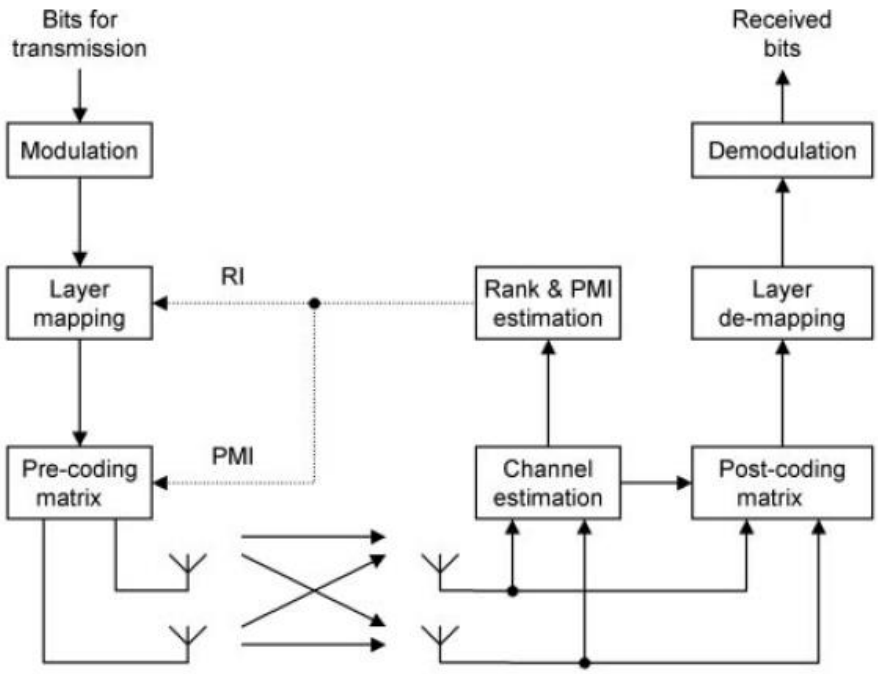

Figure 2.4 – Operation of a spatial multiplexing MIMO system (extracted from [Cox12]).

A uniform and adaptive MIMO configuration allows one to accommodate the demand for higher data rates and wider coverage, only by switching between a number of different Transmission Modes (TMs). The different TMs differ in the number of layers (streams), antenna ports used, type of reference signal and precoding type. Table E.1 shows the different DL transmission modes, defined for LTE.

LTE-A introduces higher order MIMO configurations, *i.e.,* 8×8 schemes for DL and 4×4 schemes for UL, aiming to meet the peak spectrum efficiency requirements. Moreover, LTE-A MIMO technologies were also targeted towards the increase of cell average throughput as well as cell edge performance, introducing new TMs and improving the reference signal design, multi-user MIMO, and the 4×4 DL and 2×2 UL MIMO schemes.

CA allows one to extend the maximum bandwidth in DL and UL by aggregating multiple carriers, while maintaining backward compatibility with LTE Release 8. Each aggregated carrier is referred to as Component Carrier (CC). LTE-A supports the aggregation of up to 5 component carriers, each having a bandwidth from 1.4 MHz to 20 MHz, thus achieving a maximum aggregated bandwidth of 100 MHz (5 × 20 MHz). This technique can be applied in both TDD and FDD systems, not only to provide a

larger transmission bandwidth, but also to facilitate an efficient use of the fragmented spectrum. In FDD systems, the number of UL component carriers is always lower than the number of DL ones, whereas in TDD each component carrier uses the same configuration in both DL and UL, allocating subframes in the same way.

There are three different aggregation scenarios, as shown in Figure 2.5:

- contiguous intra-band aggregation, where carrier components are contiguously located within the same operating band (Figure 2.5.a);
- non-contiguous intra-band aggregation, where carrier components are located within the same operating band, but not contiguously (Figure 2.5.b);
- inter-band aggregation, where carrier components are located in different operating bands (Figure 2.5.c).

In the inter-band scenario, CCs in different operating bands will have different path losses, thus providing different radio channel characteristics and coverage areas. Release 10 CA supports both symmetric DL/UL configurations, aggregating the same amount of DL and UL component carriers, or asymmetric DL/UL configurations, usually having more DL component carriers than UL's.

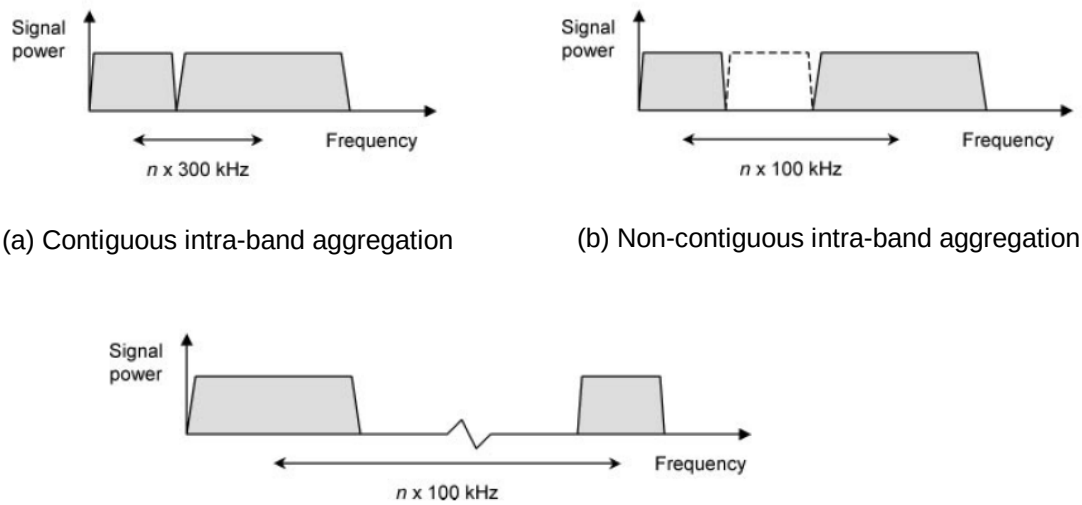

(a) Contiguous intra-band aggregation

(b) Non-contiguous intra-band aggregation

(c) Inter-band aggregation

Figure 2.5 – Different CA scenarios (extracted from [Cox12]).

The study of band aggregation started with a limited number of carrier frequencies. Initially, 3GPP identified one TDD intra-band contiguous aggregation scenario, in the 2300 MHz band, and one FDD inter-band aggregation scenario in the 800 MHz and 2100 MHz bands. Later on, other scenarios were added, and still are, in a release-independent fashion, such as the FDD inter-band aggregation in the 1800 MHz and 2600 MHz bands. Moreover, 3GPP also defined potential deployment scenarios for CA in LTE-A, allowing one to take advantage of cells overlapping areas, to improve data rates. This thesis focuses on three scenarios, which were defined in [3GPP13b] and are illustrated by Figure 2.6:

- Scenario #1: both CC1 and CC2 cells, corresponding to each Component Carrier associated cell, are co-located and overlap, providing nearly the same coverage (Figure 2.6.a). In this scenario CC1 and CC2 are likely to belong to the same band.
- Scenario #2: CC1 and CC2 cells again are co-located and overlaid (Figure 2.6.b), but CC2 has a smaller coverage area due to larger path loss. In this scenario, CC1 and CC2 are likely from different bands (*e.g.*, 1800 MHz and 2600 MHz), having different radio channel characteristics, and as a result CC1 can be used to provide basic coverage and CC2 to improve throughput.
- Scenario #3: CC1 and CC2 cells are co-located (Figure 2.6.c) but CC2 antennas have different directions/patterns, purposely shifting the direction of the beams to improve cell edge performance. Typically, CC1 and CC2 ought to be from different bands, providing different radio channel characteristics and coverage as in scenario #2.

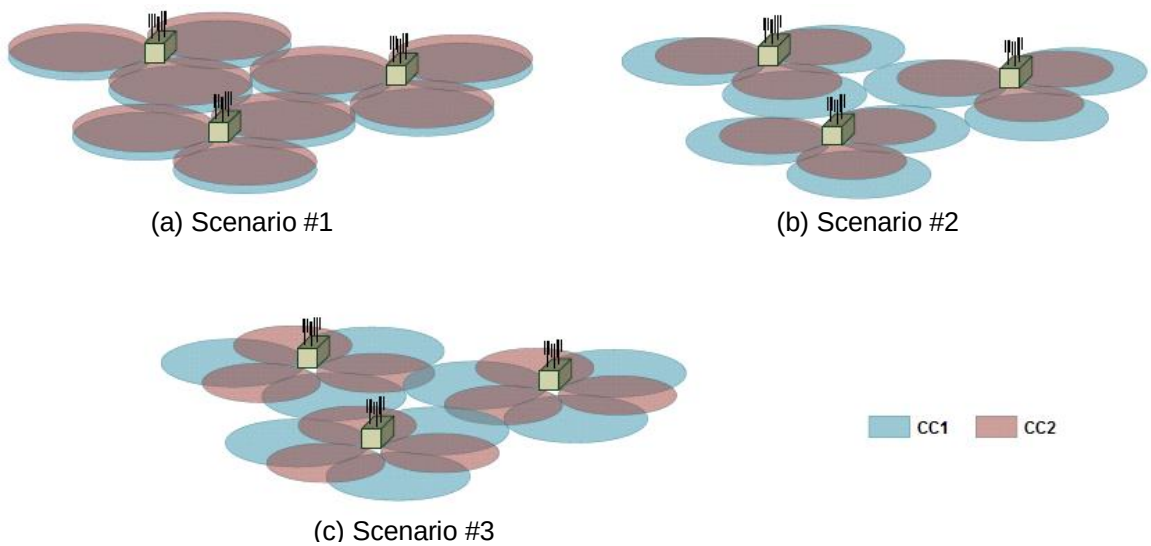

Figure 2.6 – CA main deployment scenarios (extracted from [3GPP13b]).

CCs in LTE-A are organised into one Primary Cell (PCell) and up to four Secondary Cells (SCells). In FDD, the PCell contains one DL CC and one UL CC, providing the basis for transmission in both links. It is used just like a regular cell in LTE Release 8. SCells are only used by connected UEs, being added or removed according to user-specific signalling messages. In FDD, these secondary cells should contain at least one DL CC. PCells are usually associated with the CC providing the highest received signal power to the user, serving as basic coverage cell.

2.3 Performance Analysis

The main aspects considered in this thesis regarding performance analysis are capacity, Quality of

Service and interference. These can then be split into other performance-related concepts, such as throughput, spectrum efficiency and coverage, which eventually overlap and, for that reason, are further mentioned. Moreover, 3GPP includes some of these concepts for the specification of E-UTRA requirements and advancements, in [3GPP10] and later in [3GPP12a], emphasising their importance in the performance evaluation and deployment of LTE networks.

For the particular case of cellular networks, such as LTE, capacity can be seen as the maximum aggregated data rate that one cell can handle at a given time. The aggregate data rate corresponds to the sum of the data rates from all active users within the cell and the data rates, in turn, depend on the number of allocated RBs per user. Hence, capacity also correlates with the number of available RBs and the number of users that can be assigned to them. Moreover, one can also evaluate capacity in terms of a specific service or QoS requirement, in order to determine how many users can be simultaneously served under those same conditions. It is therefore not only limited by bandwidth, requiring its efficient use, but also depends on the requirements defined for the services, which may cover a wide range of system performance parameters, such as throughput, latency and Signal-to-Interference-plus-Noise Ratio (SINR).

The main factors affecting data rates are the available bandwidth and number of RBs allocated for the transmission, subcarrier spacing, modulation scheme, number of symbols in each subframe and CP size used, the channel encoding rate, MIMO configuration and control/signalling overhead.

LTE-A provides different possible MIMO configurations – 8×8, 4×4 and 2×2 – or the possibility of not using multi-layer MIMO at all, *i.e.,* SISO. The use of MIMO is related to the channel conditions and required data rates, and provides additional modes of transmission without affecting average transmit power and frequency bandwidth, increasing system efficiency and capacity. When evaluating MIMO performance, one should not only consider the multiplicative effect on the bits per symbol, and consequently on the obtained peak data rates, but should also assess the scaled usage of bandwidth, referring to the spectral efficiency. The percentage of control and signalling overhead present in transmission depends on several factors, including the antenna configuration and frequency bandwidth used. When calculating the peak data rates over the physical layer, one should take into account the involved total overhead, which according to [HoTo11] can go from approximately 13% to 30%.

LTE Release 8 DL peak data rates can go up to 403.2 Mbit/s, using MIMO 4×4 with 64-QAM and unitary coding rate. This value assumes a normal CP length and no overhead loss. The enhancements introduced in LTE-A allow to achieve theoretical peak data rates of up to 4 Gbit/s in DL, using MIMO 8×8, and a total aggregated bandwidth of 100 MHz. Table 2.2 presents the theoretical peak data rates for a number of different configurations, using CA and higher order MIMO, and considering the maximum coding and modulation (*i.e.*, 64-QAM 1/1). These are theoretical values that do not consider any overhead loss, and would only be achieved under very specific channel conditions. In practice, the real values depend on a number of limiting factors, such as noise and interference in the network, as well as the correlation between the multiple antennas. For instance, a UE in line of sight of the BS will not be able to benefit from the MIMO multiple layer transmission, and consequently improve its data rates, due to the almost inexistent decorrelation between the multiple transmission paths.

Table 2.2 – LTE-A theoretical peak data rates, without considering overhead.

Peak Data Rate [Mbps]				
Configuration	**10 MHz**	**20 MHz**	**40 MHz**	**100 MHz**
MIMO 2×2	100.8	201.6	403.2	1008
MIMO 4×4	201.6	403.2	806.4	2016
MIMO 8×8	403.2	806.4	1612.8	4032

Another capability-related aspect considered in LTE performance requirements is latency. This is mainly due to the fact that these networks should be able to support a large number of users per cell with quasi-instantaneous access to radio resources in the active state. The control-plane (C-plane) latency takes into account the delays from the radio access and core parts of the network, resulting from the transition between connection states. On the other hand, user-plane (U-plane) latency is defined as the time elapsed since an IP packet is available in the eNB until it is received in the IP layer of the end-user terminal, and vice-versa. The use of packets retransmission mechanisms reflects on the U-plane latency and allows one to maximise spectral efficiency at the expense of increased delays while retransmissions take place. Both types of latency are mainly limited by non-radio delays, *e.g.*, distance between elements in the network and system loading, hence they do not show high correlation with radio-access improvements, such as MIMO and CA. While LTE FDD achieves a 4 ms U-plane latency, LTE-A goes further by reducing both types of latency in comparison with previous releases and providing C-plane capacity for at least 300 active users without Discontinuous Reception (DRX), in a 5 MHz bandwidth.

The design targets for LTE-A, specified in [3GPP13a], also include spectral efficiency as another important parameter for evaluating system performance, in terms of capacity, giving the total data rate that can be provided from each deployed Base Station (BS) and per Hertz of licensed spectrum. The peak spectrum efficiency corresponds to the highest bit rate normalised by the bandwidth, considering that communication is free of errors and that all the available radio resources for the corresponding link are assigned to a single user. The average spectrum efficiency corresponds to the aggregate throughput of all users normalised by the overall cell bandwidth and by the number of cells. The cell edge spectrum efficiency is obtained from the 5 % point in the user throughput Cumulative Distribution Function (CDF), normalised by the overall cell bandwidth. 3GPP defines targets for the three types of spectral efficiency, highlighting the fact that both peak and average throughputs and spectrum efficiency benefit more from MIMO than cell edge performance does, though the latter significantly challenges the dimensioning of the networks, for instance in coverage. According to the target values for peak spectral efficiency in LTE-A, by using different MIMO configurations, it is possible to estimate theoretical upper bounds on the achievable peak data rates for different channel bandwidth configurations (including CA). These theoretical upper bounds would not consider the bit rate degradation caused by CA control overhead.

Performance evaluation in terms of Quality of Service is mostly related to the end-users' experience

and to the ability of the network to provide services at assured levels of quality. It then depends on the type of services and applications, given a number of parameters to assess their quality, according to Section 2.4. The main used performance parameters are the end-to-end delay, delay jitter (variation), packet loss rate and user throughput.

User plane latency and delay jitter are very important performance metrics for real-time interactive services, such as voice/video calls, streaming applications and on-line gaming. The LTE air interface scheduler, retransmissions and the transport network, all contribute to end-to-end delay variations that may become perceptible to users. Proper network dimensioning and in-built QoS mechanisms have to be used in order to assure that end-to-end delays and delay variations do not impact negatively on the supported applications, weighting the consequences in other aspects, *e.g.,* spectral efficiency as seen earlier in this section.

User throughput takes into account the decrease in the data rates when radio resources are shared among users in the network (*i.e.*, interference), and retransmission of packets occurs due to high packet loss rates in bad channel conditions. This is a valuable concept to assess the actual level of quality perceived by users, and provides guidance to adjust network parameters in accordance. As user throughput derives from physical layer data rates, it can significantly benefit from MIMO and frequency aggregation techniques, as well as relay technologies. Moreover, it relates directly to the concepts of average and cell edge spectral efficiencies, which by definition normalise realistic values of the aggregated throughput to the overall bandwidth.

3GPP defines average and cell edge spectral efficiency targets for a base coverage urban scenario, with an inter-site distance of 500 m and pedestrian users [3GPP12a]. Special focus is given to these parameters due to the Advanced E-UTRA claim for a more homogenous distribution of the user experience over the coverage area, which is reflected in both average and cell edge user throughputs. Table 2.3 shows the targets for DL spectral efficiency, referring to the base coverage urban scenario conditions.

Table 2.3 – Targets for DL average and cell edge spectral efficiencies for different antenna configurations (extracted from [3GPP12a]).

Antenna configuration	Average Spectral Efficiency [bit/s/Hz]	Cell Edge Spectral Efficiency [bit/s/Hz/user[1]]
MIMO 2×2	2.4	0.07
MIMO 4×2	2.6	0.09
MIMO 4×4	3.7	0.12

[1] 10 users uniform-randomly dropped in the cell.

Interference is yet another aspect that has to be considered for performance evaluation in LTE. It starts by having a significant importance when its power takes higher values than noise, which mostly happens with the overlapping of different BSs coverage areas and an increasing number of users sharing the same radio resources. Interference can be of two main types:

- Intra-cell or Adjacent-Channel Interference (ACI), which is caused by signals from

adjacent channels extending into the band of the preferred signal.

- Inter-cell or Co-Channel interference (ICI or CCI), which is caused by signals of the same frequency reaching the same receiver.

The first component, ACI, is generally neglected in LTE, since perfect orthogonality between subcarriers can be assumed. On the other hand, CCI is considerably more restrictive in LTE, given the high degree of frequency reuse among cells to maximise spectral efficiency and to meet the demand in terms of data rates. With such dense frequency reuse, data and control channels experience substantial levels of interference from neighbouring cells, which in turn reduces the actual spectral efficiency, especially at the cell edge, limiting system capacity. Therefore, inter-cell interference mitigation becomes crucial to improve average user throughput.

Among some of the performance metrics that should be used in order to study the impact of interference in LTE, SINR is an important indicator to evaluate radio link conditions in cellular networks [TGBA11]. It provides a way for determining the throughput offered by a BS to the users in the cell, in scenarios where interference is more limiting than noise, *e.g.,* urban scenarios where coverage areas overlapping is far more common than in rural ones.

LTE performs continuous radio link evaluation in order to optimise transmission for a given power. This refers to the process of link adaptation, where the SINR is used to provide information about the channel quality from the serving cell, the level of interference from other cells and the noise level, matching with the necessary system parameters, such as modulation scheme, coding rate and antenna configuration (PMI and Rank). For instance, high-order modulations are only useful when the SINR is sufficiently high, given their higher sensitivity to interference, noise and channel estimation errors, whereas a low-order modulation is more robust and can tolerate higher levels of interference, though it provides lower transmission bit rates [SeTB11]. The same happens with coding rates and MIMO techniques, which can be used to achieve improved data rates by taking advantage of specific radio channel conditions evaluated through the SINR.

Scheduling is yet another important factor with direct impact on users' throughput and cell capacity. It is responsible for the allocation of resources to users, in order to maximise capacity while guaranteeing fairness in the time and frequency domains. Scheduling is also applicable to load balancing across multiple carriers in CA scenarios, as studied in [WPMS09] and [WaRP11]. The most popular scheduling algorithms are the Maximum SINR, Round Robin (RR) and Proportional Fair (PF). In the Maximum SINR scheme, resources are allocated to users according to the SINR in the respective link, hence users with higher SINR have higher probabilities to get resources than users with low SINR. In RR, scheduling provides users the same amount of resources, regardless of the radio channels conditions, in order to be as fair as possible. PF derives from the Maximum SINR, by taking into account not only the radio channel conditions but also the past scheduling, in order to avoid excluding low SINR users from scheduling.

MIMO techniques were designed to improve signal-to-noise ratios, boosting both coverage and achievable data rates. Moreover, to achieve additional throughput gains in scenarios where the SNR is already very high, LTE uses the MIMO spatial multiplexing technique, which takes further advantage

from rich multipath conditions and the transmission of parallel data streams. The increased capacity gains resulting from shared SNR between multiple data streams introduces a multiplicative effect on throughput, which in turn reflects on theoretical gains equal to the number of layers used (MIMO transmission rank). On the other hand, the enhanced reference signal design introduced in LTE-A, which allows to further improve performance when the number of antenna branches is high, also introduces more overhead in the transmission, affecting system performance especially in critical conditions. Consequently, the timing of the introduction of the new MIMO features and configuration of its parameters has to be chosen accordingly and optimised for the different types of benefit, namely in peak data rates, average capacity and cell edge performance.

According to [NoSN11], UL MIMO improvements are responsible for significantly improving peak data rates and spectrum efficiency. SU-MIMO is mainly responsible for increasing the data rates in lightly loaded networks for high-end multi-transmitter UE. MU-MIMO, on the other hand, provides significant improvements in spectrum efficiency even with single transmitter UEs. DL MIMO gains are mainly observed in multi-user transmission (MU-MIMO), which carries enhanced Channel State Information (CSI) feedback from UE to eNB.

The possibility to aggregate multiple frequency bands in Carrier Aggregation enables operators to better take advantage of the licensed spectrum by pooling resources within the same band or across different bands. This leads to improved peak data rates and more capacity, as operators will no longer be limited to the bandwidth of the contiguous spectrum. CA will enable the provision of multiple services simultaneously over multiple carriers, ensuring a better user experience while facing a lack of wider contiguous spectrum. In addition, CA can also improve network efficiency and average user performance, by allowing the dynamic allocation of traffic across the entire licensed spectrum and the aggregation of cells having different coverage, thereby enabling flexible network deployments according to traffic demands [BNCB12].

Performance analysis regarding different CA scenarios can be done by evaluating average throughput and number of active users per cell, given the impact on capacity [ShIN12]. Moreover, radio channel conditions, such as path loss and geometry (G-) factor, may differ at different frequency bands, thus being very important to take into account when implementing non-contiguous CA, where data transmission occurs over multiple carriers separated across a wide frequency range. As a result, radio channel parameters should be included along with traffic load in the design of CC selection algorithms, for performance maximisation as well as coverage optimisation [WaRP11].

Moreover, the use of multiple frequency bands in inter-band CA, allows taking advantage of the existing frequency diversity, in terms of coverage. This has direct impact on the number of covered users, depending on the PCell and corresponding coverage range, and on the average levels of interference, present in the network. Both are reflected on capacity gains of the network, thus they should be taken into consideration when describing the effects of using different combinations of frequencies, though CA.

2.4 Services and Applications

Voice services have a fairly predictable performance demand from the network, with Constant Bit Rate (CBR) and slight variations along time. The main concern for operators while delivering this kind of services lies on capacity aspects and delays. Regarding capacity, operators have to guarantee access for all their subscribers requiring voice calls, at a given time interval. Delays in turn are critical while evaluating the quality of the voice calls and user experience in this type of service.

Data services are substantially benefited by the LTE flat EPS architecture, optimised for Packet Switched (PS) services. These services assist in applications with very specific needs that usually do not require guaranteed bit rates, making it necessary to monitor each of them separately.

The LTE converged all-IP architecture requires an improved QoS provisioning, which supports the differentiation between services and applications in new generation networks. This concept of QoS has evolved from previous 3GPP defined radio access network technologies, such as UMTS, and implies a traffic differentiation and use of multiple bearers with configuration and priorities optimised to ensure sufficient service quality for each user. A bearer is defined as a point-to-point communication service between two network elements, associated with specific QoS requirements. For example, a UE can be engaged in a voice call while at the same time browsing a web page. Voice has more stringent requirements for QoS in terms of delay and delay jitter than web browsing, while the latter requires a much lower packet loss rate.

According to the 3GPP specification for UMTS and LTE QoS concept and architecture in [3GPP12b], four different classes of service, also referred to as traffic classes, are defined based on their QoS requirements. These four classes – conversational, streaming, interactive, and background – provide the basis for the multi-bearer evolved concept of QoS in LTE and LTE-A networks, and can be used as a good approach for the services differentiation:

- Conversational traffic includes the well-known telephony services, such as voice and video calls, Voice over IP (VoIP) and conferencing tools. These services are mostly characterised and performance reliant on the transfer time (delay) and time relation (variation) between the information entities of the stream.
- Streaming services, like audio-video streaming in mobile TV applications, have a strong dependence on the time relation between both ends of the stream.
- Interactive services, where one end-user requests data from a remote equipment, as in web browsing and social networking, are mainly characterised by the request response pattern from the end-user and a transparent content transfer (with low bit error rate).
- Background services, such as Email, SMS, MMS and Cloud applications, consist of end-users sending and receiving data files to a background, where they are stored and can be later accessed. Hence, they are more or less delivery time insensitive and require transparent payload transfer as well.

The 3GPP LTE/SAE specification of EPS introduced a set of QoS mechanisms that follow the new approach of differentiating traffic through the use of multiple bearers. The level of granularity for QoS

control within EPS is an EPS bearer, which means that all packet streams contained in the same bearer receive the same packet-forwarding treatment. There are two types of bearers: Guaranteed Bit-Rate (GBR) and Non-Guaranteed Bit-Rate (non-GBR). GBR bearers allocate dedicated network resources with the corresponding GBR QoS values defined for the associated services, being suitable for conversational services such as voice calls. On the other hand, non-GBR bearers do not guarantee any specific bit rate, being suitable for web browsing or background applications such as Email. Table 2.4 summarises the information about the QoS classes standardised by the 3GPP, concerning real-time requirements, symmetry between data flows, need for guaranteed bit rate, time delay restriction, extended use of data buffers, traffic burstiness and type of switching.

Table 2.4 – QoS traffic classes summary, according to the 3GPP (adapted from [3GPP12b]).

	Conversational	**Streaming**	**Interactive**	**Background**
Real Time	✓	✓	-	-
Symmetric	✓	-	-	-
Bit Rate	Guaranteed	Guaranteed	Not guaranteed	Not guaranteed
Delay	Minimum fixed	Minimum variable	Moderate variable	High variable
Buffer	-	✓	✓	✓
Bursty	-	-	✓	✓
Switching Type	CS	CS	PS	PS
Example	Voice/Video calls	Video streaming	Web browsing	SMS, MMS, Email

3GPP standardised a set of optimised parameters in order to enable QoS characterisation for each EPS bearer. The QoS Class Identifier (QCI) identifies the specific U-plane packet forward treatment associated to the bearer, being characterised by its priority, packet delay budget and acceptable packet loss rate. The Allocation and Retention Priority (ARP) specifies the C-plane treatment that the bearer will receive by means of setting priorities for admission and congestion control. The Maximum Bit Rate (MBR) and Guaranteed Bit Rate (GBR) are defined only for GBR bearers, the former sets the maximum bit rate that the traffic on the bearer may not exceed and the latter the specifies the minimum bit rate that the network can sustain and guarantee for the bearer. The Aggregated Maximum Bit Rate (AMBR) is defined for groups of non-GBR bearers and enables operators to limit the total amount of bit rate consumed by a single user.

Table 2.5 presents the set of standardised QCIs, defined by the 3GPP, that provide a common understanding of the underlying service characteristics, for LTE compatibility purposes. It corroborates some of the previous accounts about the different classes of services, *e.g.,* conversational voice requires reduced Packet Delay (100 ms) and a relatively high Packet Error Loss Ratio (10^{-2}), whereas buffered video streaming does not require such a restrictive Packet Delay Budget (300 ms), though it requires a much lower Packet Error Loss Ratio (10^{-6}).

The new functionalities introduced in LTE-A, such as enhanced MIMO support and CA, enable network performance improvements in the peak data rates, spectrum efficiency, cell edge performance, as well as new ways of cost reduction in deployment, operation and transportation. Real-time high definition video sharing services, for example in live mobile broadcasting, are limited due to the needs for very high throughputs, especially in UL, and usage capacity within the network. This limitation can be exceeded in LTE-A networks given the improved MIMO and CA features, providing much higher peak data rates and an efficient use of the bandwidth available, which increases capacity.

Table 2.5 – Standardised QoS Class Identifiers characterisation for LTE (extracted from [3GPP13a])-

QCI	Resource Type	Priority	Packet Delay Budget	Packet Error Loss Ratio	Example services
1	GBR	2	100 ms	10^{-2}	Conversational voice
2		4	150 ms	10^{-3}	Conversational video (live streaming)
3		3	50 ms	10^{-3}	Real-time gaming
4		5	300 ms	10^{-6}	Non-conversational video (buffered streaming)
5	Non-GBR	1	100 ms	10^{-6}	IMS signalling
6		6	300 ms	10^{-6}	Video (buffered streaming), TCP-based (*e.g.* www, email, chat, FTP, P2P file sharing, progressive video, etc.)
7		7	100 ms	10^{-3}	Voice, video (live streaming), interactive gaming
8		8	300 ms	10^{-6}	Video (buffered streaming), TCP-based (*e.g.* www, email, chat, FTP, P2P file sharing, progressive video, etc.)
9		9	300 ms	10^{-6}	

2.5 State of the Art

A realistic performance evaluation of LTE networks, based on drive tests measurements, is presented in [LEVB12], providing insights on potential upgraded transmission schemes. The measurements are based on radio inputs from a 3G live network and compared with link level simulation results for different LTE device categories. This includes the evaluation of MIMO 2×2 and 4×4 transmission schemes performances, based on the different devices characteristics and some analysed network key parameters, such as the Reference Signal Received Power (RSRP), inter-cell interference, DL shared channel received power and signal to noise ratio, as well as the corresponding throughputs. Results show that all MIMO 2×2 categories (2, 3 and 4) have similar performances, due to the fact that

higher LTE categories require high SNR levels, which are hardly achieved in the network, in order to provide significant improvements on the user experienced throughputs. On the other hand, LTE category 5 devices, which support MIMO 4×4 transmission, show gains of about 60% in the average throughput, compared to MIMO 2×2 devices, as well as improving performances at cell-centre and cell-edge conditions.

LTE DL system performance is evaluated in [FCDY09], using different scenarios to test different transmission modes and MIMO schemes. In one of the scenarios, the obtained average and cell-edge spectral efficiencies are investigated for different closed loop SU-MIMO transmission schemes, including MIMO 4×4. SIMO and MU-MIMO transmission schemes are also evaluated and compared with the results for SU-MIMO. The results show that average spectral efficiency of 4×4 MIMO in a static system simulation setup is, in practice, nearly 60% and 50% higher than in the 1×2 SIMO an 2×2 MIMO configurations, accordingly. Similar results were obtained for cell-edge spectral efficiencies. Moreover, 4×4 MU-MIMO simulation results also show significant improvements relatively to other configurations, with a 90% gain in average cell throughput compared to the 1×2 SIMO scheme and 20% gain over the equivalent 4×4 SU-MIMO scheme.

The potential performance gains that can be obtained with up to 8×8 MIMO transmissions, as standardised in LTE-A Release 10, are evaluated in [WAFJ12]. The tests are done through indoor measurements using a testbed implementation developed by Ericsson, thus representative of the relative performance gains of future LTE-A MIMO commercial systems. Results for a setup with well-separated antennas show increasing DL throughputs as the number of transmit and receive antennas increases, up to an average throughput of 335 Mbit/s, using an 8×8 MIMO configuration over a 20 MHz band. The tests were repeated using a more compact array size, reasonable for consumer device implementation, also showing large throughput gains for higher order MIMO and low throughput degradation compared to the well-separated antennas case, in most cases less than 10% and almost no degradation at the peak performance levels.

An overview of CA is given in [ShIN12], including different aggregation scenarios, bandwidth structure and implementation in LTE-A systems. A simulation model to investigate the impact of CA in LTE-A DL performance, in terms of average throughput and number of active users per cell, is laid out using up to five component carriers. Five different scenarios are then tested, using from 1 CC (non-CA), to 5 CCs, respectively in each scenario. The results show improvements in cell average user throughput as the number of aggregated CCs increases, with an almost tripled average user throughput when using 2 aggregated CCs and an 8 times higher average user throughput when using 5 aggregated CCs, all compared to the non-CA scenario. Furthermore, it is shown that an increasing number of aggregated CCs allows higher number of simultaneously active users communicating with the BS, thus improving system capacity. The percentage of possible active users in the cell is doubled when using 2 aggregated CCs and 5 times higher when using 5 aggregated CCs, again both compared with the non-CA case.

Multi-component carrier management for LTE-A networks is studied in [Wang10]. This includes an analysis on load-balancing and packet scheduling, across multiple CCs, outlining some of the different

techniques that can be used to assign CCs to each user, and how to multiplex users in each CC. Both random and selective load balancing algorithms are analysed and compared for different load scenarios. Then, a cross-CC packet scheduler is also proposed. Finally, the gains of using CA over independent carriers are also investigated, over different perspectives, evidencing no loss in the average cell throughput.

DL performance in LTE-A systems using inter-band carrier aggregation is investigated in [WaRP11], where radio channel characteristics and traffic load are considered key for the selection process of CCs and system performance optimisation. Simulations are carried to evaluate the performance in two different CA scenarios, including the inter-band aggregation of 20+20 MHz in the 1800 MHz and 2600 MHz bands. The results show that radio channel characteristics have greater impact to CC selection in scenarios where there is a large difference between carriers' G-factor distribution, *i.e.,* scenarios with high frequency separation (*e.g.,* 1800 MHz + 2600 MHz) and high inter-site distance (*i.e.*, cell-edge performance).

The recent advances in project SAMURAI (Spectrum Aggregation and Multi-User MIMO: Real-World Impact) are presented in [BCDD13]. This project is focused on the practical development and real-time evaluation and implementability of MU-MIMO and CA schemes in LTE-A. Starting with some of the highlights in the current standardisation status of MU-MIMO and CA features, the paper then follows to the introduction of the proposed interference aware (IA) receiver structure for MU-MIMO, realistic evaluation on the implementation of CA and some insights and practical considerations regarding the performance of the joint application of MU-MIMO and CA transmission schemes. These sections are conveyed with insights on system level performance, regarding the different investigated scenarios. MU-MIMO simulations show that up to 20% gains in cell average throughput can be achieved by using the proposed IA receiver, at the expense of some losses in cell edge throughput. CA simulations, considering a 2×20 MHz band aggregation, reveal two-folded gains in DL performances (peak and average throughputs) in the case of low load conditions. Although contiguous intra-band aggregation is most likely to be the supported by first generation LTE-A terminals, given its less drastic implementation solutions, from the network viewpoint the inter-band aggregation scheme is the most feasible in the short term due to the available spectrum constraints. Network level performance curves presented for the jointly application of MU-MIMO and CA show that under heavy load conditions this joint application can compensate for the relatively modest gains achievable with CA only. Moreover, proper scheduling and adaptive SU/MU-MIMO switching can provide up to 20% gains in average throughput performance, compared to the case when only SU-MIMO with CA is used. In UL, results show that 50% gains in average user throughput can be achieved when CA is extended by multi-cluster scheduling and MU-MIMO.

Chapter 3

Performance Models and Simulation

This chapter provides an overview of the implemented model, designed to assess LTE-A performance in terms of capacity, QoS and interference, considering realistic radio channels conditions as well as reasonable RRM strategies. In Section 3.1, the general model is described, as well as its main assumptions and approaches, together with the necessary parameters and indicators. Section 3.2 focuses on the algorithms' specifics and associated workflow descriptions. Section 3.3 provides a description of the simulator and its implementation. In Section 3.4, the simulator assessment and model's validation is performed.

3.1 Model Description

3.1.1 Initial Considerations

A model was developed to evaluate performance in a simulated LTE-A cellular network. The goal of this model was to provide information on the system's performance in terms of capacity, QoS provisioning and interference. Hence, it enables to study the impact of the considered radio technologies and techniques, as well as providing the required terms for comparison.

In essence, this model is intended for evaluating the implementation of new features in a replicated cellular network, with multiple simultaneous communication links. This is done by performing snapshot-based simulations and considering each single communication link active in the system. Then, by modelling the different dynamics, such as scheduling of radio resources and interference between links, one can obtain good approximations of the actual performance statistics.

The model relates to a defined Region of Analysis (ROA), composed by a number of BSs and users, referenced to a realistic urban scenario, as defined in Chapter 4. A similar model approach to the one in [Pire12] is adopted, together with some general assumptions suggested in [IkWR10], [ITUR08b] and [Ofco12]:

- Users are dropped independently with a pondered distribution over the ROA. Each user corresponds to an active user session that runs for the duration of the simulation.
- All users are assumed to be LTE-A compatible and to have the same UE category features.
- Line of Sight (LoS) and Non Line of Sight (NLoS) channel conditions are randomly assigned to users.
- Users connect to the closest BS, regardless of the received signal powers, due to the lack of *a priori* information on the used frequency carriers and associated radio channel conditions.
- RBs are allocated to users according to scheduling algorithms, which provide metrics to decide whether a user should, or should not, have more RBs assigned at a given moment.
- The link-level model abstracts CSI and CQI information between UEs and BSs, in order to compute SNR and SINR.
- User throughputs are obtained from the SINR-to-throughput mapping functions provided in Annex D, which were obtained from manufacturer's simulated results. These functions give the individual throughputs per RB, which can then be aggregated into corresponding user's throughput values.
- Interference is modelled through the computation of the SINR per RB, for each user, taking into account the interference signals with power higher than noise, coming from other sectors or neighbouring BSs.

Using the adequate channel and propagation (path loss) models, described in Annex B, Annex C and Annex D, it is possible to reproduce the link propagation conditions and obtain reliable performance statistics at the link-level, as well as their random fluctuations, especially in frequency and spatial

domains. Then, a system-level approach is used to account for other dynamic implications caused by overall capacity, traffic and interference conditions, through pre-defined algorithms.

Resource allocation to users is modelled by following a sequence of general steps:

- To estimate the number of RBs required for each user, taking into account general and non-precise indicators (*e.g.*, SNR, average carrier frequency) and regardless of the maximum capacity of the BSs.
- To optimise resource allocation by considering BSs' maximum capacity and the minimum services' throughputs.
- Definitive users' RBs assignment over the available spectrum, in each BS's sector, and corresponding association to precise indicators, such as carrier frequency and SINR.

After estimating the number of RBs for each user, the model needs to verify if capacity is exceeded for each sector. If so, an RB reduction is performed across that sector. This step consists of performing redistribution (optimisation) of RBs for each user, avoiding that some of them get more than they need and guaranteeing the maximum number of scheduled users, even if with a minimum service satisfaction. After the third and final step, the simulation is completed and output statistics are generated.

The model assumes that an active user is a user with one or more RBs assigned and distributed over the spectrum (scheduled RBs). An active RB can either be free from any interference or suffer interference from other RBs, which in turn may lead to a completely interfered (interfered-to-zero) RB, *i.e.*, with zero throughput. Hence, RBs can be characterised as "clean", "interfered" or "interfered-to-zero".

MIMO modes, modulation schemes and coding rates for transmission are considered to be dependent on the channel and environment conditions, as well as on the system's specific manufacturer implementation. This means that the chosen transmission modes and schemes may vary according to the specifications of the system, set as input to the simulation, adding to a certain degree of randomness regarding the channel gains. The impact of the different schemes and transmission modes is also incorporated into the SINR-to-throughput mapping functions of the Data Rate Model (DRM), rendering the influence of the different combinations in the obtained throughputs.

The adopted model considers different user scenarios, which are consistent with the defined ITU-R channel models. These scenarios represent the range of possible test environments in a simulated network:

- Outdoor to indoor and pedestrian test environment, where BSs are located outdoors and pedestrian users are located on streets or inside buildings and residences. For users inside buildings or residences, the propagation model takes building penetration loss into account.
- Vehicular test environment, where users' fading has to take vehicle speeds into account.

The EPA 5 Hz and EVA 70 Hz channel models, defined by the ITU-R, are associated with the different user scenarios, as described in Annex D. The first is considered for pedestrian and indoor users, due to the static (or almost) characteristics, while the latter is used for vehicular users.

3.1.2 SNR and SINR

The computation of SNR is the heart of the model, providing the starting point for the estimation of the necessary number of RBs to be allocated for each user. After being calculated for every user in the simulation, it will allow to extract the system's overall resource requirements and proceed to the actual distribution of resources.

When a user is dropped in the ROA and connects to a BS, the SNR is obtained from the average UE's received signal power and noise power at the MT receiver, according to equation (B.5). The obtained SNR will then be used together with the SINR-to-throughput mapping functions in Annex D to estimate the number of RBs necessary to satisfy the required QoS provisioning for that user.

The user's average received signal power is obtained from (B.1), which is based on the proposed Radio Link Budget (RLB) and the COST 231-Walfisch-Ikegami model [CiKu96], presented in Annex B and Annex C, respectively. The RLB provides general equations for the step-by-step calculations in order to obtain the average received signal power and SNR/SINR, taking propagation conditions into account. The computation of the path loss, according to (B.4), takes into account the COST 231-Walfisch-Ikegami path loss and two additional terms: one associated with the user environment, such as vehicular and indoor penetration margins, and the other referring to the Slow Fading (SF) margin. The Fast Fading (FF) Margin can be neglected, due to the fact that LTE uses sub-carrier transmission. The noise power at the receiver is obtained for each user from (B.6) provided that, at this stage, the model considers an average frequency, based on each user's relative location to the reference radius of the available frequency bands.

Interference is then considered through the computation of the SINR for each allocated RB, according to (B.7). This is done for every BS in the ROA, after the RB reduction/optimisation step, taking into account the accurate frequency carrier being used by each RB, as well as the interference power coming from neighbouring sectors. The throughput per RB can then be accurately mapped, now using the values of SINR instead of SNR.

The total interference power can be calculated by 1, as the sum of the interfering signals reaching the receiver with equal or greater power than noise and using the same frequency carrier. These interfering signals can be originated in other sectors of the same BS or in neighbouring BSs. Each of the interfering powers can be obtained using (B.1), as in the calculation of the user's average received signal power.

$$I_{[\mathrm{mW}]} = \sum_{i=1}^{N_I} I_{i_{[\mathrm{mW}]}} \tag{3.1}$$

where:

- I_i: interference power coming from Tx i;
- N_I: number of interfering signals reaching the Rx.

3.1.3 Throughput

During the first stage of the simulation, the throughput per RB is estimated using the mapping functions in Annex D, taking into account the approximation of the users' SNR. This is a preliminary step that serves as a basis to estimate the number of necessary RBs to allocate for each user, depending on the required and minimum service throughputs.

In order to estimate the achievable user throughput, the model starts by computing the throughput of one single RB, considering a reference frequency assigned to that user, and then multiplies it by the total number of allocated RBs, according to:

$$R_{b\,[\mathrm{Mbit/s}]} = N_{RB} \cdot R_b^{RB_c}{}_{[\mathrm{Mbit/s}]} \tag{3.2}$$

where:

- N_{RB}: number of used RBs;
- R_b^{RB}: throughput per RB, obtained in the reference frequency assigned to the user.

The maximum theoretical throughput per RB can be obtained from (3.3), in terms of the different time-frequency elements in the RB structure.

$$R_b^{RB}{}_{[\mathrm{Mbit/s}]} = \frac{N_{RB} \cdot N_{sub}^{RB} \cdot N_{sym}^{sub} \cdot N_b^{sym}{}_{[\mathrm{bit}]}}{T_{RB\,[\mu\mathrm{s}]}} \cdot G_{MIMO} \tag{3.3}$$

where:

- N_{sub}^{RB}: number of subcarriers per RB (assumed 12 for 15 kHz subcarrier spacing);
- N_{sym}^{sub}: number of symbols per subcarrier (7 symbols for normal CP or 6 for extended CP, in one slot period);
- N_b^{sym}: number of bits per symbol;
- T_{RB}: RB slot duration (*i.e.*, 500 µs);
- G_{MIMO}: Maximum achievable capacity/throughput gain associated to the use of MIMO.

The SNR-to-throughput mapping functions used for calculating RBs' throughput were obtained for the different available modulation schemes, QPSK, 16-QAM and 64-QAM, and also for the different MIMO transmission modes (*e.g.*, Rank-1 and Rank-2 transmissions), as shown in detail in Annex D. The effect of AMC link adaptation, supported by LTE, is replicated through the selection of the best modulation scheme, which is the one that maximises the throughput in each RB calculation.

The final user throughput, with the inclusion of interference effects, is obtained after the computation of the SINR values for each allocated RB. Once again, these are mapped onto new values of throughput per RB, according to the allocation distribution along the available carrier frequencies, and then summed for each user:

$$R_{b_{[\mathrm{Mbit/s}]}} = \sum_{i=1}^{N_{RB}} R_b^{RB_i}{}_{[\mathrm{Mbit/s}]} \tag{3.4}$$

where:

- $R_b^{RB_i}$: throughput obtained for the ith RB.

This model allows taking into consideration some additional losses together with the obtained throughputs, in order to account for the control and signalling overhead along multiple layers of the OSI model. The expressions provided in Annex D already include a share of these throughput losses, depending on the overheads considered by each manufacturer. The inclusion of the loss ratios in the analysis enables realistic approximations of the physical layer throughputs, as well as having a better notion of the actual throughputs experienced by end-users, at the application layer. The following set of pre-defined overheads is considered:

- Other physical channels (PCFICH, PDCCH and PHICH): 15.5%;
- Reference Signals: 9.5%;
- PBCH and Synchronisation Signals: 0.4%.
- Additional overheads (*e.g.*, protocol stack headers): 4.8%;
- Retransmissions (*e.g.*, HARQ, ARQ and TCP): 4.27%.

Summing the indicated overhead values, which were taken from Optimus' control and signalling dimensioning recommendations [Opti13], based on real network data, an approximate loss of 25.4% is obtained at the physical layer, and a total loss of 34.5% is obtained up to the overall application layer throughput. The application layer throughput is related with the physical layer one through (3.5):

$$R_b^{APP}{}_{[\mathrm{Mbit/s}]} = \left(1 - \eta_{overhead}^{APP/PHY}\right) \cdot R_{b_{[\mathrm{Mbit/s}]}} \tag{3.5}$$

where:

- $\eta_{overhead}^{APP/PHY}$: sum of all the overheads, up to the application layer;

Three different user throughput metrics are used in order to characterise network performance: average user throughput, top 5% user throughput, bottom 5% user throughput. The first corresponds to the average user throughput, from all active users in the network. The remaining two metrics, top- and bottom-performing user performances, are obtained by ordering all users' throughputs, from lowest to highest, and then taking the 95th and 5th percentiles of this throughput distribution, respectively. These two metrics can be used to characterise the cell-centre and cell-edge throughputs obtained in the network.

3.1.4 Cell Capacity

Capacity can be evaluated in terms of the number of users that can be simultaneously served by a BS. This depends on the QoS provisioning and required throughput for each user, as well as on the radio conditions among the different used RBs. Taking this into account, one can inspect the BS load by

calculating the aggregate cell throughput, *i.e.,* the sum of the throughputs of all active users in the cell:

$$R_b^{BS}{}_{[\mathrm{Mbit/s}]} = \sum_{i=1}^{N_u^{BS}} R_b^i{}_{[\mathrm{Mbit/s}]} \tag{3.6}$$

where:

- N_u^{BS}: number of users served by the BS;
- R_b^i: throughput of user i served by the BS.

Moreover, the capacity of a cell also depends on the scheduling and load balancing algorithms, which are used according to the radio channel, traffic and user priority (*i.e.*, QoS) conditions. The impact of all these aspects on overall capacity can be evaluated by looking at the total accumulated throughput served, over all the BSs in the network. This can be done by computing the product of the number of users served with the average user throughput in the network.

3.1.5 Coverage

Coverage estimation is performed to determine which users are served by the network. Moreover, this model considers coverage estimation as an additional tool to assess the impact of the different used techniques (*i.e.*, MIMO and CA) and weigh its influence on the remaining performance parameters, such as capacity and throughput. In particular, coverage estimation for each frequency band is required to be able to segment users within a cell and establish priorities among the different CCs being assigned to users.

The RLB equations are combined with the adequate environment propagation model for the path loss, in order to determine the maximum cell or coverage radius. The result from manipulating (B.4), (C.1) and (C.2), provides two expressions for the cell radius, considering LoS or NLoS propagation:

$$R^{LoS}{}_{[\mathrm{km}]} = 10^{\frac{P_{t[\mathrm{dBm}]}+G_{t[\mathrm{dBi}]}+G_{r[\mathrm{dBi}]}-P_{r[\mathrm{dBm}]}^{ref}-L_p^{LoS}{}_{[\mathrm{dB}]}}{26}} \tag{3.7}$$

where:

- P_t: power fed to the Tx antenna;
- G_t: gain of the Tx antenna;
- G_r: gain of the Rx antenna;
- P_r^{ref}: Rx antenna sensitivity for a specific reference service, according to (B.8);
- L_p^{LoS}: path loss for LoS propagation.

$$R^{NLoS}{}_{[\mathrm{km}]} = 10^{\frac{P_{t[\mathrm{dBm}]}+G_{t[\mathrm{dBi}]}+G_{r[\mathrm{dBi}]}-P_{r[\mathrm{dBm}]}^{ref}-L_p^{NLoS}{}_{[\mathrm{dB}]}}{20+k_d}} \tag{3.8}$$

where:

- L_p^{NLoS}: path loss for NLoS propagation;

- k_d: average power decay.

The maximum cell radius estimation using (3.7) and (3.8) can be imprecise, due to the fact that BSs coverage areas are influenced by many factors that cannot be precisely described by the adopted propagation model. The actual covered area is, in most cases, smaller than the area spanned by the maximum cell radius, especially in dense urban networks. For that reason, the model assumes that the radius of each frequency band equals the maximum distance where an NLoS user can still achieve the established reference throughput. This reference throughput and corresponding distance are only indicative values, adaptable to the reality of the simulator. The reference service throughput is selected according to the target throughput that is desirable for a typical urban cell. Then, using the RLB equations it is possible to obtain the maximum coverage radius for each available frequency band, computing the minimum SINR, necessary to guarantee the reference throughput.

3.1.6 Load Distribution

When using CA, RBs can be allocated over different frequency bands. It is then important to evaluate the load distribution of active RBs over the available CCs. This can be done by taking the number of used RBs (*i.e.*, assigned to a user) in every BS, for each of the frequency bands available (CCs), according to:

$$N_{RB}^{CC_j} = \sum_{i=1}^{N_{BS}} n_{RB}{}_{i}^{CC_j} \tag{3.9}$$

where:

- N_{BS}: number of BSs;
- $n_{RB}{}_{i}^{CC_j}$: number of used RBs assigned in the jth CC, allocated by BS i.

Also, the number of used RBs per available LTE frequency band (*i.e.*, 800 MHz, 1800 MHz and 2600 MHz) can be extracted, according to:

$$N_{RB}^{Y} = \sum_{j=1}^{N_{CC}^{Y}} N_{RB}^{CC_j} \tag{3.10}$$

where:

- N_{CC}^{Y}: number of CCs in frequency band Y.

Finally, another important metric is the accumulated throughput offered by each of the available CCs and corresponding LTE frequency bands. This follows the same rationale as in the computation of the number of used RBs, first obtaining the accumulated throughput per CC and then for the corresponding LTE frequency band:

$$R_b^{CC_j}{}_{[\mathrm{Mbit/s}]} = \sum_{i=1}^{N_{BS}} \sum_{k=1}^{N_{RB}^{CC_j}} R_{b_k}{}_{[\mathrm{Mbit/s}]} \tag{3.11}$$

where:

- R_{b_k}: throughput in the kth RB.

These metrics vary according to the load offered to the network, as well as with the CC assignment algorithm (*i.e.*, RB distribution over the available spectrum). They provide a starting point for the analysis of the impact of the load distribution over the different available CCs on the system's performance and capacity.

3.1.7 Interference

One way of evaluating interference in the network is to take the number of interfered RBs and compare it with the number of active RBs, according to (3.12). An RB is considered interfered when its throughput has been affected by signals coming from other sectors or neighbouring BSs, with a power above noise level. The particular case of "interfered-to-zero" RBs (critical interference), which had their throughput reduced to zero, according to the ICI analysis algorithm, should also be considered. From the relation between the number of interfered/interfered-to-zero and active RBs, one can extract percentages of interference:

$$P_{I_{[\%]}} = \frac{N_{RB}^{I}}{N_{RB}} \times 100 \tag{3.12}$$

where:

- N_{RB}^{I}: number of interfered RBs.

Regarding CA, it is also interesting to evaluate the percentage of interference in each of the available CCs and LTE frequency bands. For instance, take the percentage of interfered RBs in each CC or the relation to the total number of active RBs, over all CCs, according to:

$$P_I^{CC_j}{}_{[\%]} = \frac{N_{RB_I}^{CC_j}}{N_{RB}} \times 100 \tag{3.13}$$

where:

- $N_{RB_I}^{CC_j}$: number of interfered RBs assigned in the *j*-th CC.

Another metric that was used for evaluating interference is the difference between dB values of SNR and SINR, which is given by:

$$\Delta\rho = \rho_{N_{[\mathrm{dB}]}} - \rho_{IN_{[\mathrm{dB}]}} = 10\log_{10}\left(\frac{P_{r_{[\mathrm{mW}]}}}{N_{[\mathrm{mW}]}}\right) - 10\log_{10}\left(\frac{P_{r_{[\mathrm{mW}]}}}{I_{[\mathrm{mW}]} + N_{[\mathrm{mW}]}}\right)$$
$$= 10\log_{10}\left(1 + \frac{I_{[\mathrm{mW}]}}{N_{[\mathrm{mW}]}}\right) \tag{3.14}$$

where:

- ρ_N: SNR;
- ρ_{IN}: SINR;
- N: noise power.

When comparing two scenarios where average noise levels are kept constant, an increase in this difference ought to represent an increase in interference. In other words, if noise is kept constant and the difference between dB values of SNR and SINR increases, the interference-to-noise ratio in equation (3.14) increases, meaning that interference is also increasing.

3.1.8 MIMO Model

In general, the performance of different multi-antenna configurations depends on a number of factors, such as the channel state, signal quality, the speed of the user and the correlation between received signals at the receiving antennas. According to the explanation provided in Annex E, there are multiple transmission modes available for LTE, employing different multi-antenna schemes. The effect of the MIMO transmission mode selection (*e.g.*, transmit diversity and spatial multiplexing), and associated gains, is incorporated into the mapping functions, which always return the maximum achievable throughput for each different scenario, and into the adopted gain model.

The MIMO model takes into account the dependence of the capacity improvements on multiple factors, such as distance or the number of transmitting and receiving antennas, according to the Relative MIMO Gain (RMG) Model, described in Annex E. This dependence translates into gain values that complement the throughput results obtained from the mapping functions, in order to compensate for the capacity gains of the different evaluated MIMO schemes.

The throughput expressions provided by the DRM allow one to obtain values for up to MIMO 4×4 transmissions, according to Annex D. Thus, when modelling MIMO 8×8 transmissions, one should consider the normalisation of the corresponding RMGs towards the gain of a MIMO 4×4 scheme.

Since all users are assumed to have the same UE category features, the model takes only one single MIMO scheme for all the evaluated communication links. The relative gains applied in the model, already consider an average loss due to the variable conditions of the radio channel, which limit the use of maximum supported schemes. In other words, the average gain of a MIMO 4×4 transmission does not correspond to double the gain of MIMO 2×2, due to the fact that Rank-2 transmission does not always happen.

3.2 Algorithms

One of the main motivations of this thesis is to evaluate the impact of CA on the performance and overall capacity of the system. For that reason, it requires the use of algorithms to model the allocation of resources to users and subsequent distribution over the whole available spectrum.

Figure 3.1 shows the RRM framework of a multi-carrier LTE-A system, supporting the aggregation of up to 3 CCs. This scheme guarantees backwards compatibility with LTE Release 8 users, since the same physical layer and data link layer configurations can be used [ShIN12]. The RRM algorithm starts by performing admission control and then employs Layer-3 carrier load balancing (CC assignment) to allocate users on different CCs. Once users are assigned to the corresponding CCs, the RRM performs Layer-2 Packet Scheduling (PS), which is responsible for the allocation of the time-frequency resources to the different UEs in each CC [WPSM10].

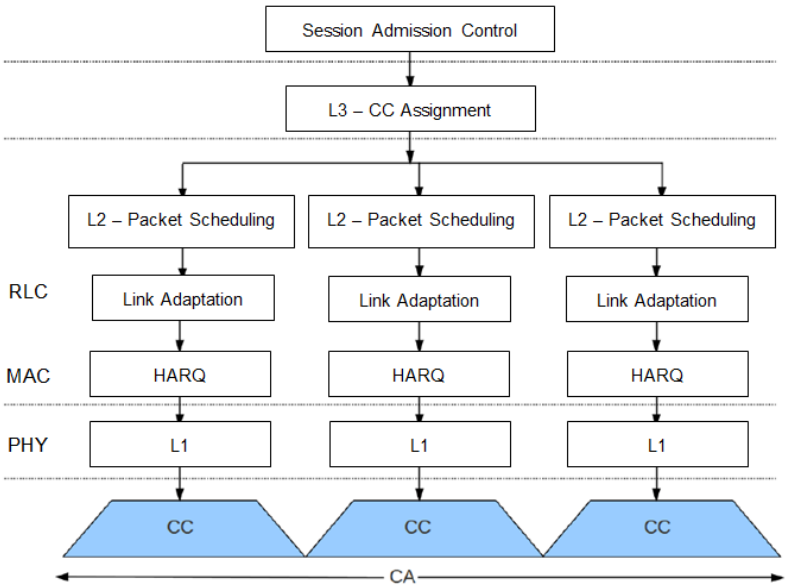

Figure 3.1 – Multi-carrier RRM framework structure, with up to 3 CCs (extracted from [SPZG12]).

The simulator's framework towards CA and multi-carrier allocation of users is based on the described RRM structure. It tries to mimic the results observed with a real RRM, while implementing a slightly different sequence of steps, adapting to the snapshot-based nature of the simulations. The assignment of different CCs to users is done through the distribution of RBs along the available carrier frequencies. At this point, the RB distribution algorithm should decide which frequency bands to use according to different criteria, such as user distance, frequency band coverage and load distribution. It assumes that all users are LTE-A compatible, which makes it possible for every user to be allocated in all available CCs and frequency bands, as long as it has enough RB demand.

Assuming that RBs can be distributed over a whole continuous (aggregated) bandwidth, the distribution algorithm will have to determine the set of carrier frequencies where the user's RBs can be scheduled. From this point on, RBs can be randomly or sequentially distributed over the different sets of carrier frequencies defined for each user. This is a key point for the model, since it provides the

most relevant variations in the results, regarding the impact of CA.

Every LTE-A user always has to have a PCell active and the possibility to dynamically activate/deactivate one or more SCells, as described in Section 2.2. This possibility relies on different parameters, such as radio channel conditions and the data rates required. While the PCell will always be active, meaning that the user's RBs can always be assigned in the corresponding CC, the SCells will work as an extension of available bandwidth. According to [Opti13], the amount of data sent on each carrier is proportional to the bandwidth and DL channel quality of the carrier. Splitting of data onto multiple carriers will only happen if the data to be sent exceed a certain threshold. If the data are less than this threshold then the transmission happens only on the carrier that could potentially send more data given the constraints of carrier bandwidth and DL channel quality on the carrier.

The PS functionality for multi-carrier LTE-A is very similar to the one in LTE Release 8, except that it allows scheduling of users separately across multiple CCs. In this thesis, it is modelled as a simple RB allocation algorithm. The simulator implements an adapted version of the PF algorithm, illustrated in Figure 3.2, in order to estimate the required number of RBs to allocate for each user. Since the simulator is snapshot-based, it does not have the time depth to be able to explore average levels over time, as in the traditional PF algorithm. Hence, the algorithm tries to allocate the number of RBs necessary to satisfy the average service throughput or the minimum service throughput, depending on the number of available RBs in the sector. This is done before the interference reduction algorithm takes place and regardless of the average throughput history of the user. Since all users are assumed to be LTE-A compatible, allowed to potentially make use of any of the available CCs, the RBs are laid together in one unique source of resources (*i.e.*, continuous available spectrum) and treated as in a single-carrier system. This approach simplifies the use of different Frequency Reuse Schemes (FRSs) as well as the whole process of optimisation and reduction of the resources in each sector, as explained further below.

This model considers an intermediate step that is responsible for defining the available bandwidth and associated RBs in every sector of each BS. This is prior to the users' RBs distribution over the spectrum, which sets specific carrier frequencies for each available RB. The Universal Frequency Reuse Scheme, or just Reuse-1 scheme, is adopted as the fundamental FRS for every BS in the network. This scheme consists of using the whole bandwidth in each sector, reusing the same carrier frequencies three times in every BS (*i.e.*, one for each sector). Other FRSs, such as the ones described in [Pire12], can be used together with CA, providing evolved bandwidth schemes that aim to reduce interference among sectors. However, these are not the focus of this thesis and for that reason are not further treated here.

Regarding the allocation of RBs over multiple CCs, one has also to consider load balancing between multiple carriers as a relevant aspect affecting system's performance. Once the number of allocated RBs is determined for every user, an algorithm is performed in order to consistently associate these RBs to specific carrier frequencies, thus completing the process of resource allocation and distribution over the spectrum. This algorithm is the core of the model, in terms of CA, since it allows one to take advantage of the frequency diversity available over the whole aggregated spectrum. At this point, there

are two different approaches to distribute user RBs over the available spectrum:

- To randomly distribute users over the available bandwidth, disregarding RBs carrier frequencies. This method resembles the Mobile Hashing (MH) algorithm described in [WPSM10] and [Wang10], which aims to provide balanced load across all CCs, in the long term.
- Selective distribution of users across the CCs depending on their distance to the BS. In other words, users close to the BS (*i.e.*, cell-centre users) are allocated the highest frequencies, whereas users further away from the BS (*i.e.*, cell-edge users) are allocated the lowest ones.

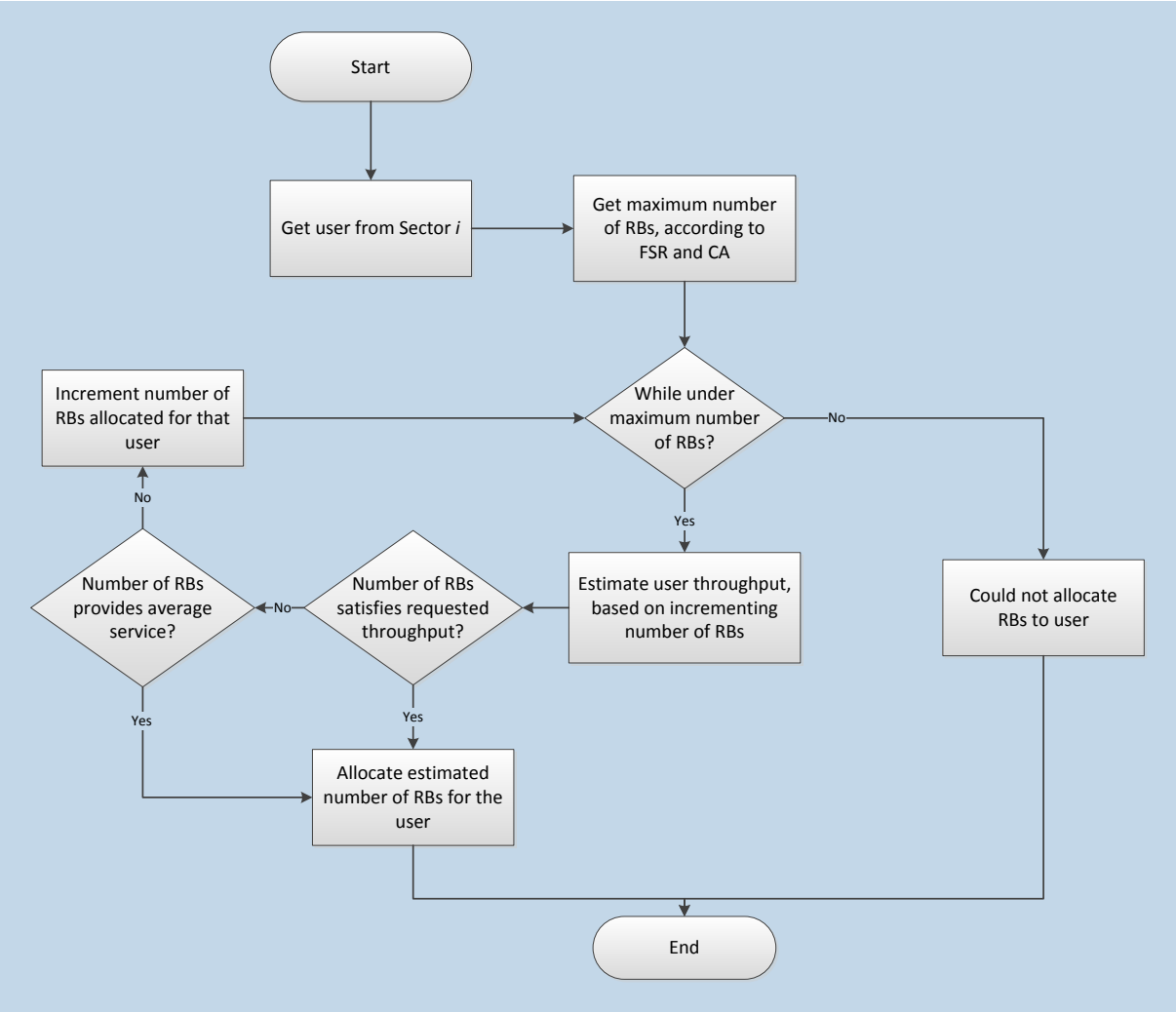

Figure 3.2 – PF based estimation of the number of RBs for each user.

While the first approach provides better load balancing across CCs, reducing the probability of interference between RBs, it does not benefit from the available frequency diversity. The second approach is based on the fact that lower frequencies span wider coverage areas than higher ones, due to smaller path loss, thus being more adequate to users farther away from the BS.

When employing selective distribution over the spectrum, RBs can either be distributed sequentially or randomly within each CC, exploring the impact in terms of the interference caused by the reuse of the same carrier frequencies. If sequential distribution is adopted, RBs from cell-edge users are distributed

starting from the lowest frequency CC and cell-centre users' RBs are distributed starting from the highest frequency CC. This means that, in high load scenarios, RBs' frequency location is more adequate to the associated users, taking advantage from the existing frequency diversity. However, the allocated RBs are predominantly concentrated in the two opposite ends of the available spectrum, and in low load scenarios middle range carrier frequencies end up not being used at all.

Alternatively, one can look at the random selective distribution of users' RBs as an intermediate between the random algorithm (*i.e.*, MH algorithm) and the sequential selective algorithm. This distribution first decides which CCs should be allowed to a user, providing an analogy between the selection of PCell and SCells in a real LTE-A system, and only after RBs are randomly distributed over the assigned CCs. The decision of which CCs should be assigned to a user is based on the user distance to the BS. Considering a reference cell range for each of the available frequency bands (*i.e.*, central frequencies), based on a reference throughput, it is possible to segment users according to their distance to the centre, thus enabling a more accurate CC-selection criteria. When using the random selective distribution algorithm, the lowest frequency band is always available, working as a PCell, while the other frequency bands are only available to the users with a distance equal or smaller than the corresponding reference cell ranges, or in case of full load in the PCell.

The flow diagram in Figure 3.3 provides an overall representation of the RB allocation process, including the three main stages described in this section: RB estimation, optimisation and distribution over the spectrum. As shown in the flow diagram, first the RBs are laid over the available carrier frequencies, in a consecutive order, and only after they are sorted or shuffled, according to the selected distribution algorithm. The optimisation of the resources is done via a reduction algorithm, which is responsible for reducing the number of allocated RBs, according to specific criteria, in sectors where capacity is exceeded. This thesis concentrates on the QoS-based reduction algorithm, which reduces users from the same service by one RB, according to a pre-defined list containing the services' priorities [Duar08].

Figure 3.4 represents a scenario where RBs from three different users were sequentially redistributed over the three available CCs, according to the sequential selective method. The three represented CCs are not necessarily contiguous in frequency. The first user is at the cell-edge, hence he has all the RBs (coloured in red) consecutively located in the lowest frequencies. The second user is in the cell-centre, thus all his RBs (coloured in blue) were moved to the highest frequencies. Finally, the third user, also at the cell-edge, has all his RBs (coloured in green) in the frequency positions right next to the RBs of the first user. At the end of this algorithm, users in the cell-centre occupy the highest frequencies of the available bandwidth, and the users in the cell-edge occupy the lowest ones.

Likewise, Figure 3.5 represents a scenario where RBs from three different users were distributed according to the random selective algorithm. In this scenario, the two first CCs belong to a different frequency band than the third one, and the users also differ in their distances to the serving BSs. Assuming that only the second user is inside the reference coverage area of both frequency bands, according to the random selective algorithm, only RBs from this user are randomly distributed using all three CCs. RBs belonging to the first and third users are exclusively allocated on the first two CCs.

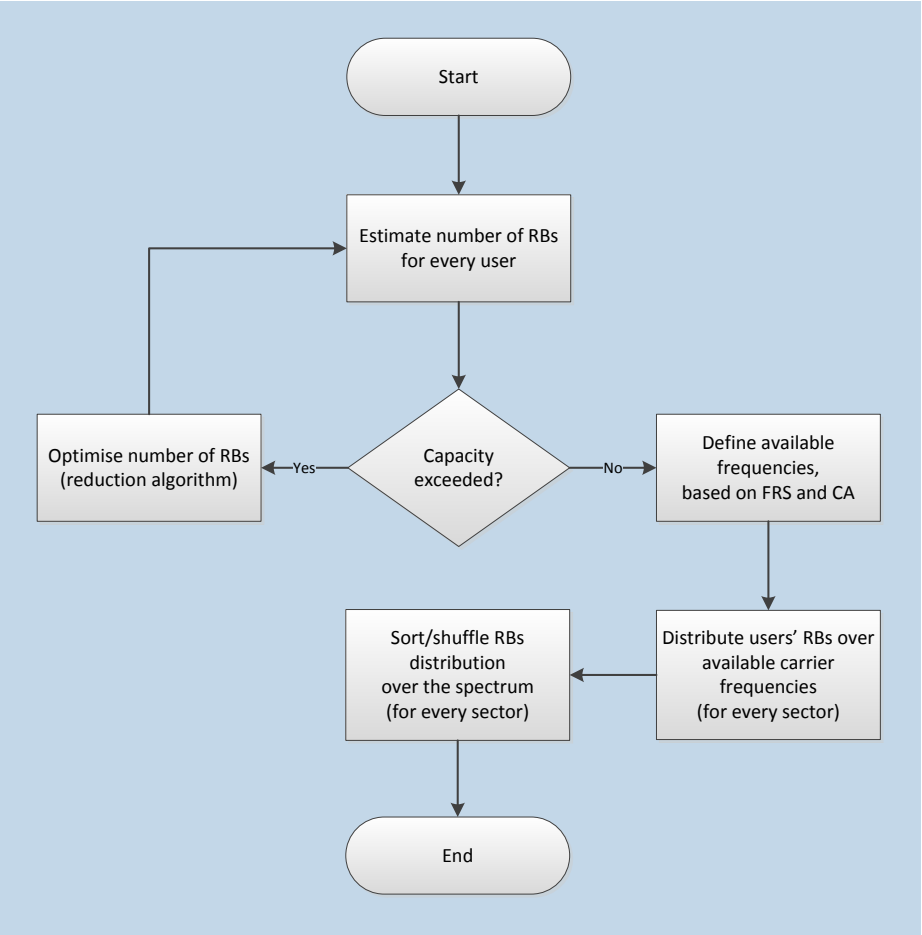

Figure 3.3 – RB allocation and distribution algorithm.

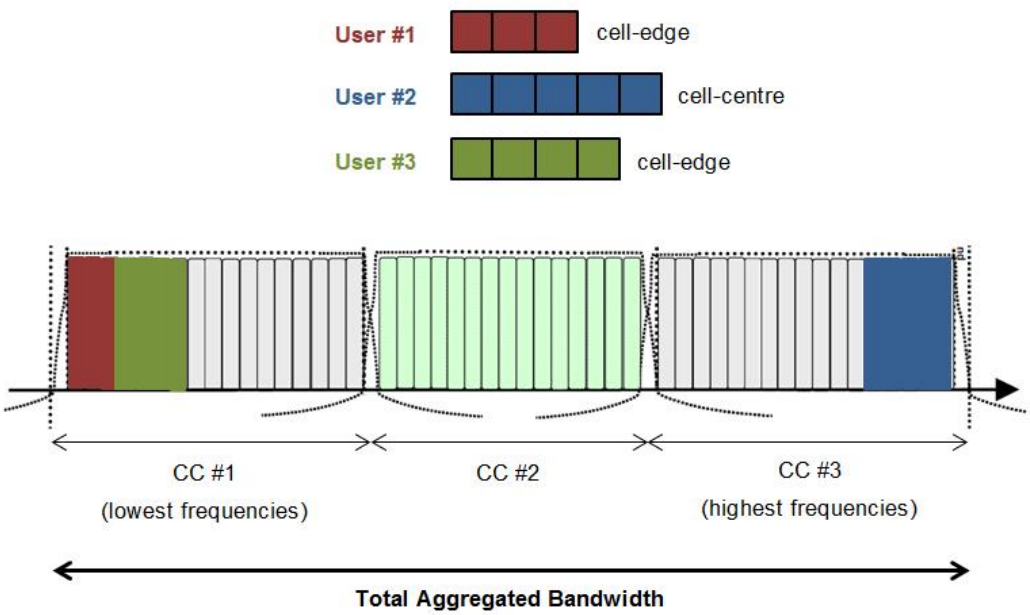

Figure 3.4 – Sequential selective RB distribution algorithm, considering users' distance to the BS.

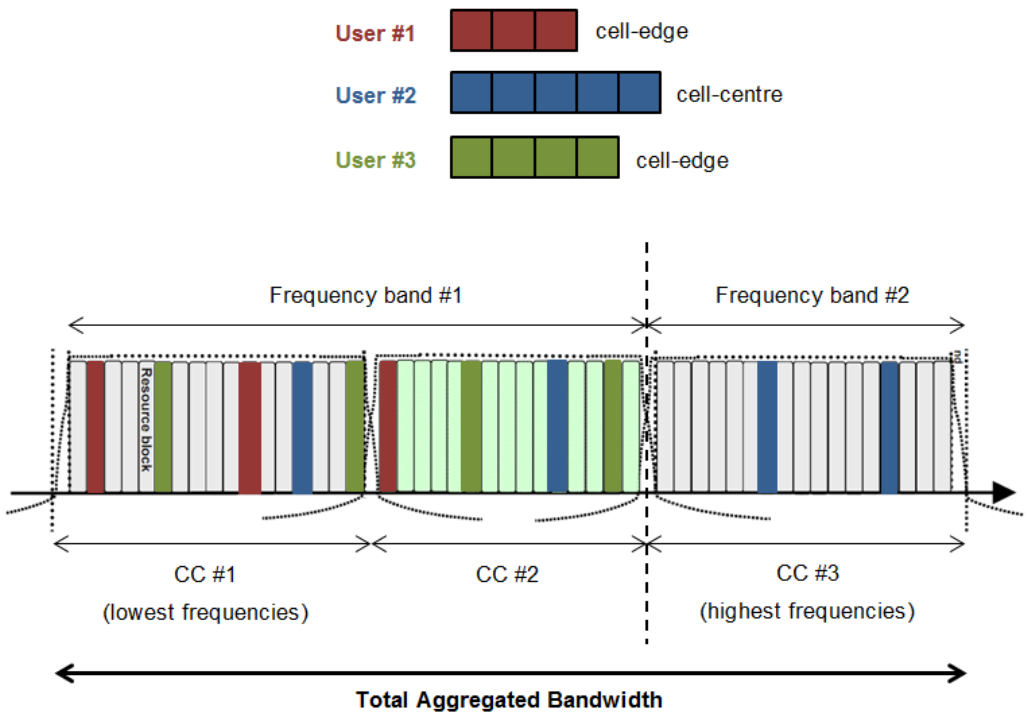

Figure 3.5 – Random selective RB distribution algorithm, considering users' distance to the BS and different reference coverage areas for each frequency band.

3.3 LTE-A Simulator

The developed LTE-A program routines are introduced in this section. First, in Subsection 3.3.1, the simulator is presented, with its implementation being described in Subsection 3.3.2 and the input and output parameters and files in Subsection 3.3.3. Finally, a global simulator evaluation is performed in the last subsection.

3.3.1 Simulator Overview

The developed simulator is composed of several parts, the result being the work from previous studies, namely [SeCa04], [Card06], [LaCo06], [Lope08], [Salv08], [Duar08], [Perg08] and [Jaci09], plus the modules developed in this thesis. Its global structure is presented in Figure 3.6, representing the main stages of the simulation: users' generation, network deployment and LTE-A DL performance analysis. The last two required major modifications, in order to implement the performance models and algorithms described in Sections 3.1 and 3.2. Also, some new statistics were added to the output data files, in order to obtain specific results related to CA, according to the described model.

The Users Generator module, or SIM program, is described in detail in [Lope08] and [Salv08], and is responsible for generating a file that contains information about the users (*e.g.*, location, user-specific scenario, service). Users are randomly distributed over a selected ROA, and services are also

randomly assigned to users, according to a given service penetration percentage. The traffic distribution and services penetration percentage, as well as the QoS priority lists, used as default for the SIM program, are described in Chapter 4.

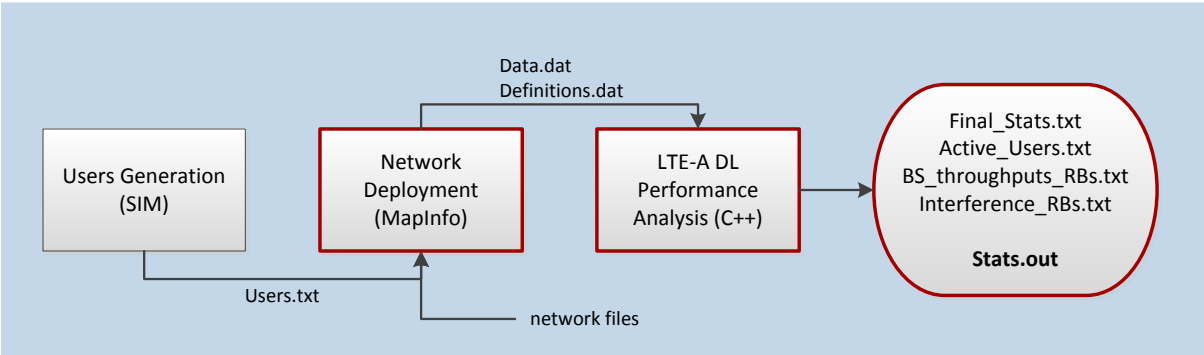

Figure 3.6 – Simulation overview and input/output files (modified modules highlighted in red).

The network deployment module is described in detail in [CoLa06]. It is responsible for the distribution of users, from the output file of the SIM program, and BSs throughout the different areas of the ROA. It also offers a visual and geographical representation of the actual simulation, supported by the MapInfo environment. After placing all users in the map, the network is deployed. Then, a preliminary analysis of the network concerning coverage is conducted, and an estimation of the cell radius for each service is obtained. Additionally, it performs inclusion (exclusion) of covered (non-covered) users, to be considered in the following performance analysis. All users within the coverage area are the ones that are passed to the LTE-A DL performance analysis module.

The LTE-A DL performance analysis module is the core of the simulator, being responsible for processing the whole snapshot activity in the network (covered users) and obtaining statistics of interest, in terms of cell capacity, QoS and interference. These statistics are then sent to the MapInfo environment, or printed over files. The whole process of obtaining the performance statistics is based on the models and algorithms described in Sections 3.1 and 3.2.

3.3.2 Implementation Analysis

The LTE DL module was developed to enable the analysis of performance of LTE-A systems supporting CA and up to 8×8 MIMO transmission. This means that both the Network Deployment, using the MapInfo environment, and the DL Performance Analysis module, developed in C++, had to be adapted to provide snapshot based calculations consistent with the previously described model.

Before going into the implementation of the LTE-A Performance Analysis module, it is essential to understand how data are processed by the Network Deployment module and the kind of operations it performs, in order to pass the required inputs to the C++ program. Users generated by the SIM module, with specific characterisation (*e.g.*, geographical position, service, environment scenario), are placed over the map of the ROA along with the network's available BSs. Then, this module performs an overall coverage analysis of the cellular network, computing the radius of the multiple cells, and estimating which are the users that are covered by the network. These are the users that will be

included in the performance analysis, done by the C++ module. The coverage analysis is only an estimate, using the cell radius corresponding to two different reference throughputs, *i.e.*, one for a dense urban environment (higher demand) and another for a regular urban environment (moderate demand), in the ROA. The two reference services define the BSs' cell coverage, according to the propagation models adopted in this thesis. Moreover, only the lowest available frequency band operating in the network is considered in this analysis, according to the selected CA configuration and corresponding PCell.

The first part of the C++ performance simulator is to read from the input files, containing the information about users and deployed network, as well as the system's parameters, *i.e.*, Data.dat and Definitions.dat files. This step is essential to collect both general and specific information about the network and enable the analysis at cellular and user levels, associating each user to the closest BS and distributing the available RBs according to the required services and corresponding throughputs. Since the simulator follows a snapshot based approach, the network is (re)created in every simulation, which means that all the information regarding previous occupied resources, as well as user and BS statistics are discarded. Henceforth, even in situations of overlapping BSs' coverage areas, users are connected to the closest one, disregarding the load of the BSs involved.

In order to estimate the reference coverage radius of the BSs, the simulator assumes that the cell range for each frequency band is equal to the corresponding reference service distance, according to the explanation provided in Section 3.1.5. These calculations are done assuming NLoS propagation, in order to provide more realistic coverage scenarios in a typical (dense) urban environment. Each user is associated to a reference frequency, depending on its distance to the serving BS and on the computed cell radii for each of the available frequency bands.

The CA module is responsible for creating the data structures that support the aggregation of carrier frequencies coming from different CCs and frequency bands, according to the selected bandwidth configuration. These structures provide a way of dealing with a single pool of carriers, ordered from the lowest carrier frequencies to the highest ones, enabling a selective distribution of RBs over the spectrum, if selected.

Estimation of the number of RBs to be allocated is done regardless of their location within the available spectrum. This means that, if CA is used, the number of available RBs refers to the sum over all aggregated CCs. If the required capacity exceeds the maximum available one (*i.e.*, sum of all RBs over all CCs assigned), the RB provisioning takes into account other factors, such as service class priorities, in order to perform RB reduction and guarantee an optimised allocation of resources.

Once the number of required RBs is determined for every user, the simulator proceeds to their distribution over the available spectrum. This is done following the rationale explained in Section 3.2, where three distribution strategies are described: "Random Distribution", "Sequential Selective Distribution" and "Random Selective Distribution". In order to simplify the implementation, the "Sequential Selective Distribution" was implemented as an extension of the random distribution, resulting from a simple sorting algorithm. This means that, when this algorithm is selected, firstly a random distribution is employed, and then the sequential reordering is done. Alternatively, the

“Random Selective Distribution” firstly distributes RBs consecutively in the CCs assigned to the corresponding users, and only after it redistributes them randomly over the spectrum, assuring that all the CC-assignment restrictions are fulfilled.

After the RB allocation to users and distribution over the spectrum, an interference analysis is performed on every active RB, according to ICI algorithm described in [Pire12]. The detected interference powers, reaching to a certain RB, are used to calculate the corresponding SINR, which in turn is mapped onto a definitive throughput value for that same RB. Some key adjustments were made, at this point, to enable an accurate computation of the SINR in carrier aggregation scenarios. In these cases, RBs may be located in non-contiguous CCs, thus requiring individual path loss calculations, using the correct frequency values.

Finally, the simulator generates relevant statistics for the performance analysis, based on the simulation results and the equations given in Section 3.1. The workflow of the simulator is presented in Figure 3.7, where the performed algorithms along the processes are identified.

The simulator offers the possibility to tune a number of radio and system parameters, as shown in Annex F. These parameters correspond to the main inputs of the link-measurement and link-performance models, setting the appropriate definitions and assumptions for the LTE-A simulation:

- Propagation model parameters (COST 231-WI);
- Services QoS priorities;
- Services minimum and maximum data rate;
- DL transmission power (BS);
- BS and MT antenna gains;
- User and cable losses;
- Noise figure;
- Interference and penetration margins;
- Operating frequency;
- Bandwidth configuration(s) and number of CCs;
- MIMO configuration;
- Urban scenario characterisation for the channel and propagation models;
- Scheduling algorithm;
- RB reduction strategy;
- FRS;
- RB distribution algorithm;
- Antennas downtilt angle;
- Percentage of LoS users;
- Throughput overhead;
- Number of PDCCH symbols.

Other parameters such as the number of users, their associated services and service penetration values are defined in the Users Generation module, completing all the necessary information and user

data for the system-level simulation.

Frequency and bandwidth, together with MIMO, are key input parameters in this analysis, affecting maximum achievable user data rates and cell capacity. The number of available RBs is directly related to the chosen bandwidth configuration, according to Table 2.1, whereas the throughput per RB depends on the MIMO configuration, modulation and coding rate. The selection of different frequency bands (*i.e.*, operating frequencies) affects coverage and capacity, through the path loss of received signals. The difference in path loss can go up to 23 dB, between the 800 MHz and 2600 MHz bands, offering a trade-off concerning capacity and interference. On the one hand, the higher path loss associated with higher frequencies reduces both cell radius and SNR (*i.e.*, received signal) for users further away from the cell-centre. This, in turn, limits the use of higher order modulation schemes and, consequently, the user data rates and cell capacity. On the other hand, higher path loss also means lower interference powers reaching the neighbouring BSs, improving performance over increased SINRs.

CA provides for the use of additional frequency and bandwidth configurations, introducing a number of different combinations to this study, as shown in Figure F.4. The simulator offers the possibility to select CCs from the same or different LTE frequency bands, allowing for simulations of intra- or inter-band scenarios. Moreover, one can select specific CCs within each of the chosen frequency bands, enabling the study of a particular intra-band non-contiguous aggregation scenario. Each configured aggregation scenario corresponds to a deployment scenario, according to the explanation in Section 2.2. By combining different LTE frequency bands and bandwidth configurations with the adequate RB distribution algorithm, one can approach the conditions of specific CA deployment scenarios. For instance, the second and third CA deployment scenarios, represented by Figure 2.6.b) and Figure 2.6.c), are mostly directed towards the performance improvement of specific sets of users connected to a BS (*i.e.*, cell edge and cell-centre users). The corresponding impact on performance can be evaluated using a selective RB distribution algorithm combined with an aggregated bandwidth configuration, to provide improved RB selection for users at different distances of the BS.

The SINR-to-throughput mapping functions, described in Annex D, allow one to obtain the throughput per RB for a reference MIMO 2×2 configuration. These reflect a mix of different transmission modes (*e.g.*, MIMO mode, modulation and coding rate), using a 2×2 antenna scheme. The equations were extracted and adapted from up-to-date simulation results, from recognised LTE manufacturers, and from Optimus' proposed link budget [Opti13]. Since higher order MIMO (*i.e.*, MIMO 4×4 and MIMO 8×8) is the main focus of this thesis, other "intermediate" antenna configuration schemes are not explicitly considered in the simulator, such as SISO and SIMO schemes. The MIMO option, available in the simulator, mostly impacts the gains that are added to the reference throughput values, obtained for each RB. These gains refer to the RMG model, described in Annex E, and provide a way to estimate the performance of higher order MIMO transmissions based on the simulation results for a reference scenario of MIMO 2×2. Although the RMG model was not developed for the same conditions as this work, it can be considered a fairly good approximation.

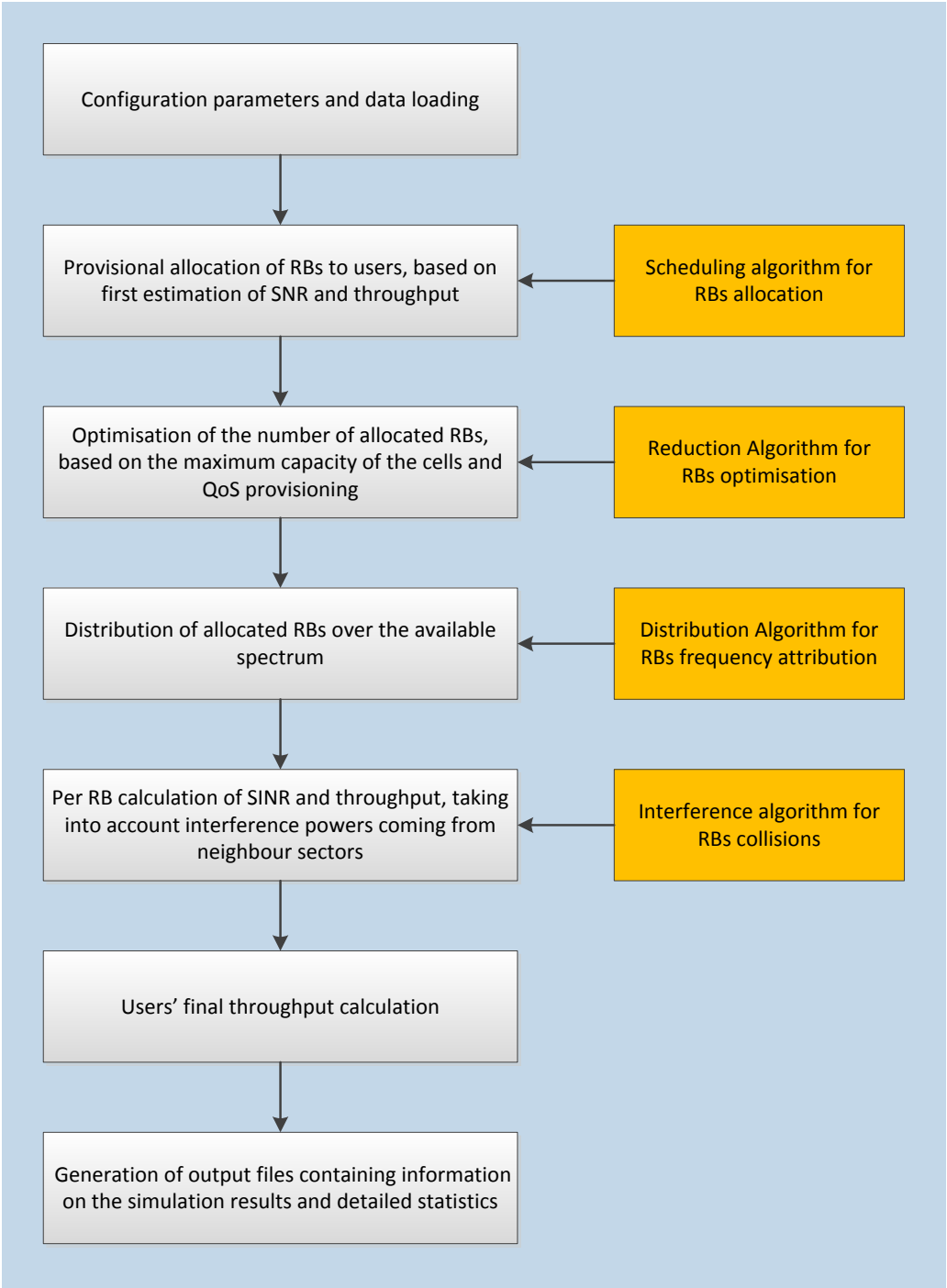

Figure 3.7 – LTE-A DL performance analysis workflow.

The reference SINR-to-throughput mapping functions retrieve the throughput for three different set-up scenarios, with a specific Modulation and Coding Scheme (MCS) and transmission mode. Then, the simulator returns the highest value obtained for the different set-ups, maximising system's performance for a given SNR/SINR value. Due to the lack of information and complexity involved, adaptive coding rate is not further explored in this thesis, which means that only one coding scheme is indexed to each modulation scheme and antenna configuration.

The slow fading margin, used in the path loss calculation, described in Annex B, is taken as a Log-Normal Distribution, which is characterised by its standard deviation and percentage. The

simulator also receives an input reference SF margin, to be used in the estimation of the maximum cell radius, for each frequency band. Additionally, the path loss computation accounts for environment-specific losses (*e.g.,* indoor/penetration margin), which are received as input to the simulator and used according to each user's specific scenario. This characterisation is based on the extended ITU channel models, described in Annex D, and go down to four different possible scenarios: pedestrian, vehicular, indoor low-loss, and indoor high-loss. In some cases, where path loss has to be computed regardless of the exact location of the RBs in frequency, the simulator considers reference SF and interference margins to make intermediate results in the simulation more consistent with reality.

Users are assigned random LoS/NLoS conditions, according to the percentage of LoS users that is specified as input in the simulator. Whenever a user is added to the data structures of the performance analysis simulator, a random number between 0 and 100 is generated. If it falls under the LoS percentage value the user is set with LoS conditions, whereas if it falls above the percentage value the user is set with NLoS conditions. The same rationale is used when computing interference, where the simulator considers a random distribution of LoS/NLoS propagation conditions for the interfering signals, based on a fixed percentage of 30% LoS signals.

PF will be used as the default RB allocation algorithm, as described in Section 3.2. While allocating RBs to users, the algorithm takes into account the target throughput within the range of the corresponding service. Throughput ranges for every service are defined in the User Profile window of the Network Deployment module (MapInfo), as shown in Figure F.5. The PF algorithm computes the number of RBs needed for every user, targeting an average throughput value between the maximum and minimum values. If the number of available RBs is not enough to deliver the corresponding average service, then the algorithm targets for the minimum service throughput.

The FSR parameter allows selecting between different ICI avoidance strategies through frequency reuse, as described in [Pire12]. Since studying ICI avoidance is not the focus of this thesis, it is considered only as an additional feature. The simulations were only done using the Reuse-1 scheme, where the whole available bandwidth is used in every sector of the BS, with equal power, and the RBs are freely assigned between users, regardless of their position in the cell (*e.g.*, cell-centre, cell-edge).

Different RB reduction strategies are also available in the simulator, in particular, overall throughput reduction and QoS-based reduction strategies. In the first, users' throughput is reduced by a fixed number of RBs, regardless of any QoS condition, whereas in the second, throughput is reduced according to QoS classes and services priorities. The implementation of these algorithms is entirely based on the work done in [Duar08] and in the developments introduced in [Pire12], to support the tri-sectorisation of BSs (*i.e.*, reduction employed in each sector) and to solve other problems, such as users' starvation for RBs, as detailed in the latter. The implementation of the CA module considers only one pool of RBs, which is indexed to the total aggregated spectrum available, as in a single-carrier system. This allows one to keep the previous structure supporting the reduction and optimisation algorithms. Given its best performance and consistency with reality, the proposed simulations were only done using the "QoS Class Reduction" strategy. For more detailed information

on the implementation of the “QoS Class Reduction” and the remaining RB reduction algorithms available in this simulator, one should refer to [Duar08] and [Pire12].

3.3.3 Input and Output Parameters

The simulator requires the following list of input files in order to run the network simulation and performance analysis modules:

- “Ant65deg.tab”, containing the BS’s antenna gain for every direction (*i.e.*, radiation pattern);
- “Kathrein Horizontal.txt” and “Kathrein Vertical.txt”, containing the horizontal and vertical radiation pattern of the antennas, respectively;
- “DADOS_Lisboa.tab”, containing information about the geography and different districts of the city of Lisbon.
- “ZONAS_Lisboa.tab”, containing the area characterisation of Lisbon, such as streets and gardens;
- “<users>.txt”, output from the SIM module (*i.e.*, users generator), containing information about the users;
- “Optimus LTE Network.tab”, containing the coordinates of the co-located BSs over the city of Lisbon.

The Network Deployment module internally generates two files that are used as input to the LTE-A DL Performance Analysis module:

- “Definitions.dat”, containing the radio parameters, CA configuration, minimum and maximum throughputs for each service, QoS service’s priorities, and other simulations settings;
- “Data.dat”, containing a list of all users and associated BS location, as well as the distance between them. For each user, additional information, such as the user scenario and requested service, is also present.

After the LTE-A DL performance analysis simulation is completed, the simulator generates multiple output files, one of which is used by the Network Deployment module to present the results in the MapInfo environment:

- “stats.out”, which includes results concerning the network performance analysis and services statistics.

In addition, other text files are generated, presenting general and specific information on the different elements of the system:

- “Final_Stats.txt”, containing general statistics about the users, RBs, CCs and used frequency bands;
- “Active_Users.txt”, containing a list of the served users, along with the respective number of used RBs, interfered RBs, distance to serving BS, average RBs SNR and SINR, average signal and interference power at the user’s MT, service performed and position in the cell (*i.e.*, cell-centre or cell-edge);

- “BS_throughputs_RBs.txt”, containing the list of the active BSs along with the number of used RBs, interfered RBs, served users and radius.

The information contained in these output files was obtained directly from the data kept in the inner data structures of the simulation, such as users’ distance, average throughput and SNR/SINR. Other statistic calculations, such as Probability Density Functions (PDFs), Cumulative Density Functions (CDFs) and standard deviation values, were done afterwards using Microsoft Excel.

3.4 Simulator Assessment and Model Evaluation

This section covers the assessment of the simulator in order to validate the simulation results and generated output. It is also important to reach an estimation of the minimum number of simulations necessary to ensure statistical relevance of the obtained results. In order to be able to characterise the simulation results, statistical parameters, such as average and standard deviation [Mora10], were computed for the output data generated by the simulator. These statistics allow one to analyse and to understand the variation and meaning of the vast amount of results produced in each simulation. The average and standard deviation values were computed using (3.15) and (3.16), respectively.

$$\mu_X = \frac{\sum_{i=1}^{N_X} X_i}{N_X} \tag{3.15}$$

where:

- N_X: number of samples of variable X;
- X_i: value of sample i of variable X.

$$\sigma_X = \sqrt{\frac{1}{N_X}\sum_{i=1}^{N_X}(X_i - \bar{X})^2} \tag{3.16}$$

where:

- $\bar{X}$: mean value of variable X (μ_X).

The first step in this assessment was to estimate a reasonable number of simulations necessary to ensure statistical relevance of the analysis. Since users’ geographical location and radio channel conditions are randomly distributed between simulations, several of them must be taken to assure result validation. As the simulator is intended for scenarios with thousands of users located in an urban network with hundreds of BSs, one can expect that the minimum number required to ensure statistical relevance will not be as high as in single user simulations. This analysis is done looking at the evolution of the average and standard deviation for some results and how it varies through different sets of simulations. Figure 3.8 shows the standard deviation over average ratio, also known as the

Coefficient of Variation (CV), for some relevant parameters, going from sets of 5 to 30 simulations. The considered parameters are the number of active users in the network, average user throughput, average BS throughput, which are the main performance/capacity indicators in this thesis, as well as the average number of used RBs per user and average active user distance to the serving BS.

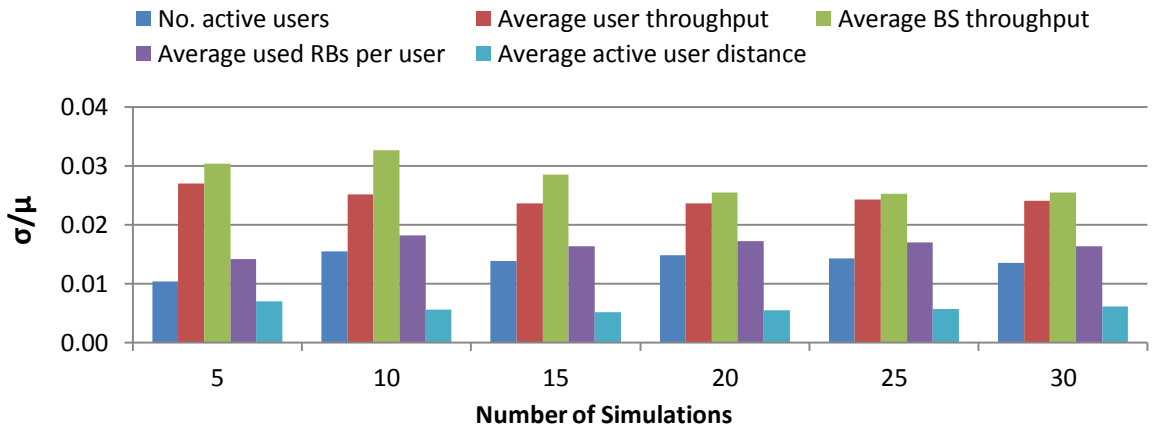

Figure 3.8 – Standard deviation over average ratios, going from 5 to 30 simulations.

The assessment was done using a reference scenario, described in Chapter 4. The total number of users per simulation approaches 2 000, this number being the result from the coverage estimation performed in the Network Deployment module, described earlier in this section. Figure 3.9 shows the evolution of the average and standard deviation over different sets of simulations, for four of the previously mentioned parameters.

Figure 3.8 and Figure 3.9 show that results have considerably low variations around the mean values, in the different sets of simulations. Also, it is shown that average and standard deviation values have almost no variation along the sets of simulations. One can further notice in Figure 3.8 that all values of CV fall below 0.05, and are consistent among the different sets of simulations, meaning that an increase in the number of simulations does not have a relevant impact on the results variability. Henceforth, 5 simulations can be taken as a reasonable number in order to obtain statistically relevant results in the simulator. This is an important assumption due to the fact that each single simulation can take 45 to 60 minutes, depending on the growing number of users and BSs in the network, as well as its load, thus consuming a substantial amount of time.

Several tests and appropriate debugging were performed regularly throughout the development of the simulator, as well as a set of critical tests that were made at the end, in order to validate its implementation. Moreover, these tests allowed one to understand if the simulator was performing a good approximation of the RRM processes, distributing the limited number of radio resources among users, as in a real network. Figure 3.10 shows that the number of active (served) users increases with the number of covered users, until the system reaches the saturation of radio resources, *i.e.*, and saturation of the number of served users. From that point on, an increase in the total number of users no longer means an increase in the number of active users. One can observe from Figure 3.10 that saturation starts shaping right after reaching 8 000 covered users, which means that this can be taken as a reference point to simulate median high-load conditions.

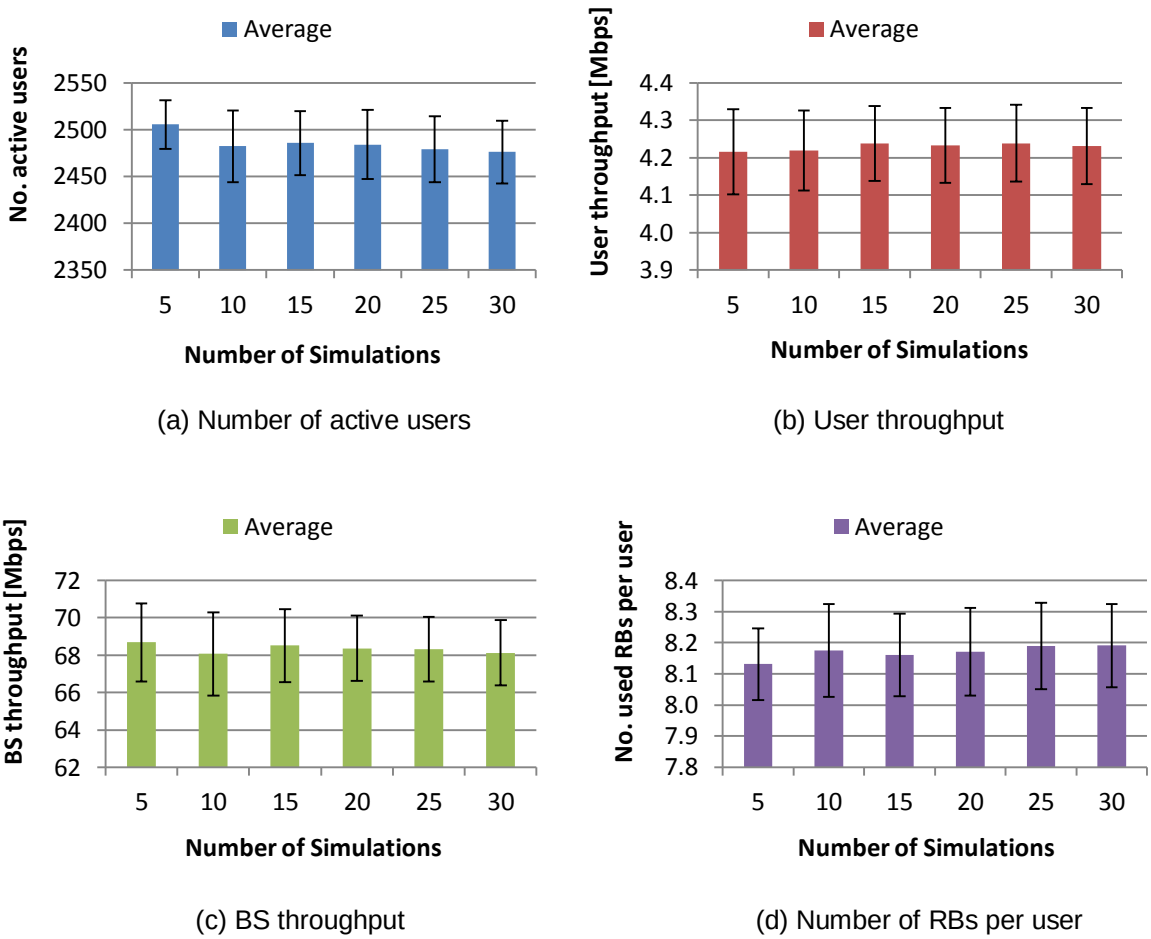

Figure 3.9 – Evolution of average and standard deviation for different parameters, going from 5 to 30 simulations.

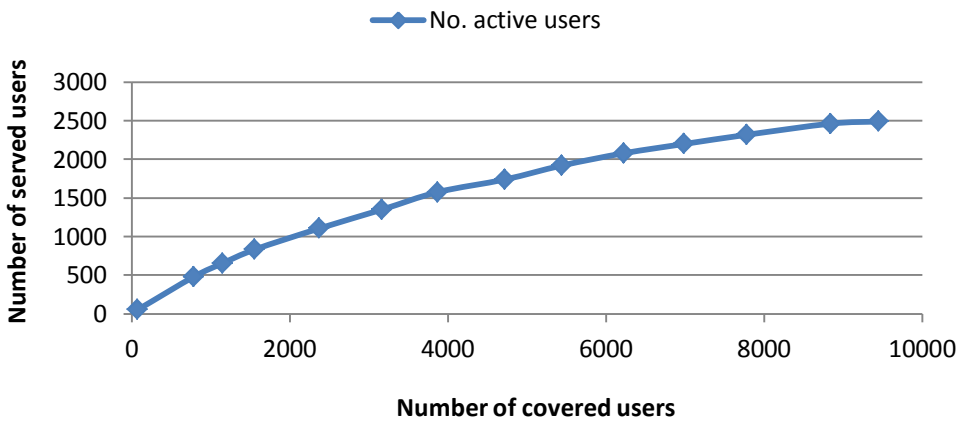

Figure 3.10 – Number of served users versus the total number of users covered by the network.

Figure 3.11 shows how interference varies along different frequency bands, being represented by the percentage of interfered/interfered-to-zero RBs in relation to the total number of available RBs, as described earlier in this chapter. It confirms the expected decrease in interference when using higher frequencies, due to the higher path losses. This analysis was performed for the reference scenario, and simulating for nearly 2 000 users in the network.

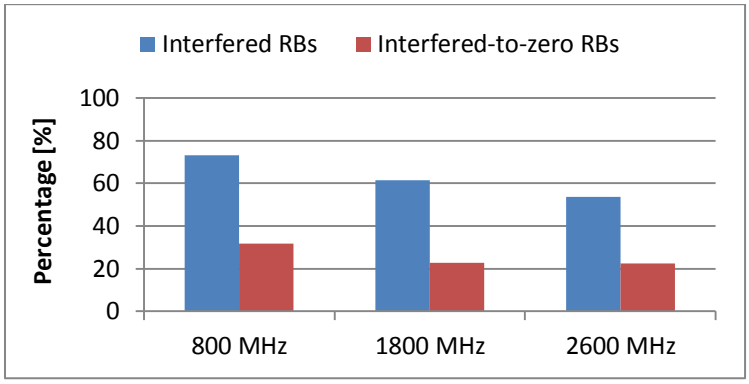

Figure 3.11 – Percentage of interference for different frequency bands.

Another way of validating the simulator was to test it for the limit scenario of a single user, asking for a highly demanding service. These results are taken from a user who is alone in the cell and closely located to the corresponding BS (LoS). In this particular scenario, it is possible to extract information about the maximum achievable user throughput and see if the maximum number of RBs is being used, free from the impact of the multi-user distribution of radio resources. These results can be cross-checked with theoretical values of achievable throughputs, in order to validate the simulator. Table 3.1 presents the results of the single-user assessment simulation, considering three different bandwidth scenarios (including CA feature), all using the 1800 MHz band.

Table 3.1 – Single-user assessment simulation.

	Available bandwidth		
	20 MHz	**40 MHz**	**100 MHz**
Distance to BS [m]	3	3	3
Number of used RBs	100	200	500
Maximum data rate [Mbit/s]	201.6	403.2	1008
Expected throughput[1] [Mbit/s]	151.2	302.4	756
Served throughput [Mbit/s]	**142.4**	**284.7**	**710.9**

[1] considering overhead.

In these simulations the user is only 3 m away from the BS, with LoS conditions, and for each bandwidth scenario it requests the corresponding maximum data rate at the physical layer, according to Table 3.1. All three simulations result in full usage of the available bandwidth and in served throughputs close to the expected throughput values, which consider an average loss ratio of 25%, at the physical layer, as defined in Section 3.1.3. Served throughputs correspond to a fraction of, approximately, 70% of the theoretical maximum data rates, which can be explained by the additional randomness of the simulated radio channel, also impacting on average user performance gains.

Chapter 4

Results Analysis

This chapter contains the description of the low-load and high-load scenarios tested in simulations, and corresponding results analysis. Firstly, a brief description of the default parameters and considered environment is given. Secondly, low-load results are presented, including both field measurements and simulated results, as well as a comparison between the two. High-load simulations are then presented and compared with the previously defined reference scenario, changing relevant input parameters one-by-one, such as CA configuration, aggregated bandwidth, MIMO scheme and RB distribution algorithm.

4.1 Scenarios Description

Starting with the definition of a reference scenario, this thesis works around a number of different variations and particular cases, derived from the former, in order to obtain results on the performance of a fully operational LTE-A network. In addition to the multi-user simulations performed, this thesis also includes the analysis of single-user test results, measured in a real deployed LTE-A network. Most of the simulation parameters were chosen based on information provided by the operator, given the settings of its own deployed network.

The default scenario is defined for the city of Lisbon, an urban environment with heterogeneous distribution of users and services. It can be characterised by a centre region, with a higher density of users and BSs (higher average service demand), and an outer region, with lower user and BS densities.

Figure 4.1 shows a map of Lisbon, illustrating different elements of the city's topology. The centre zone is highlighted in blue, corresponding to the downtown of Lisbon, whereas the outer region is depicted in yellow. Annex F presents the different steps in the configuration of the simulator, showing, in Figure F.6, the distribution of users over the city. As one can observe, users' density is more accentuated in the blue zone, *i.e.*, downtown Lisbon, and in the outer region just above the north-centre. Figure F.7 shows the distribution of BSs and respective coverage areas over Lisbon, according to the information provided by Optimus on the location of the BSs and corresponding coverage estimation performed by the simulator. The network comprises *[Confidential Information]* BSs, which are assumed to be capable of operating in the considered three frequency bands, *i.e.*, 800 MHz, 1800 MHz and 2600 MHz. In general, the location and density of the BSs follows the same pattern as the user distribution, in order to provide consistent coverage with the number and type of users (capacity and QoS demands), within the different areas of the city.

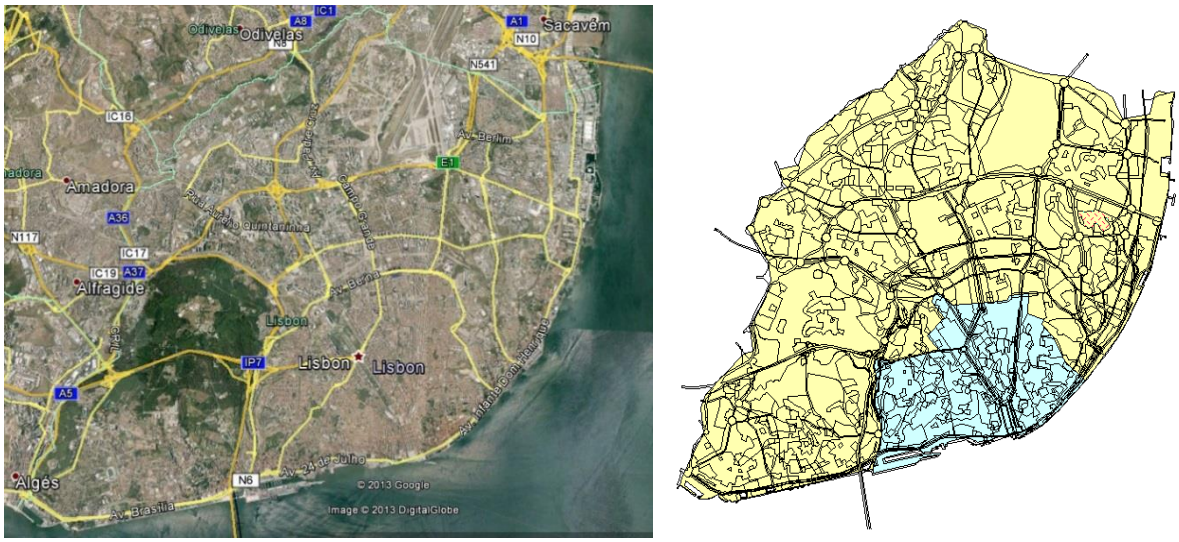

Figure 4.1 – Satellite view of Lisbon and topographic information.

This thesis considers four different types of user environment: outdoor pedestrian, inside vehicle and indoor with low or high losses. Each of them represents an additional path loss that will be assigned to users, in order to characterise transmission in the corresponding scenarios. The pedestrian scenario is considered for users at street level with low attenuation margins (approximately 0 dB); the vehicular scenario is applicable to users moving at high-speeds, *e.g.*, when driving a car; indoor scenarios are considered for users performing services inside a building. The two types of indoor scenarios, *i.e.*, high or low losses, stand for users in more or less "deep" indoor locations, with accordingly higher or lower penetration margins. The percentages of users associated with each environment, when considering multi-user simulations, are presented in Table 4.1. They take into account that indoor environments represent the largest share of overall users, corresponding to the most suitable situation to perform data services in smartphones, tablets or laptops (more than half).

Table 4.2 shows the values for the parameters used in the computation of path loss. These are according to the adopted propagation model, *i.e.*, the COST 231-Walfisch-Ikegami model, which is described in Annex C. The values adopted for average buildings and streets dimensions are consistent with the type of dense urban environment existing in Lisbon.

Table 4.1 – Additional user scenario loss and respective penetration.

User environment	Additional loss [dB]	Scenarios penetration [%]
Pedestrian outdoor	0	30
Vehicular	11	15
Low loss indoor	11	20
High loss indoor	21	35

Table 4.2 – COST 231-Walfisch-Ikegami Model parameters.

Parameter	Default values
BS height (h_b) [m]	26
Buildings height (h_{Roof}) [m]	24
Streets width (w) [m]	24
Buildings separation (b) [m]	48
Street orientation angle (φ) [º]	90
MT height (h_m) [m]	1.80

Table 4.3 presents the default values for the DL reference scenario parameters, regarding radio interface and adopted algorithms. BS's transmission power is set to 46 dBm, according to the information provided by the operator on the maximum reference power in each MIMO branch (dedicated feeding power). The reference bandwidth configuration corresponds to a single component carrier of 20 MHz, in the 1800 MHz band, corresponding to Optimus' preferable network configuration. A fixed downtilt angle of 6° was chosen as default, assuming that it maximises the whole network's

performance and capacity. Typical values for MT antenna gain, user and cable losses, as well as noise figure were also used [Pire12]. The antennas used in the simulator correspond to the Kathrein 80010675 model, whose horizontal and vertical radiation patterns can be consulted in [Kath13].

The reference scenario takes MIMO 2×2 case as default. This is mainly due to the fact that the throughput equations in Annex D are optimised for the results of this particular MIMO scheme, which makes it a more reliable reference scenario to be adopted. Also, since MIMO 2×2 is the lowest order scheme considered in this thesis, it can work as a good starting point for the analysis of other higher order configurations.

Both reference services 1 and 2, used for coverage estimation in the Network Deployment module, are set to average throughput values that characterise the user demand in the centre and outer ROA, respectively. The first, being related to the downtown area of the city, is greater than the second, due to the fact that users in this area are more concentrated and perform more demanding services.

Regarding RRM algorithms, the reference scenario uses a combination of the PF for resource allocation (scheduling), the Reuse-1 for the distribution of bandwidth among sectors, the QoS Class Reduction algorithm for the optimisation of RBs among users, and the Random Distribution algorithm, responsible for assigning carrier frequencies to the allocated RBs. The first three will remain unchanged throughout the multiple simulations and studied scenarios along this work. Table 4.4 presents values for the QoS priorities, minimum and maximum (target) throughputs, as well as penetration percentages, of the different data services being performed by users in the reference scenario. This table was adapted from the services characterisation provided in [Pire12], keeping most of its values, with the exception of the maximum throughputs for Web, FTP, Email and P2P services. These were changed to the maximum throughput that can be obtained with a Category 5 UE, *i.e.*, 300 Mbit/s (see Table A.1), taking it as the default device category for all users in the network. A combination of different priorities with minimum and target values for throughput was chosen in an effort to establish fairness in the distribution of resources among users, and considering increased throughput targets for some specific services, with unlimited demand. One can also note that voice services are not included here, since this thesis focuses on LTE-A, only supporting data services.

Taking the previously described reference scenario, multiple simulations were performed considering different loads on the network (total number of users). Starting with low load simulations, with few users in the network, one can evaluate the system's performance in scenarios where such is not limited by the lack of resources. In these cases, it is possible for some users to achieve the maximum peak data rates using the different transmission schemes available, according to Table 2.2. The present situation of LTE networks in Lisbon can be best described by low load scenarios, due to its recent launch. When moving to simulations with increased number of users, the load becomes a limiting factor in the network, resulting in more interference and in generalised scarcity of resources. Thereby, in high loaded scenarios it becomes more interesting to evaluate the impacts of increasing the available bandwidth (*i.e.*, resource blocks), or using alternative CA configurations and RRM algorithms. Multiple variations of the described reference scenario are then used to study the impact of different variables and elements in the system, with low or high load on the network.

Table 4.3 – Radio interface parameters and algorithms used in the reference scenario.

Parameter	Default values (DL)
Central frequency [MHz]	1840
Bandwidth Configuration [MHz]	20 MHz (single carrier)
MIMO Configuration	2×2
Modulation	QPSK/16-QAM/64-QAM
BS Transmission Power [dBm]	46
Maximum BS Antennas Gain [dBi]	18
Antennas Feeding Power	Dedicated
MT Antenna Gain [dBi]	0
Downtilt Angle [º]	6
User Losses [dB]	1
Cable Losses [dB]	3
Noise Figure [dB]	7
LoS Percentage [%]	40%
Scheduling Algorithm	PF
Frequency Reuse Scheme	Reuse-1
Reduction Algorithm	QoS Class Reduction
RB Distribution Algorithm	Random Distribution
Reference Service 1 [Mbps]	12
Reference Service 2 [Mbps]	7

Table 4.4 – Default data services characterisation.

Service	QoS Priority	Throughput [Mbps]		Penetration [%]
		Minimum	Maximum	
Streaming	1	1.024	6	36.0
Chat	2	0.064	0.384	5.5
Web	3	1.024	300	25.0
FTP	4	1.024	300	9.5
Email	5	1.024	300	6.0
P2P	6	1.024	300	18.0

The analysis of the different scenarios is done by selecting the statistics that are more relevant to each case. Each presented statistic comes with a standard deviation that is related to the average network performance, *e.g.*, the average throughput of all users being served in the network, or just to the average of the simulations that were considered. The latter is related to the results obtained during the

simulator's assessment, being proof of consistency among multiple runs of the same scenario.

4.2 Low-Load Results Analysis

This section covers an analysis on peak performance and capacity of the network, by testing it under low-load conditions. It includes results from both the simulator, running with just a few users, and from single-user DL field measurements collected through a number of drive tests, which were performed in cooperation with Optimus.

The analysis focuses mainly on achieving the theoretical performance values, discussed in previous sections. Firstly, results from the field measurements are presented as a reference for the subsequent low-load simulations. Then, the same network configurations are recreated in the simulator, with less than 100 users spread over the whole city, in order to provide simulated results. Besides, from the previous scenarios, additional simulations were made, using higher order MIMO configurations, in order to complete information on the performance achievements of these options.

The results are mainly represented by the distributions of throughput versus signal power and SINR levels. Also, some benchmarking between scenarios is included through the comparison of average, top- and worst-performing throughput metrics, and number of users.

4.2.1 Field Measurements

As stated earlier, single-user DL measurements were collected by drive tests, performed in one of Optimus' trial sites, in Póvoa de Santo Adrião, Odivelas. These were done using a pre-commercial category 5 UE, connected to 4 outdoor antennas and 2 laptops, used for data generation and results acquisition and storage, respectively. The latter was done using a recent version of the probe software GENEX, released by the LTE RAN vendor Huawei. Setup characterisation is presented in Table 4.5.

Most of the equipment was placed inside a car, used to move around the area of the cell site, except for the four antennas, which were placed outside on the rooftop of the vehicle. This allowed to get rid of the attenuation caused by the vehicle's structure and windows, providing clearer radio channel conditions. In addition, efforts were made to move the car as slow as possible, in order to mitigate higher variations of the radio channel conditions, imposed by the Doppler frequency shifts.

Despite the use of 4 antennas in the UE, this setup only works as the aggregation of two separate MIMO 2×2 transmission schemes, dedicated to each of two frequency bands. The setup follows an approach similar to the one described by Figure 3.1, but in this case data aggregation, along with throughput aggregation, are done at the Radio Link Control (RLC) level. Below this point, transmission is dealt separately through both CCs, using dedicated MIMO 2×2. The maximum expected throughput in a 10 MHz component carrier, using MIMO 2×2 transmission, is given by the theoretical peak data rate, presented in Table 2.2, and an overhead reduction factor of, approximately, 25%, giving a maximum 75.6 Mbit/s per CC. Combining the data streams coming from two CCs, it is possible to

achieve an aggregated throughput of, approximately, 150 Mbit/s.

Table 4.5 – Field measurements setup characterisation.

Parameter	Values	
Central Frequency [MHz]	1840	2660
Bandwidth Configuration [MHz]	10	10
Transmission Mode	TM1, TM2, TM3, TM4	
MIMO Configuration	SISO and 1×2 (Rank-1) 2×2 (Rank-2)	
Modulation	QPSK/16-QAM/64-QAM	
BS Transmission Power [dBm]	46	

During the drive tests, data were acquired and stored using Huawei's probe software, which also allows measuring and monitoring the radio channel conditions, and showing information in real time. A second computer was used to generate a continuous 150 Mbit/s UDP stream in DL, using a server from Optimus' back office. A huge amount of parameters was collected, although only the most relevant ones were selected to be analysed in this section, such as throughput and radio channel condition parameters. Also, the data points, which normally refer to different positions and radio channel conditions, were processed in order to keep only the ones that are relevant for comparison with simulated results.

The field results include measurements in three different setup scenarios: one using CA and the other two using each of the CCs, separately. Hence, data collection had to be done in three phases, one for each setup, repeating the same drive route for the sake of consistency among results:

- Scenario 1: 10 MHz in the 1800 MHz band;
- Scenario 2: 10 MHz in the 2600 MHz band.
- Scenario 3: 20 MHz aggregated in the 1800 MHz and 2600 MHz bands.

Results for the DL RLC throughput using each of the two frequency bands alone, in two different setups, are represented in Figure 4.2 and Figure 4.3. The former plots throughput values in terms of the corresponding RSRP, whereas the latter plots throughput in terms of SINR.

The results in Figure 4.2 show that the two ranges of RSRP values, from both scenarios, are slightly shifted from one another. When using the 2600 MHz band, the range of values is [-128, -64] dBm, whereas in the case of the 1800 MHz one, they range in [-121, -57] dBm. This evidences a shift of 7 dB, which is explained by the difference in coverage between the two frequencies. By covering the same area in two repetitions of the drive tests, it is expected that the 2600 MHz band measurements show lower levels of received power, than the ones performed using the 1800 MHz band. Moreover, results show that it is possible to achieve nearly 70 Mbit/s in each of the two 10 MHz carriers.

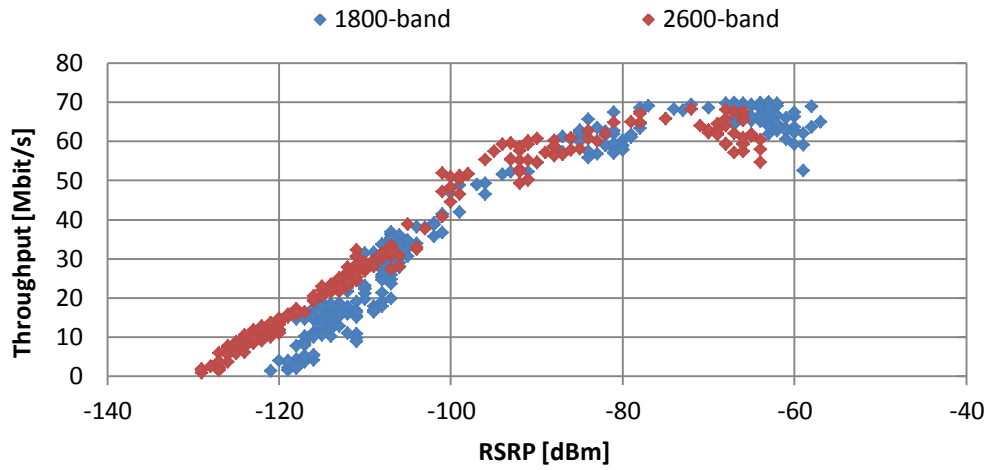

Figure 4.2 – DL RLC throughput versus RSRP, in scenarios 1 and 2.

SINR introduces a compensation of the levels of interference in each frequency, increasing the correlation between points of the two distributions, according to Figure 4.3. Furthermore, these distributions translate the effect of the link adaptation algorithm, performed by the LTE scheduler, which reflects on the slightly changed curve of evolution of the throughput with the radio channel conditions, and increased correlation between both metrics, *i.e.*, throughput and SINR level.

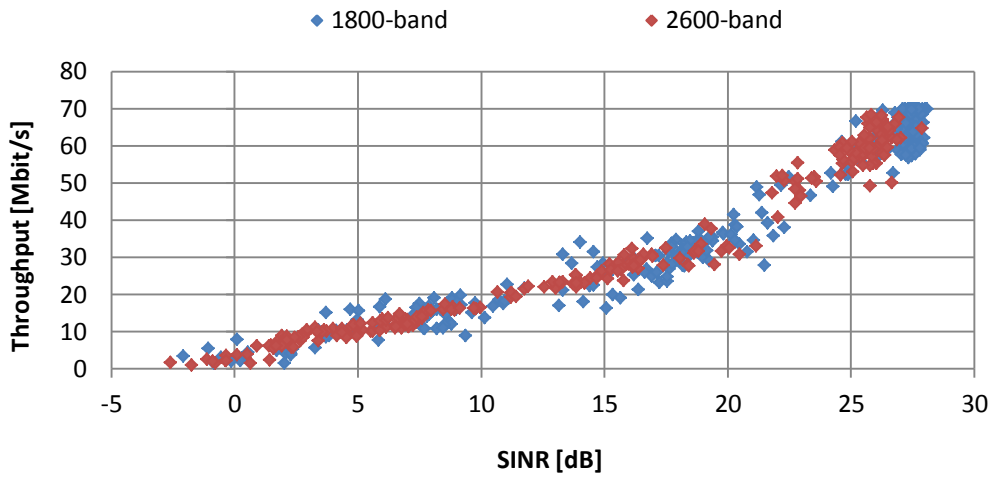

Figure 4.3 – DL RLC throughput versus SINR, in scenarios 1 and 2.

Figure 4.4 and Figure 4.5 present the variation of the DL RLC throughput in terms of the RSRP and SINR level, respectively. The values of throughput go up to 140 Mbit/s, which corresponds to the arithmetic sum of the previous separate throughputs, per 10 MHz of band. The maximum aggregated throughput obtained corresponds to 69% of the maximum peak data rate (without considering overhead), meaning that the RLC throughput suffers a total loss of 31%, due to control and signalling overheads. This is in line with the expected values of throughput loss, described in Section 3.1.3. Measured RSRPs vary in [-124, -58] dBm, whereas SINR varies in [-3, 29] dB. Both parameters fall into the expected ranges.

The results in Figure 4.4 show a well-defined, almost linear, variation of the throughput with lower values of received signal power. Then, at higher received powers, the throughput tends to a limit

value, which is around 140 Mbit/s. The larger amplitude observed in this region can be associated with an increased sensitivity with respect to the speed of the car and resulting Doppler shift.

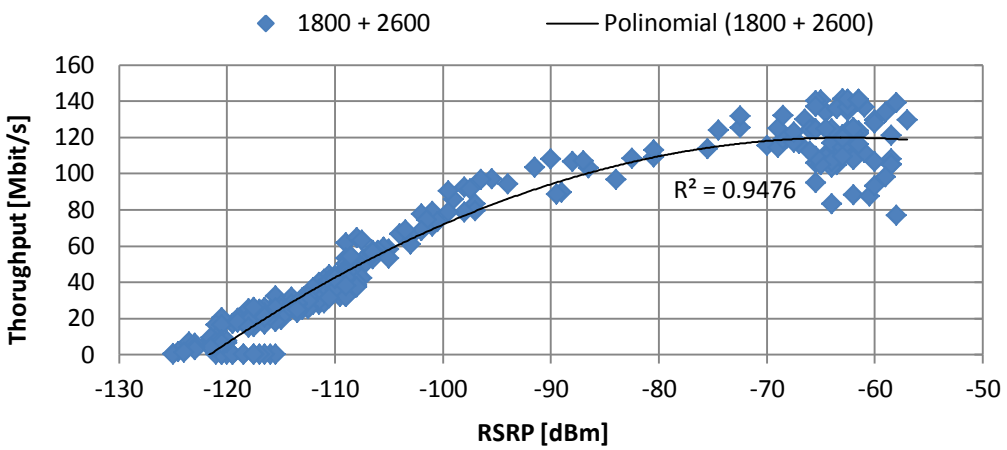

Figure 4.4 – DL RLC throughput versus RSRP, in “1800+2600” aggregation scenario.

The variation of throughput with SINR corresponds to a well-shaped exponential curve, limited at 30 dB. This curve translates the same effect of link adaptation, as observed in each separate band transmission, resulting in a higher correlation between the values of throughput and corresponding SINR level. One can observe that only at excellent radio channel conditions (above 25 dB) it is possible to achieve throughput values over 100 Mbit/s.

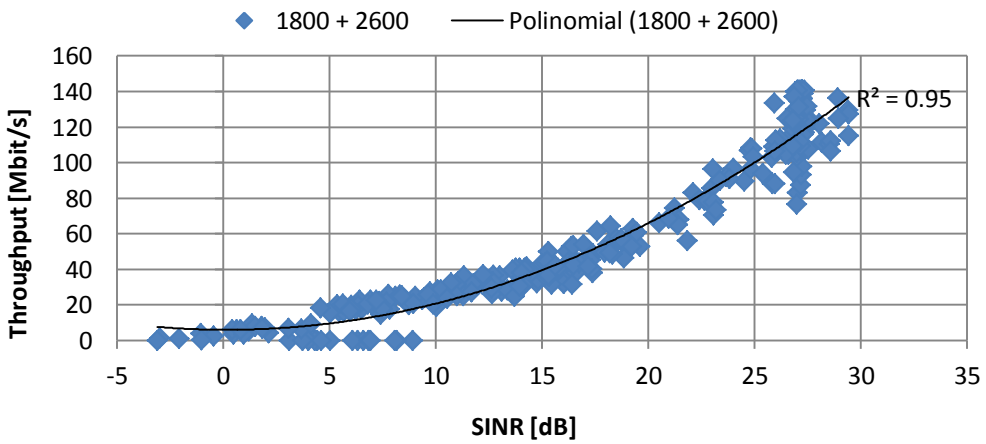

Figure 4.5 – DL RLC throughput versus SINR, in “1800+2600” aggregation scenario.

Figure 4.6 plots the contribution of each CC to the total aggregated DL throughput, versus the RSRP values of the PCell. These contributions correspond to the obtained ratios between each CC MAC layer throughput and the total aggregated RLC throughput. It is evidenced that, as coverage deteriorates (*i.e.,* lower received powers), the contribution from PCell to the aggregated throughput increases, reaching 80%. At higher RSRP values, the contributions from both CCs concentrate around 50%, meaning that cell capacity becomes less influenced by the existing frequency diversity. The PCell is responsible for assuring transmission at cell-edge conditions, while SCells allow one to improve capacity in the cell-centre.

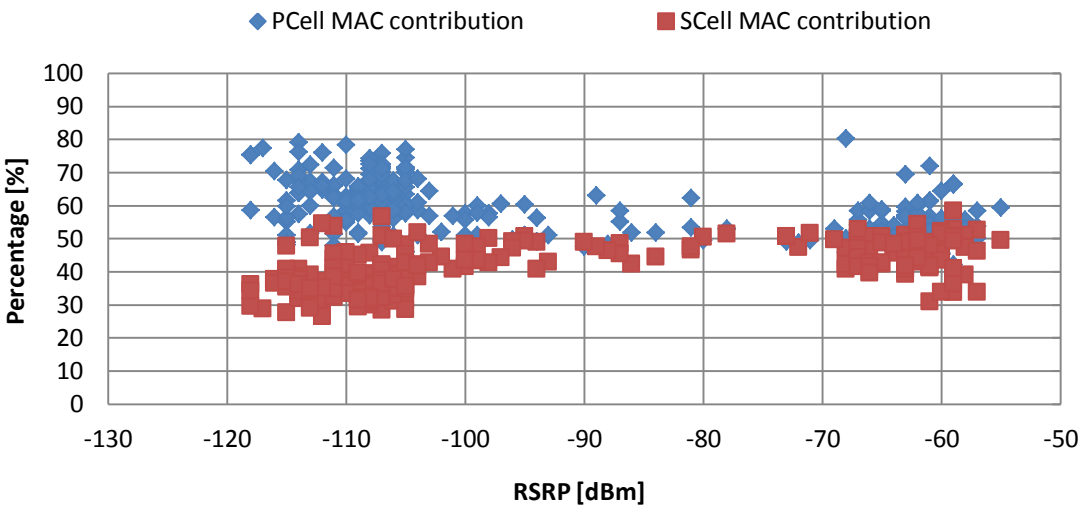

Figure 4.6 – PCell and SCell MAC layer contributions for the DL RLC aggregated throughput.

4.2.2 Carrier Aggregation Simulations

In order to obtain results for the same low-load scenarios described in the previous subsection, several simulations were performed assuming only 80 users in the whole city. All users were assumed to request the same type of service, FTP, with the maximum allowed throughput for a Category 5 device and same priority level. This was done in order to achieve maximum use of the available resources, in the cells where users were present. The results were grouped into sets of 5 simulation runs, in order to achieve statistical relevance, according to the assumptions in Section 3.4.

It is important to highlight that the following results refer to snapshot simulations of an entire network, with multiple users in it, which is clearly different from the performed field measurements, consisting of different data points collected in a single cell site. Regardless of the dissimilarities between both testing methodologies, the small number of users simulated in the second, and consequently low overall interference, allows taking it as a satisfactory single-user/single-cell test approximation.

Figure 4.7 and Figure 4.8 plot results from the simulated CA scenario, using the 1800 MHz and 2600 MHz bands, in low-load conditions (80 users). These figures also include the data points obtained from field measurements, allowing the comparison of both results, plus the average user throughput in the simulated network.

Simulation results match satisfactorily with the data obtained from the field measurements, especially when plotting the throughput versus received power, in Figure 4.7. The differences between the two ranges of received powers are justified by the small amount of points that the simulations provide, given the reduced number of users. This can be overcome by simulating the network with a greater amount of users, though it would introduce a lot of interference, which invalidates the comparison with the single-user field measurements.

These results show that under low-load conditions, the network can provide users with the maximum expected data rates for an aggregated bandwidth of 20 MHz, which were also obtained during the field

measurements. One out of two scenarios can happen to a user under excellent radio channel conditions: either being allocated with the maximum number of RBs available in the sector, which allows to reach maximum throughput, or being allocated with a smaller number of RBs, due to conflicts with other users, in the same sector. Both figures show the existence of these two types of users, even in a scenario with only 80 users. Increasing the number of users in the network would also increment the number of capacity conflicts between them, which would drastically lower the average user throughput in the network.

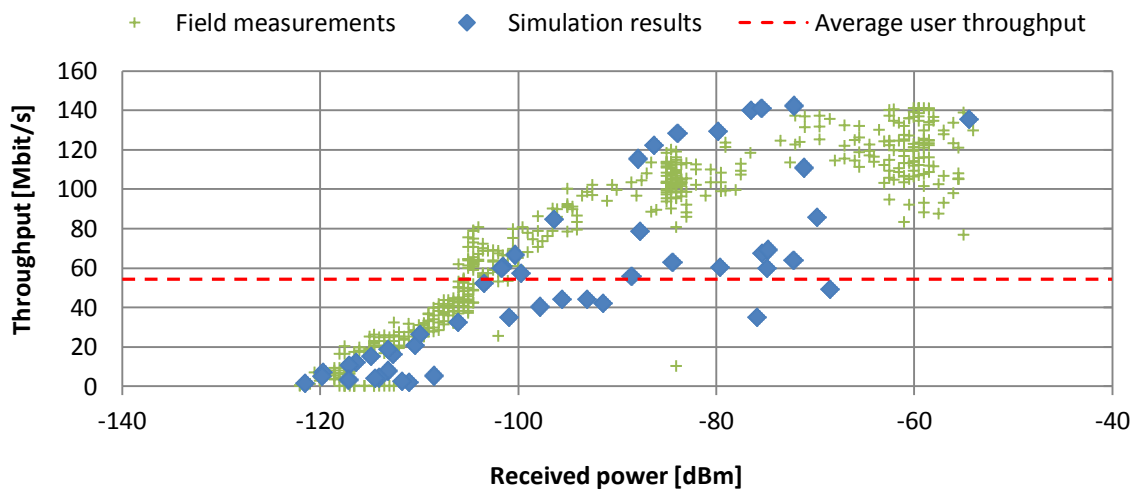

Figure 4.7 – DL throughput versus received power. Comparison between simulation results and field measurements data.

The dissimilarities found between curves of the simulated results and field measurements in Figure 4.8 can be explained by the differences that exist in the scheduling algorithms of both test environments. The way throughput is obtained in the simulator does not follow the exact same procedure as in a real LTE scheduler, as described in Chapter 3. Also, it is clear from the field measurements, that the LTE scheduler truncates points with SINR levels below -5 dB and above 30 dB. This restriction is not followed by the simulator.

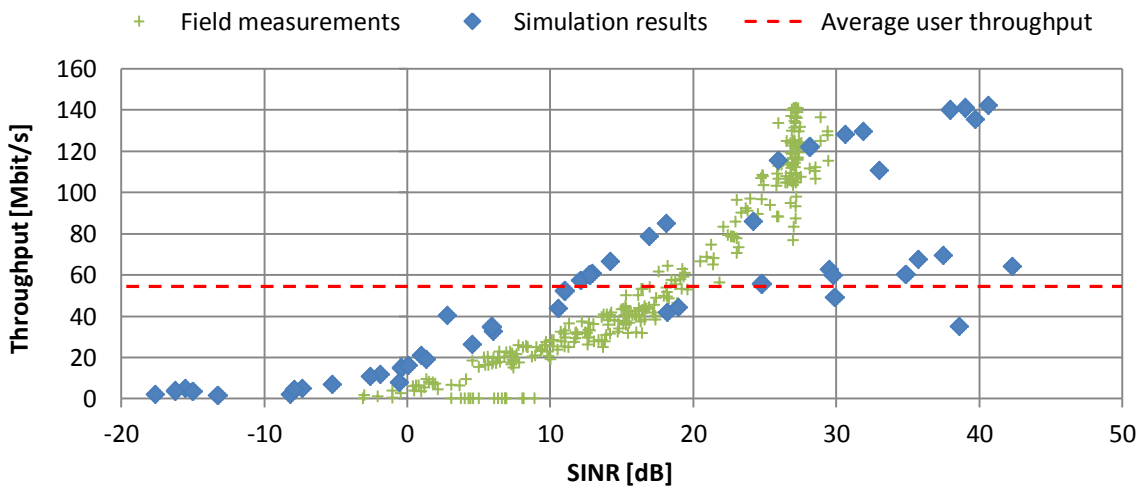

Figure 4.8 – DL throughput versus SINR. Comparison between simulation results and field measurements data.

According to the simulated results, users can only achieve the maximum throughputs under extremely good conditions, *i.e.*, over 35 dB of SINR. Comparing with the field measurements, it is possible to assume that the simulator provides a slightly pessimistic perspective of user peak performances.

4.2.3 MIMO Simulations

This section analyses the impact of using different MIMO configurations, under low-load conditions, presenting the results for 4×4 and 8×8 MIMO schemes and comparing them with the reference scenario, defined in Section 4.1. The purpose of these simulations is to estimate the peak performance gains that can be obtained by using higher order antenna configurations. Moreover, it is also interesting to assess how these gains are distributed over the different capacity aspects of the system, depending on the simulator's algorithm behaviour.

Performance gains associated to the use of MIMO 4×4 and 8×8 configurations can be extrapolated from the comparison between peak data rates, presented in Table 2.2. These indicate doubled and quadrupled gains in performance, respectively, compared to the reference 2×2 case. In practice, results show that the gains of using higher order MIMO configurations do not match theoretical expectations due to multiple factors, most of which are derived from the adopted Data Rate and RMG models, described in Annex D and Annex E, respectively.

Low-load simulation results, performed over the same distribution of users, show that MIMO 4×4 achieves user performances of 187 Mbit/s, whereas MIMO 8×8 can achieve 300 Mbit/s, according to Figure 4.9. These results represent peak performance gains of 34% and 115%, respectively, compared to the maximum throughput achieved in the reference scenario (*i.e.*, MIMO 2×2).

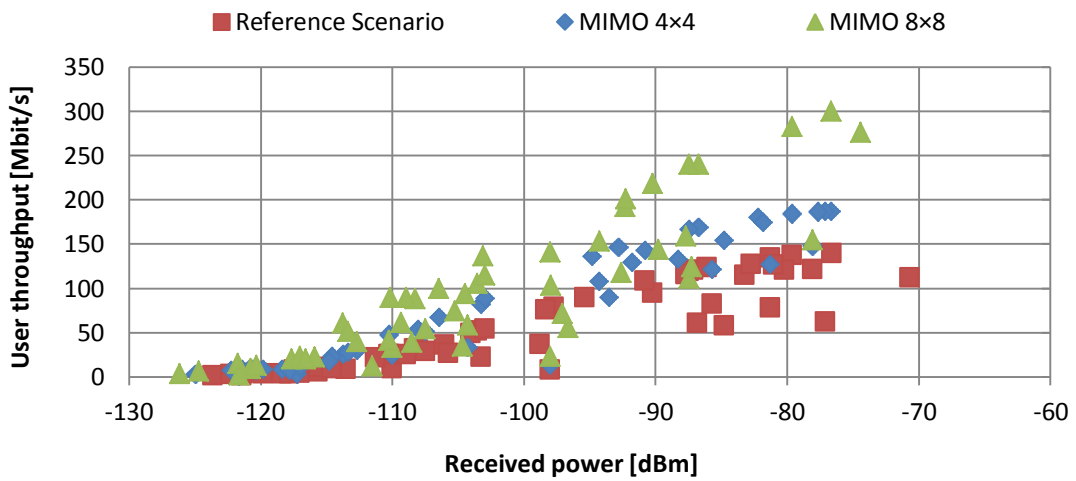

Figure 4.9 – User throughput versus received powers, using different MIMO configurations in low-load scenarios.

By multiplying the number of served users by the average user throughput, one obtains the total DL throughput that is being served across the whole network. It provides a means for evaluating the aggregated capacity gains in the network, which in this case are exclusively determined by user performance gains resulting from the use of higher order MIMO. Total aggregated throughputs of

3.76 Gbit/s and 4.79 Gbit/s are obtained when using MIMO 4×4 and MIMO 8×8, respectively, based on the average user throughputs presented in Figure 4.10, plus additional results presented in Figure G.1, concerning the number of users. These results correspond to, approximate, gains of 36% and 73% in relation to the 2.77 Gbit/s of aggregated throughput observed in the reference scenario. It is evident, as one should expect, that the total capacity gain of using MIMO 8×8 transmission is nearly twice the gain of using MIMO 4×4.

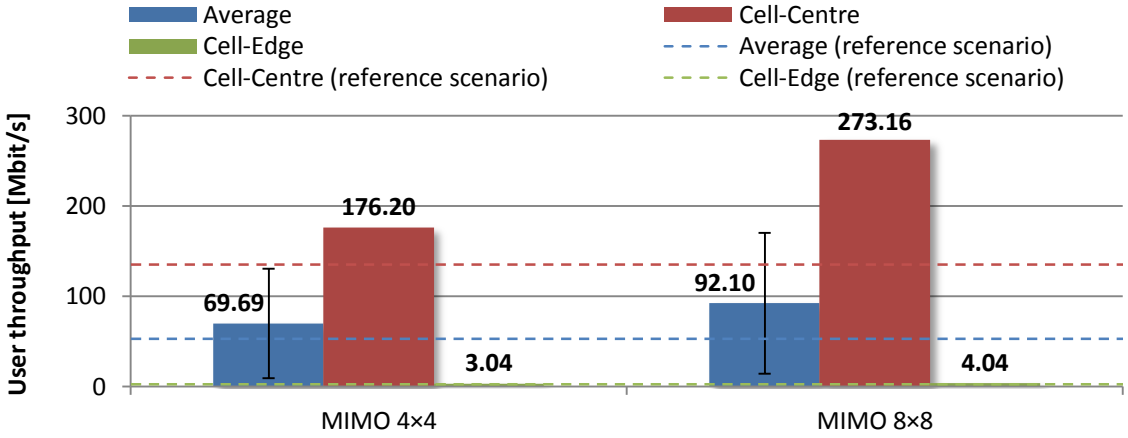

Figure 4.10 – User throughput metrics obtained for different MIMO configurations, in low-load conditions.

4.3 High-Load Results Analysis

In this section, the reference scenario is tested under heavy load conditions, using the multi-user simulator described in Section 3.3. An analysis on the influence of several radio and scheduling input parameters is presented, changing them, one by one, in order to fully characterise the system's behaviour and overall performance. Output parameters and indicators such as BSs' and users' throughputs, SNR/SINR values, path loss and received powers, as well as number of served users and number of active RBs, are used to characterise the obtained results.

4.3.1 Reference Scenario

In order to obtain results for the reference scenario, under high loaded conditions, several simulations were performed inserting a total of, approximately, 8000 users in the network. Results were taken using the same approach as in the low-load simulations, only this time with a much larger processing time. Some results were taken from a single simulation run, in order to study the snapshot distribution of specific parameters.

Figure 4.11 shows the distribution of covered and active users in the network over the available data services, for a single run of the reference scenario. From a total of 7626 users, only 2180 are actually served. This corresponds to only a 29% of all the users connected to the network, which raises a matter of capacity and calls for the study of the impact on other aspects of the system. Also, one

should note that the distribution of users among services is predominantly affected by the corresponding priorities and target throughputs, besides the number of covered users. Services requiring high throughputs and carrying medium-high priorities, such as Web services, show a higher percentage of served users.

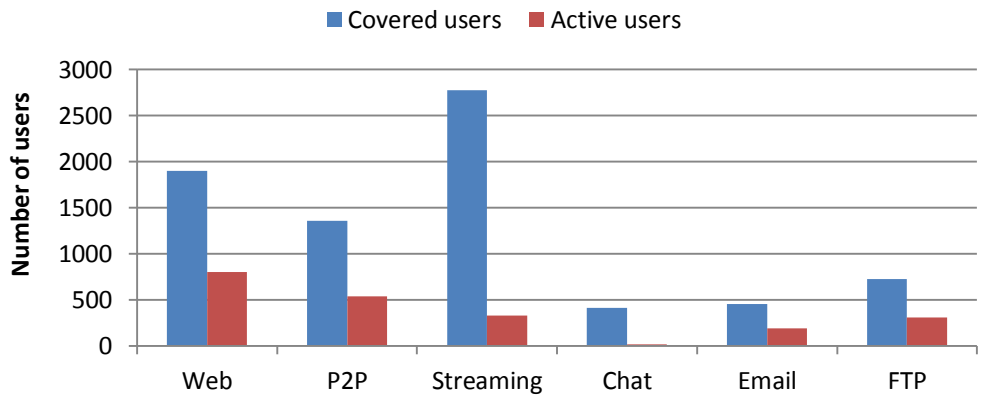

Figure 4.11 – Number of covered and served users, obtained in the reference scenario.

Figure 4.12 shows the distribution of distances for all served users in the network, using both the corresponding PDF and CDF. As one can observe, a good percentage of the users (approximately 80%) are located between 100 m and 400 m from the serving BS. Also, all served users fall below the reference coverage radius, computed for this scenario. This means that, in theory, every served user is able to achieve the reference throughput, which was set to 7 Mbit/s.

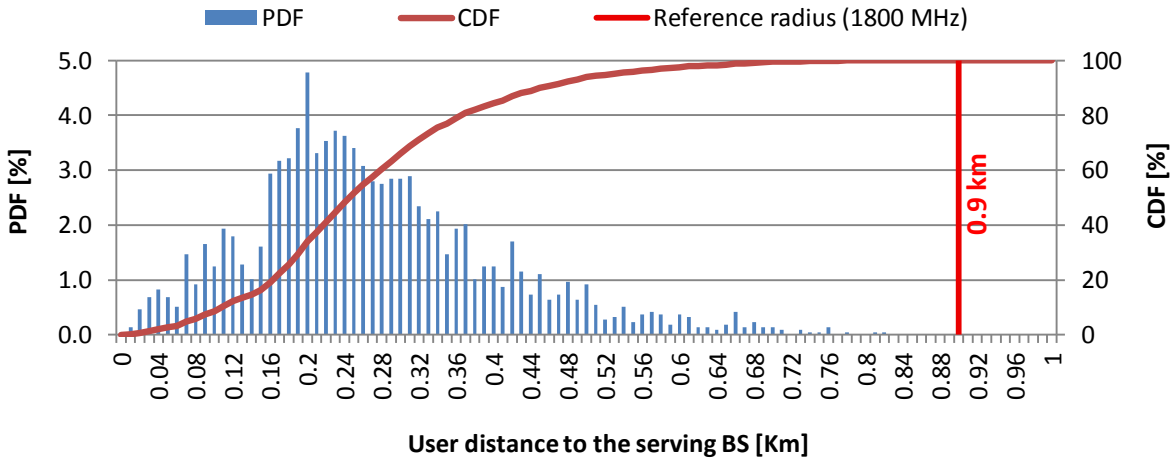

Figure 4.12 – Users' distance to the serving BS distribution (PDF and CDF), obtained for the reference scenario.

Figure 4.13 shows the distribution of BSs' throughput over the network. The CDF grows almost linearly between 0 and 217 Mbit/s (minimum and maximum BS throughputs, respectively), meaning that throughputs in this range are evenly distributed among all active BSs. The impact of the distribution of users and services along the network, as well as heavy interference, can be seen in this example distribution, by looking at the maximum BS throughput achieved. This is significantly below the theoretical maximum for a BS, which is nearly three times the maximum value for a 20 MHz sector, *i.e.*, 604.8 Mbit/s (see Table 2.2).

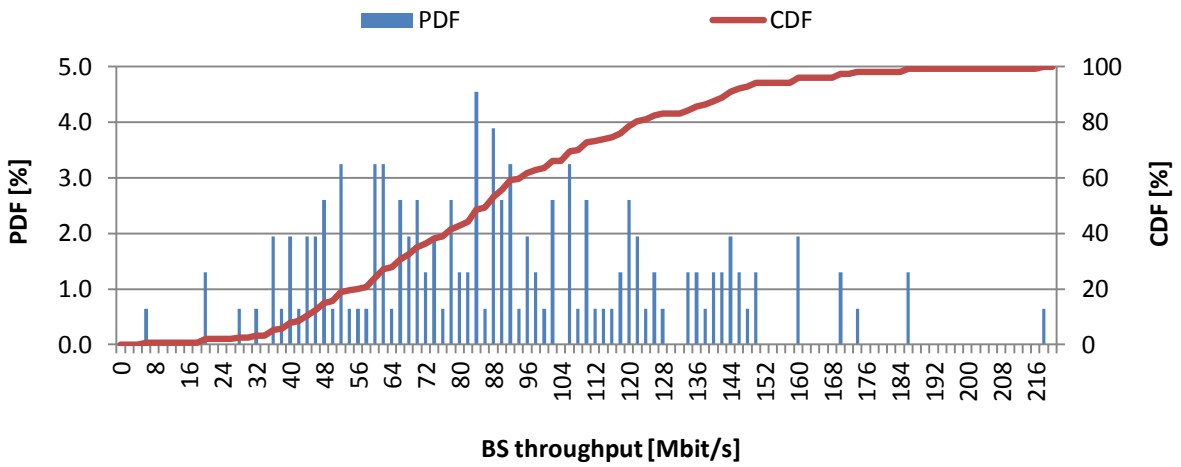

Figure 4.13 – BSs' throughput distribution (PDF and CDF), obtained for the reference scenario.

Figure 4.14 presents the mean values for the average, cell-centre and cell-edge user throughputs, taken from a set of 5 simulation runs. The "cell-centre" throughput was taken from the 95th percentile of the user throughput distribution, corresponding to the 5% top-performing user being served. Similarly, the "cell-edge" throughput corresponds to the 5th percentile of the same distribution, corresponding to the 5% worst-performing user being served. These metrics refer to a single throughput, thus do not carry a standard deviation. Cell-edge throughput approaches the minimum defined for an LTE-A user (*i.e.*, 1.024 Mbit/s for most services), which means that this statistic captures mostly users that are concentrated in the threshold of acceptable throughputs. Average user throughput remains at 6.40 Mbit/s, which is only 4% of the maximum achievable value. The cell-centre throughput, corresponding to the 5% top-performing user, reaches 17.08 Mbit/s, still far from the maximum theoretical value. While the cell-edge metric is mostly influenced by the number of users that are satisfied with the minimum service throughput, the average and cell-centre metrics are limited by capacity (*i.e.*, bandwidth) and interference, generated by a great density of users. These factors have a strong impact on the distribution of the users' throughputs, as shown later in this section.

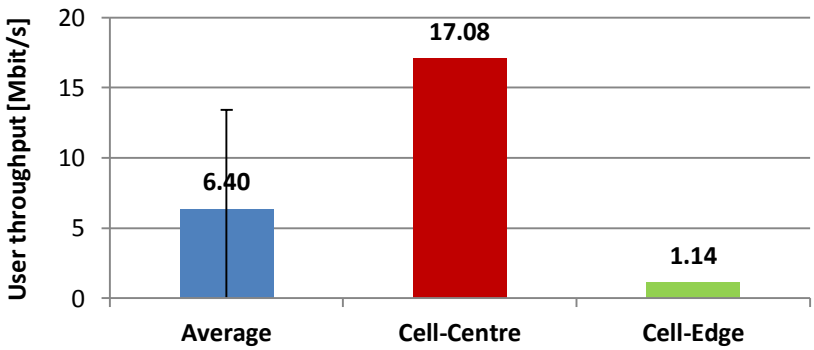

Figure 4.14 – User throughput indicators (average, cell-centre and cell-edge), obtained for the reference scenario.

Moreover, the large standard deviation observed in the average user throughput, reflects the effect of having a huge mix of users, carrying different radio channel conditions (*e.g.*, distance, line of sight) and services. This also explains why it is so difficult to achieve a uniform average performance level close to maximum capacity.

The relation between user throughput and corresponding received power and SINR are plotted in Figure 4.15 and Figure 4.16, respectively. Received powers vary in [-122, -55] dBm, approximately, which is consistent with the range defined for this parameter, [-140, -44] dBm according to [3GPP13c]. SINR values fall between -16 dB and 47 dB. Both distributions concentrate around the network's average user throughput, the first being more "concentrated" than the second. This can be explained by the fact that RSRP only gives a perspective of the users' performance limitation due to their location and radio channel conditions, disregarding interference. Looking at the users' throughput versus SINR distribution, one can distinguish two different tendencies, represented by the dark lines: one that grows almost linearly with SINR, and another that tends to a value near the cell-centre throughput. The former line fits the portion of users that are not limited by cell capacity and corresponding service priority, while the latter tends to a saturation limit, due to the high number of users sharing a limited pool of resources.

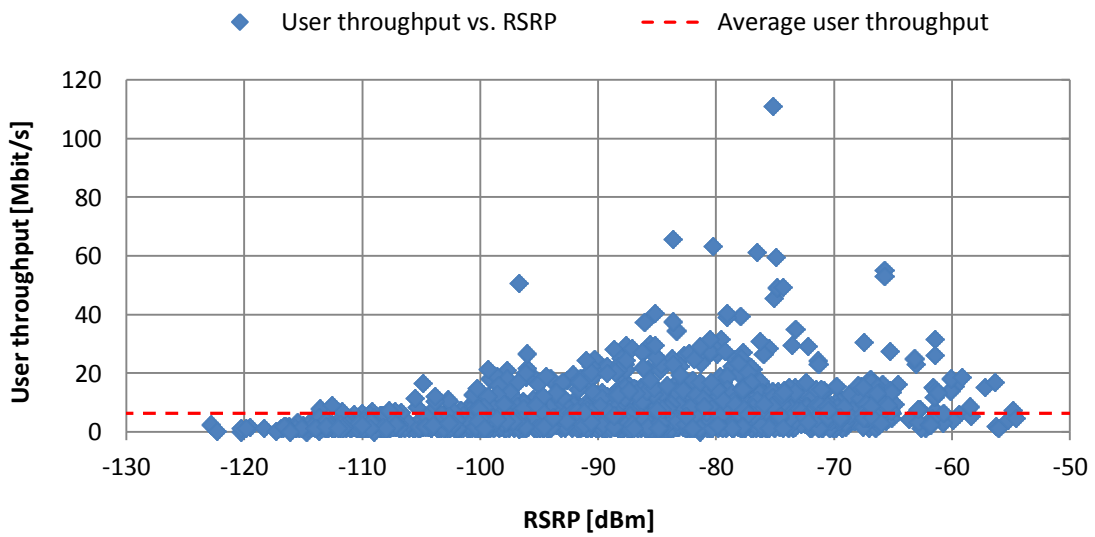

Figure 4.15 – Users' throughput versus RSRP.

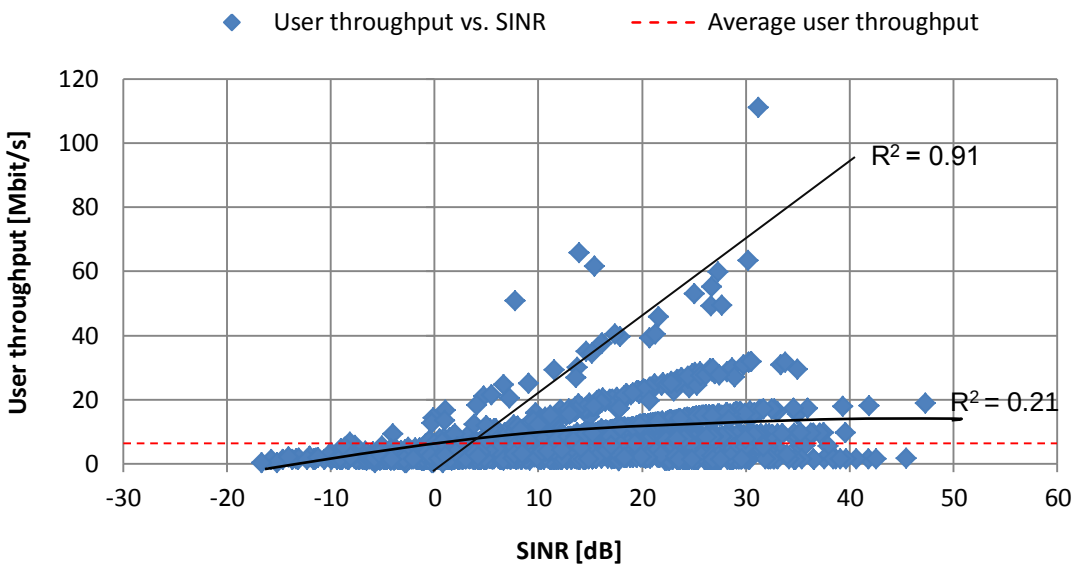

Figure 4.16 – Users' throughput versus SINR.

4.3.2 Carrier Aggregation Configuration

This section presents the results for using different Carrier Aggregation configurations. The analysis is done for a number of combinations, using the three available frequency bands: 800 MHz band, 1800 MHz band, and 2600 MHz.

Different frequencies can be combined, resulting in a balance between coverage and interference, to achieve better overall performance. On the one hand, the use of lower frequencies allows the system to cover a larger number of users, though it carries additional interference problems. On the other, higher frequencies provide low levels of interference in the network, though they only allow to cover much smaller areas.

Six scenarios were defined in order to test the gains of combining two or three frequency bands, through CA. These scenarios were tested with an aggregated bandwidth of 20 MHz, as in the reference scenario. Due to the large number of possibilities of combining multiple CCs from different frequency bands, this study is limited to a few cases that also take into account the maximum available bandwidth in each band, *i.e.*, that is owned by the operator. Table 4.6 characterises the six scenarios in terms of the component carriers used and type of aggregation (*i.e.*, intra- or inter-bands).

Table 4.6 – CA configuration scenarios.

Scenario	Aggregation type	CC Configuration	
		Bandwidth [MHz]	Central Frequency [MHz]
Scenario 1	Inter-band	10	820
		10	1830
Scenario 2		10	820
		10	2640
Scenario 3		10	1830
		10	2640
Scenario 4	Intra-band	10	1830
		10	1850
Scenario 5		10	2620
		10	2640
Scenario 6	Inter-band	5	820
		10	1830
		5	2635

The first three scenarios and the last one correspond to inter-band aggregations, whereas the fourth and fifth ones correspond to intra-band non-contiguous aggregations. This choice of scenarios allows one to take some conclusions regarding the advantages and disadvantages of employing each of the two types of CA.

Starting with the numbers of covered and served users in the network, Figure 4.17 shows that, in general, the tested configurations keep almost the same ratio as the one observed in the reference scenario. One should note that, according to the coverage estimation algorithm performed by the

MapInfo simulator, the number of covered users in each scenario is strictly related to the lowest frequency band used, associated to the carrier aggregation PCell. Although resulting in the lowest number of served users, the fifth scenario (two CCs in the 2600 MHz band) results in the highest ratio to the number of covered users, reaching 30% in this case. This means that, despite the much lower number of users that can be covered using the 2600 MHz frequency band, this option offers other kind of performance advantages, allowing one to keep satisfactory levels of capacity in the network.

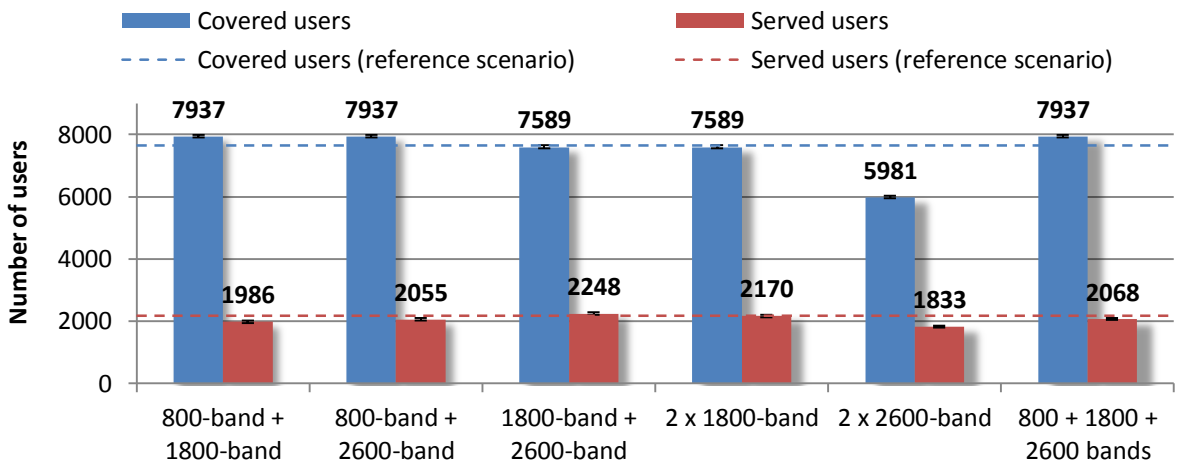

Figure 4.17 – Number of covered and served users for different CA configurations.

The previous observation can be further verified by comparing the average user throughput metrics among the different tested configurations, represented in Figure 4.18. While results for the worst-performing users (cell-edge) are almost kept constant, around 1.1 Mbit/s, both average network and top-performing throughputs are visibly changed along the different scenarios. The average user throughput varies between 5 Mbit/s and 10 Mbit/s, while cell-centre throughput varies between 15 Mbit/s and 25 Mbit/s. Low variation of the worst-performing (cell-edge) users' throughput is due to the truncation of the minimum throughput that is acceptable for a (served) user, as explained in Subsection 4.3.1. Moreover, the large variations in user throughput across the network, which are expressed by the standard deviation, explain why the average user values are so below the expected maximum.

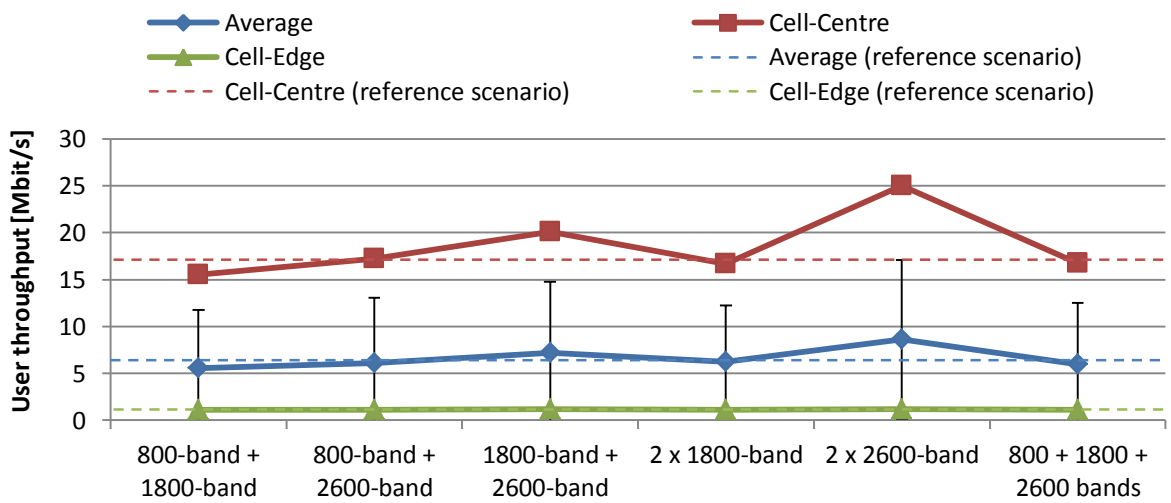

Figure 4.18 –User throughput metrics for different CA configurations.

Results on average user and cell-centre throughputs verify that user performance is, in general, lower in scenarios that use the 800 MHz band. When higher frequencies are used, *i.e.*, 1800 MHz and 2600 MHz bands, user performance is increased. These results can be explained by the lower levels of interference that are originated in higher frequencies, improving average performance at RB and user levels. The results indicate that, by simply changing from a reference single-carrier configuration of 20 MHz, in the 1800 MHz band, to an intra-band carrier aggregation scenario, using two CCs on the 2600 MHz band, one can obtain a 30% (approximate) gain in average user throughput, under heavy load conditions.

By combining the results of both charts in Figure 4.17 and Figure 4.18, through the average user throughput and number of served users, one can obtain an estimate of the aggregated bit rate capacity of the network. The third scenario, which uses CCs from the 1800 MHz and 2600 MHz bands, is the one that maximises capacity, achieving a total of 16.1 Gbit/s served. This corresponds to a 15.5% gain in the total capacity of the network, compared to the reference scenario.

Figure 4.19 shows how average user SNR and SINR levels vary along the six scenarios. SNR varies marginally above the reference scenario level, between 26 dB and 31 dB. The two intra-band aggregation scenarios show the highest levels of SNR, which can be explained by the fact that using higher frequencies alone, the resulting cell coverage areas are smaller, compared to scenarios using the 800 MHz band as PCell. By having smaller cell areas, the served users in the network will, in general, be located closer to the BSs, meaning that the average received signal powers will be higher. Average SINR values vary around the reference scenario level, between 10 dB and 18 dB. Configurations that use higher frequency bands result in higher values of average user SINR.

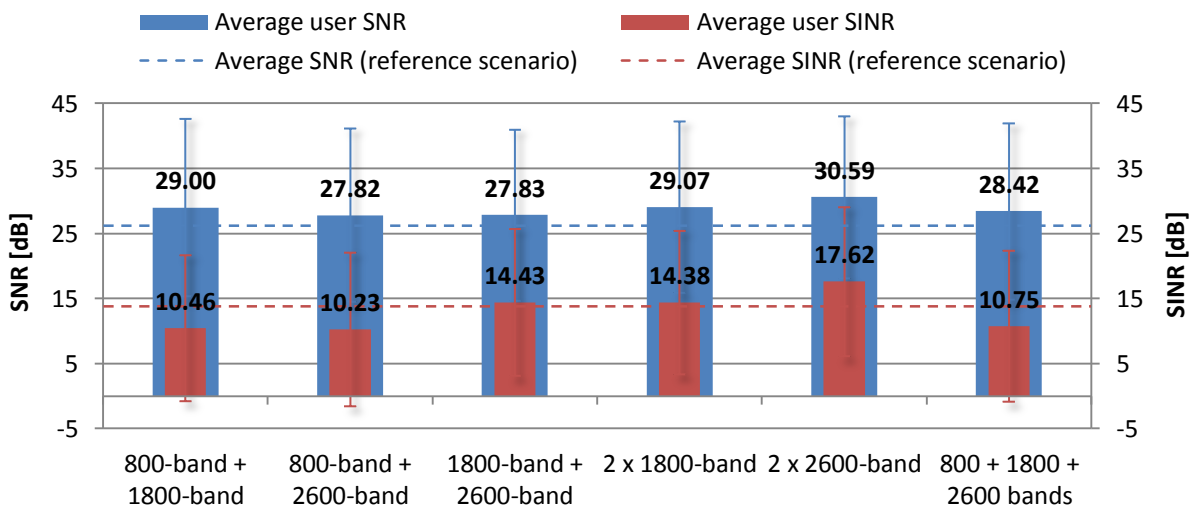

Figure 4.19 – Average user SNR and SINR levels for different CA configurations.

The difference between SNR and SINR levels gives a metric of interference for each scenario, when average network noise levels are kept constant. The 2600 MHz intra-band scenario provides the lowest level of interference, compared to all the other tested configurations, which is reflected on the improved average user performance (throughput), observed in Figure 4.18. The same is true for the third scenario, where a small difference between average SNR and SINR levels leads to good user throughput performances as well.

Figure 4.20 provides information on the BSs' average throughput for each of the tested scenarios. This information allows one to get another perspective of which of the configurations is taking better advantage of the available resources, maximising network capacity at BS level. The third scenario presents the highest average BS throughput, which means that, on average, BSs are either capable of serving higher throughputs and/or more users, than BSs in any of the other configuration scenarios. This duality has to be analysed, as peak performances are, in many cases, obtained at the expense of the number of served users. In this case, as shown earlier in this section, the number of served users prevails as a dominant factor for capacity, leading to a larger network accumulated throughput in the third scenario, which represents a 15% increase in relation to the reference scenario. Also, one should notice the difference between standard deviations. Scenarios with improved average capacity, such as the fifth scenario, will have more disparity between BS throughput values, meaning that served throughputs, across the network, are less harmonised, for instance, due to lower levels of interference.

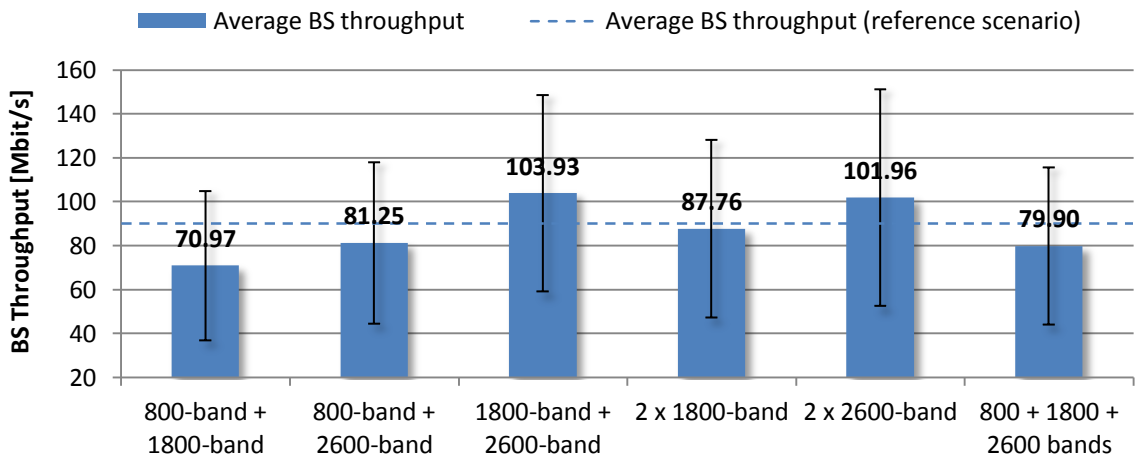

Figure 4.20 – Average BS throughput for different aggregation scenarios.

4.3.3 Bandwidth

This section includes the results of using different bandwidths, through the aggregation of multiple CCs. The analysis is only considered for scenarios where the aggregated bandwidth is equal or greater than the 20 MHz available in the reference scenario.

Results in Subsection 4.3.2 indicate a better overall performance of the "1800-band + 2600-band" configuration, compared to other configurations. For that reason, it is adopted as the default inter-band aggregation scenario, and used through different combinations of bandwidths, to test impact on performance and capacity. Table 4.7 presents the scenarios that were defined using different bandwidths (*i.e.*, CCs) per frequency band, from an aggregated bandwidth of 20 MHz to 100 MHz.

Despite the small adjustments, in respect to the number of used CCs and bandwidth proportion between frequency bands, along the simulated scenarios, the results are plotted in a sequence of aggregated bandwidths, from 20 MHz to 100 MHz, each scenario separated by 10 MHz.

Table 4.7 – Bandwidth configuration scenarios.

Scenario	Bandwidth configuration [MHz]		Aggregated bandwidth [MHz]
	1800-band	2600-band	
Scenario 1	10	10	20
Scenario 2	20	10	30
Scenario 3	20	20	40
Scenario 4	20 + 10	20	50
Scenario 5	20 + 20	20	60
Scenario 6	20 + 20	20 + 10	70
Scenario 7	20 + 20	20 + 20	80
Scenario 8	20 + 20 + 20	20 + 10	90
Scenario 9	20 + 20 + 20	20 + 20	100

In theory, capacity should be increased in direct proportion with bandwidth. One has to look across different aspects of capacity, such as number of users, resource usage and achieved performances, in order to conclude on the previous observation. In practice, results should indicate additional losses that are related to the heavy load simulated on the network. These losses are evidenced both in absolute values and in relative proportions to the increase of bandwidth or maximum expected values.

While the number of covered users remains practically the same in all cases, the number of served users grows almost linearly with bandwidth, as shown in Figure 4.21, which translates into an average increment of 100 served users per 10 MHz of additional bandwidth. This variation also reflects in the network's "efficiency", allowing one to go from a 30% ratio between served and covered users, to a 40% one. The increase in number of served users is due not only to the increase in the available resources, but also to other factors, such as interference between them.

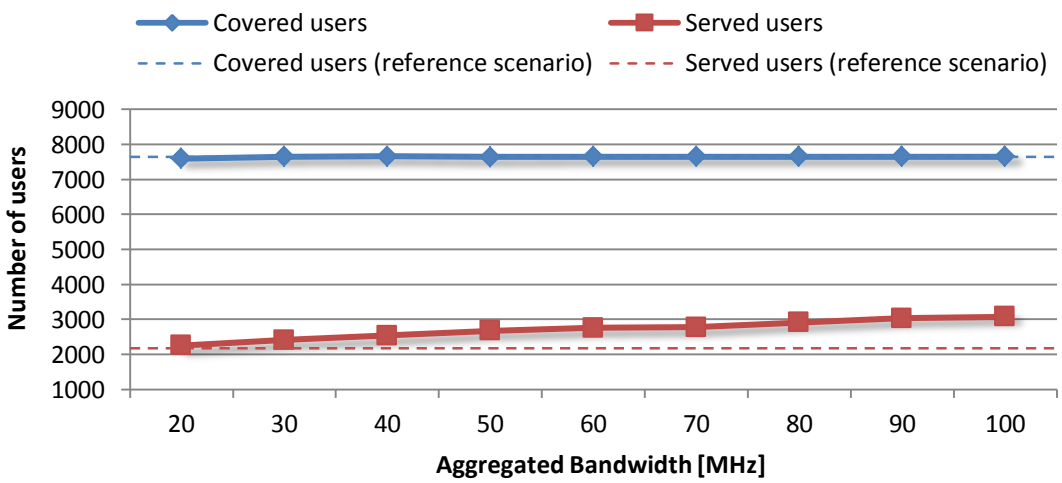

Figure 4.21 – Number of covered and served users, for different aggregated bandwidths.

Figure 4.22 shows the evolution of the user throughput metrics over variable aggregated bandwidth scenarios. As in the different CA configurations, worst-performing users' throughput does not vary

significantly. On the contrary, the average user and top-performing throughputs increase significantly with the aggregated bandwidth. The first varies between 7 Mbit/s and 18 Mbit/s, which translates into an approximate 150% increase in average user performance of the network, going from 20 MHz to 100 MHz of aggregated bandwidth. Cell-centre throughput shows a more expressive variation, by going from 20 Mbit/s to 63 Mbit/s, which represents a 215% increase. In theory, both metrics should increase in the same proportion as bandwidth, but, again, interference and large deviation of user performances along the network have strong impact on average results, explaining the discrepancy between results and the maximum expected values. Furthermore, as bandwidth increases, the increments in user performance begin to loose significance, contradicting, in some cases, the growing tendency observed. These contradicting results are balanced by the other capacity aspects of the network, such as the number of served users.

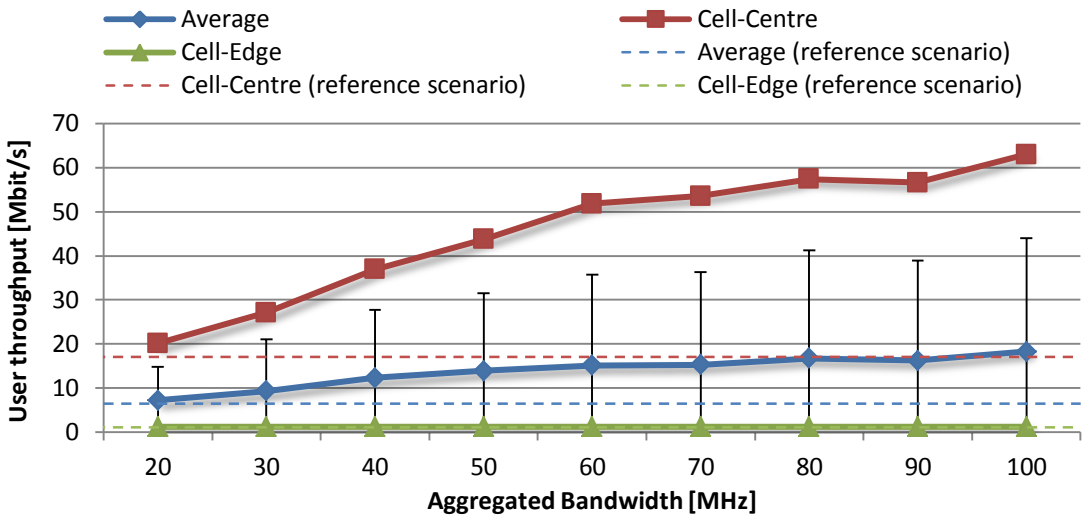

Figure 4.22 –User throughput metrics for different aggregated bandwidths.

Another interesting fact from these results is the fact that throughput metrics increase almost linearly with bandwidth up to 60 MHz of aggregated bandwidth, and then variation becomes less correlated with bandwidth increase. This observation evidences the effect of the requested service throughputs and number of users per sector in the variation of user performance. Users are limited to a maximum of 300 Mbit/s, achievable by Category 5 devices, and keep the same average geographical distribution across Lisbon. Since these two aspects are kept constant throughout the simulations, there is a point where sectors' available bandwidth loses predominance in the variation of users' performance.

Improvements in user performance can be explained by a combination of the results in Figure 4.23 and Figure 4.24. These two figures show a variation of the average network SNR and SINR levels and average number of RBs per user, respectively, for different aggregated bandwidth scenarios. Figure 4.23 shows a decrease in both SNR and SINR levels, whereas Figure 4.24 evidences an increase in the average number of RBs per user. These results are directly correlated, since by having more bandwidth available, users will be able to have more RBs with lower SNR/SINR levels in order to achieve the desired service satisfaction. Also, the difference between SNR and SINR levels decreases with bandwidth. This indicates a decrease in average levels of interference in the network, when

average noise levels are kept, approximately, constant.

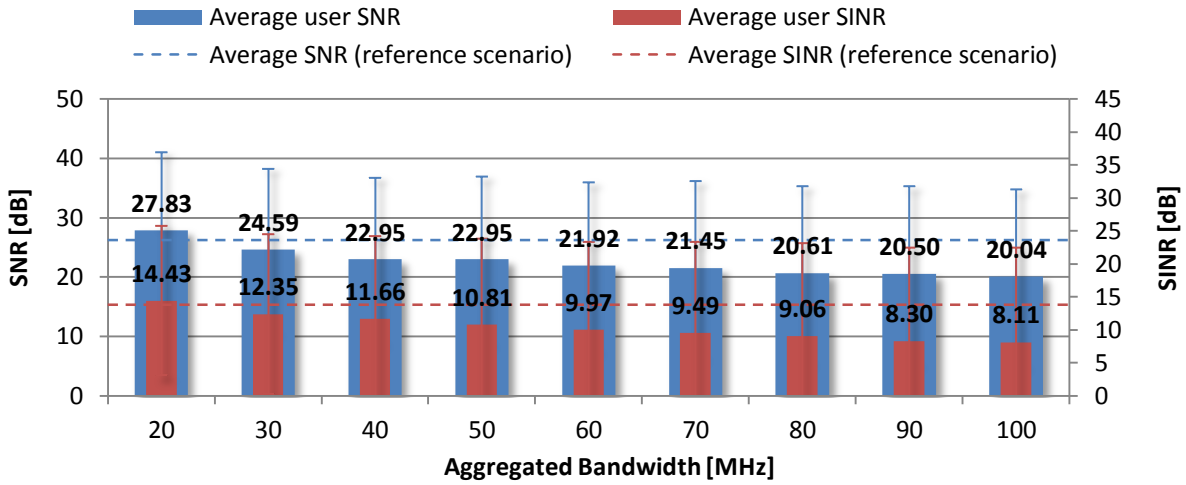

Figure 4.23 – Average user SNR and SINR levels for different aggregated bandwidths.

Variation of the average number of RBs per user, plotted in Figure 4.24, show a linear increase from 12 to 49, which translates into an average increase of 4.5 RBs per 10 MHz of additional bandwidth, approximately. According to the information provided in the graph, on average, a user takes 10% of the total number of available resource blocks, in the corresponding sector. This ratio is merely indicative, due to the large standard deviation observed over the network, resulting from the diversity of radio channel conditions and services requested by users. The standard deviation also increases with bandwidth, as in the case of average user throughput, mostly due to top-performing users that will be able to have more resource blocks and satisfy the maximum throughputs.

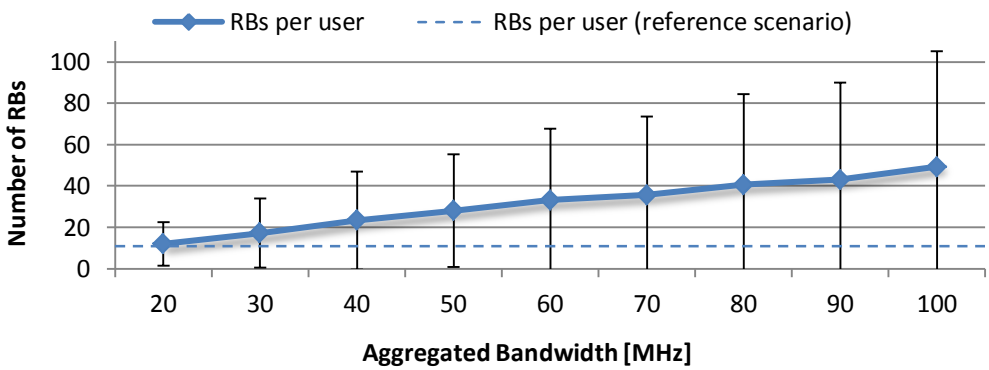

Figure 4.24 – Average number of resource blocks per user for different aggregated bandwidths.

Previous information on per user resource usage can be linked with average number of users per BS or per sector, in order to have a perspective on the use of the available resources over the network. Multiplying the values of average number of users per BS, plotted in Figure 4.25, by the average number of active RBs per user, one obtains the average number of active RBs per BS. According to the adopted Reuse-1 FRS, each BS provides three times the amount of RBs available in one single aggregated bandwidth. For instance, in the case of a 20 MHz bandwidth configuration, 300 RBs would be made available by each BS. Results show that, in this particular scenario, only an average 58% of the total amount of RBs in each BS would actually be used. Again, this is explained by the large deviation observed in relation to the average values, evidencing that many users do not request the

maximum number of resources available. Average numbers of users per BS and per sector do not increase in the same proportion as bandwidth and other capacity vectors. This is compensated by an increase in individual performances, at RB and user levels. The fluctuations between multiple capacity aspects can be impacted by the resource allocation algorithms used in the simulator.

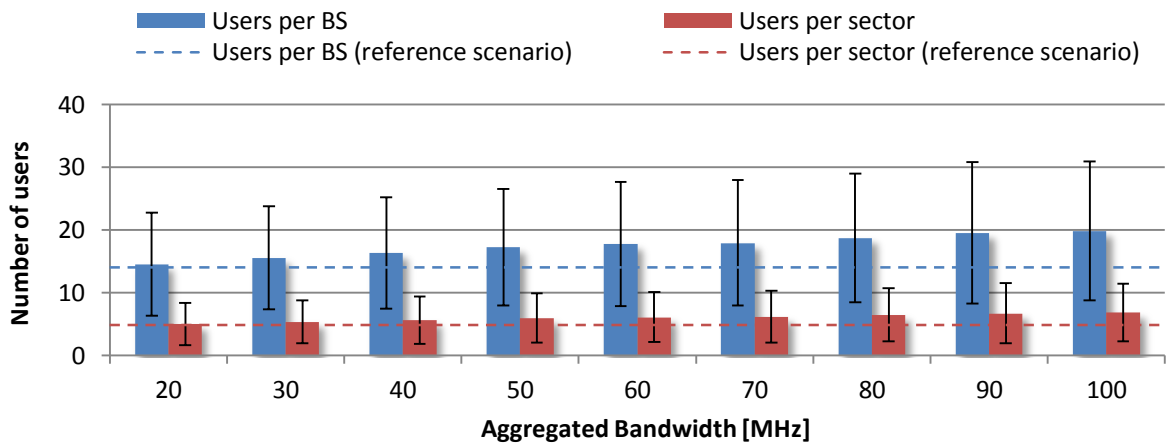

Figure 4.25 – Average numbers of users per BS and per sector for different bandwidths.

Figure 4.26 plots the evolution of the network's average BS throughput when going from 20 MHz to 100 MHz of aggregated bandwidth, available in each sector. An approximately linear variation between 104 Mbit/s and 361 Mbit/s, translates into an average increase of 32 Mbit/s per 10 MHz of additional bandwidth. This is still very far from what should be expected in theory, which is in line with previous observations on the average usage of available resource blocks in the network, and corresponding absolute values. Results indicate that it is possible to achieve, roughly, twice the cell capacity of the reference scenario when aggregating 40 MHz of bandwidth, and up to four times the same capacity when aggregating 100 MHz of bandwidth.

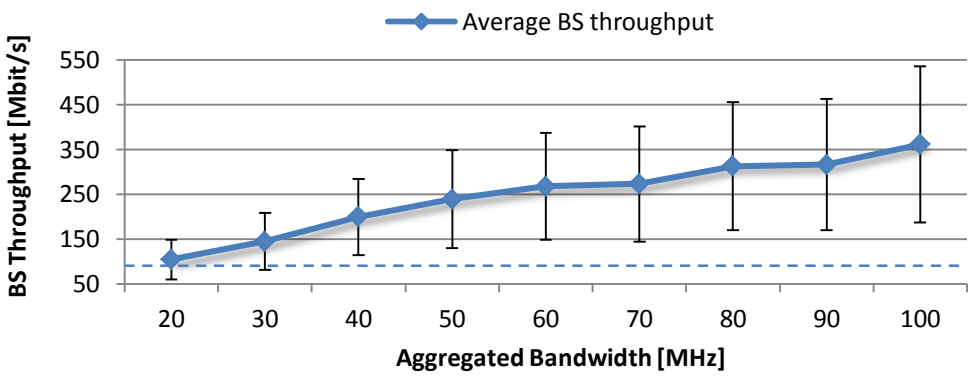

Figure 4.26 – Average BS throughput for different aggregated bandwidths.

4.3.4 MIMO Configuration

This section analyses the impact of using different MIMO configurations, under heavy load conditions, presenting the results for 4×4 and 8×8 schemes and comparing them with the reference scenario (*i.e.*, MIMO 2×2 case). The tested MIMO configurations are expected to improve user performance, leading to an increase in overall capacity. However, one should also take into account that these simulations were done on heavily loaded networks, which means that, although users have the potential of

achieving higher peak data rates, the capacity of the system is still limited by the conflicts among users for the available resources.

Performance gains associated to the use of MIMO 4×4 and 8×8 configurations can be extrapolated from the comparison between peak data rates, presented in Table 2.2. These indicate doubled and quadrupled gains in performance, respectively, compared to the reference 2×2 case. In practice, results show that the gains of using higher order MIMO configurations are significantly limited due to the high number of users in the network, which reflects in overall capacity.

Figure 4.27 shows the number of covered and active users in the network, when using different antenna configurations. From a total of 7912 users covered by the network, only 2315 are served, when using MIMO 4×4. In the case of MIMO 8×8, the numbers are nearly the same with 2312 users served and a total of 7937 covered. These numbers reflect almost the same ratio between served and covered users, which is close to 30% in both situations. However, one can observe that the number of served users actually decreases between MIMO 4×4 and MIMO 8×8. These results indicate that the aggregated network capacity must be compensated in some other aspects, such as user performance, which is possibly causing user starvation.

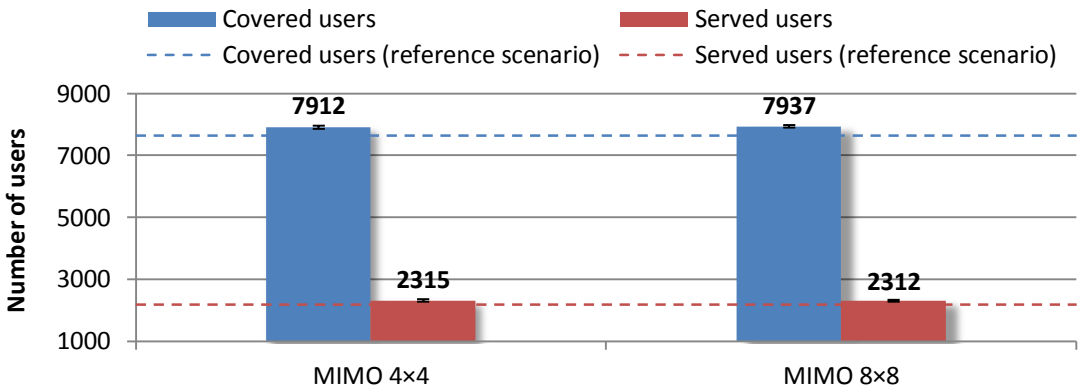

Figure 4.27 – Number of covered and served users for different antenna configurations – high load scenario.

The chart represented in Figure 4.28 shows increases in user performance, which are then reflected in capacity. This evidences the impact of the allocation algorithm in the simulator, by favouring an increase in average user performance, rather than increasing the number of users being served. This is mostly related to the highly demanding services that users are requesting, which target the maximum throughputs in the corresponding UE category (300 Mbit/s in Category 5). As in the low-load analysis, average and cell-centre performance gains are still very far from the ones that would be obtained, in theory, by using twice and four times the number of antennas of the reference scenario. This can be explained by the fact that the DRM and RMG models, adopted in this thesis, consider maximum gains that are already limited by the assumption that users can never reach theoretical gains, due to typical radio channel conditions and situation of the users. In other words, even users located at less than 10 m of the serving BS, will not achieve double or quadruple data rates of the reference scenario, which is according to the equations and correction factors that were defined by adopted the models.

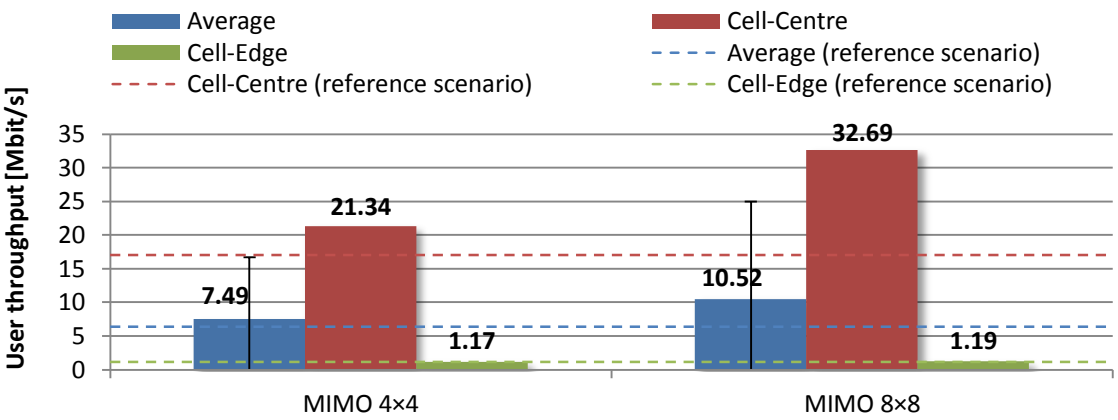

Figure 4.28 – User throughput metrics for different MIMO configurations.

The total aggregated throughputs being served in the network are calculated for the different scenarios, using the number of served users and average user throughput, from Figure 4.27 and Figure 4.28. The product between these two metrics gives total aggregated throughputs of 13.95 Gbit/s, 17.34 Gbit/s and 24.32 Gbit/s, for MIMO 2×2, MIMO 4×4 and MIMO 8×8, respectively. These values represent average network capacity gains of 24% and 74% for MIMO 4×4 and MIMO 8×8 schemes, respectively, in relation to the reference scenario (*i.e.*, MIMO 2×2 case).

Cell-centre throughput (*i.e.*, top 5% performing user throughput) increases in both cases, showing that users that are close to the BS, and not limited by cell capacity, can substantially benefit from using higher order antenna schemes. MIMO 4×4 evidences a gain of 24% in top user performance, and a gain of 91% for MIMO 8×8. Bottom user performance is not affected in the same way as top user, due to the same reasons, explained in previous sections, concerning the high concentration of users being served with the minimum service throughput.

Figure 4.29 shows comparable capacity gains with the ones obtained for the network aggregated throughput served, for different MIMO configuration scenarios. Average BS capacity is increased by 24% and 74%, when using MIMO 4×4 and MIMO 8×8, respectively, in high-load conditions. Once again, absolute values evidence the difference existing between theoretical values and those obtained in practice, under heavy load conditions. Only an average 37 Mbit/s is used per sector, when using MIMO 4×4, and an average 52 Mbit/s per sector, when using MIMO 8×8, which is still very far from the maximum values presented in Table 2.2.

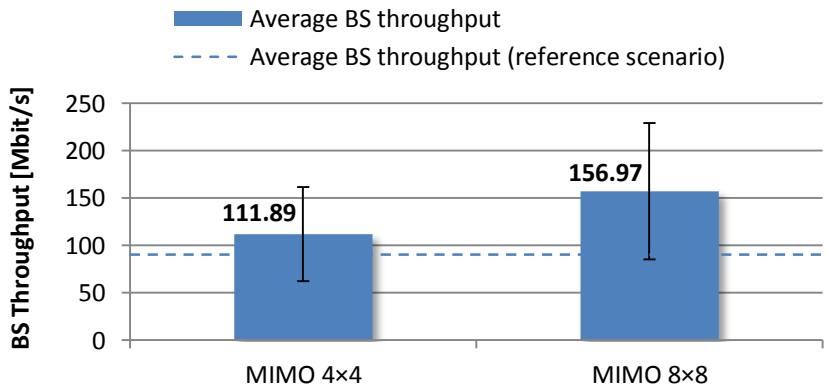

Figure 4.29 – Average BS throughput for different MIMO configurations.

4.3.5 Resource Block Distribution Algorithm

This section analyses the impact of using different RB distribution algorithms, which aim to take advantage of a selective positioning of resources within the spectrum. Three scenarios were defined, according to the different distribution algorithms defined in Section 3.2. Both 1800 MHz and 2600 MHz bands were used, through the aggregation of two 10 MHz component carriers, to be able to observe any improvements that may result from frequency diversity.

In order to establish a cell border area in the Sequential Selective scenario, the algorithm assumes that cell-edge users are located further than 70% of the reference radius of the cell. Using this segmentation of users, it is possible to preferably assign high frequencies, with shorter range, to cell-centre users and low frequencies to cell-edge ones. Alternatively, users' segmentation in the third scenario is done by assigning "reference frequencies", based on the users' relative positions to the reference coverage radii of the frequency bands available.

Despite the multiple differences that exist among the three algorithms, results show that performance and, consequently, capacity are not visibly affected by them. Annex G provides some of these results, showing that user performances and levels of received signal, noise and interference do not change significantly. Although it may seem irrelevant to the focus of this thesis, it is rather important to see that slightly different interpretations of the scheduling procedures, to the reality of the simulator, do not impact significantly on results. These results indicate that, even with CA, scheduling is still not as limiting to the network as other factors, such as interference and scarcity of resources.

The percentage of active RBs per used frequency band is presented in Figure 4.30, when using different RB distribution algorithms. While in the first scenario the percentages of active RBs, for both frequency bands, tend to the same value due to the random character of the distribution, the second scenario evidences a clear difference between the two percentages of active RBs. In this case, the 2600 MHz band is preferably used due to the fact that most users are considered to be located in the cell-centre, according to the assumptions defined in Section 3.2.

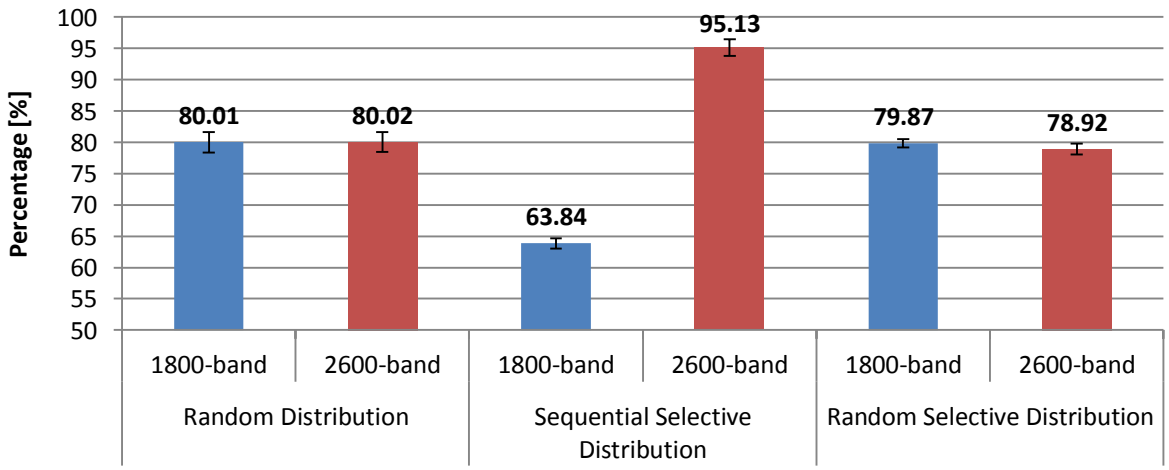

Figure 4.30 – Percentage of active RBs per frequency band, for different RB distribution scenarios.

The Random Selective algorithm shows an almost imperceptible difference between percentages of

active RBs, approaching the results of the first scenario, *i.e.*, Random distribution. In this case, the percentage of active RBs in the 2600 MHz band is slightly lower than the one observed in the 1800 MHz one. This is explained by the portion of users that are located beyond the reference radius of the 2600 MHz band, preventing them to have RBs in these higher frequencies, whenever cell capacity is not exceeded.

By relating these results with the distribution of users' distances, presented in Figure 4.31, it becomes clear that the parameterisation of the reference cell radii is crucial to differentiate the gains of using each of the three algorithms. This distribution shows that only a 10%, or less, of users is affected by the frequency selective criteria, reflecting into insignificant performance gains.

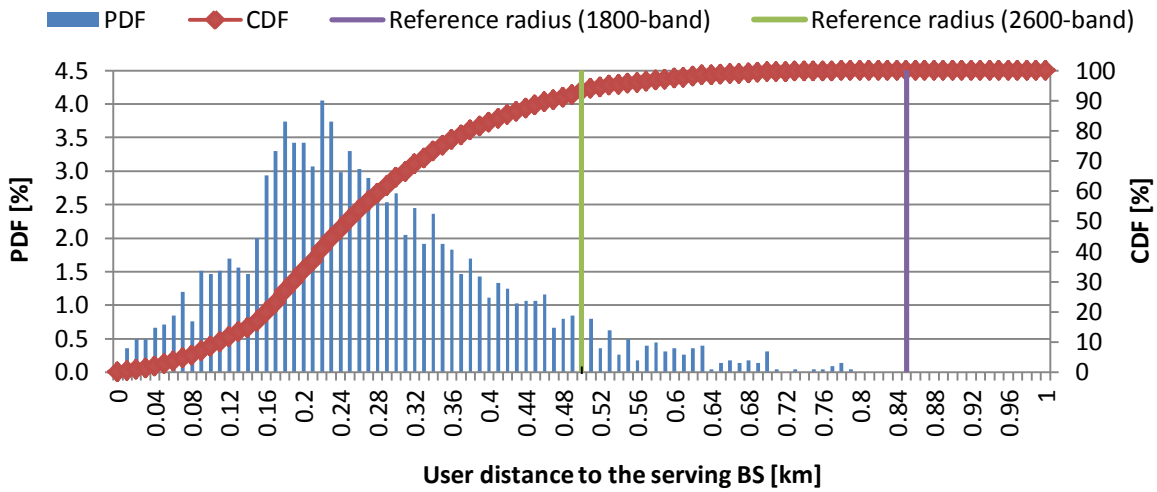

Figure 4.31 – Users' distance to the serving BS distribution (PDF and CDF), obtained for the "1800+2600" aggregation scenario.

An increase in the reference throughput considered in the network would pull the reference radii of both frequency bands towards the average distance of users. This would guarantee that more users are included into the "selective area" of both Sequential and Random Selective algorithms, which would generate more significant variations in average RB (and user) performance. The focus of this thesis is not to cover extensively the differences in performance, among the three algorithms, but only to provide a general idea of how differently they perform and the degree of the impact on performance.

Chapter 5

Conclusions

This chapter concludes the present work, summarising a critical analysis and discussion of the results, as well as pointing out some of the aspects to be developed in future work.

The main objective of this thesis was to study the impact of including MIMO and CA advanced features in LTE networks, giving special emphasis to capacity, performance and interference related aspects.

Chapter 2 focuses on describing the fundamental concepts of LTE and LTE-A networks, covering network and radio technology aspects, performance analysis and services and applications. These are key to understand the chapters that follow, how the system works and what are the main features that were taken into account when developing the model. The first section addresses the network architecture, describing its main elements and orientation towards data services. A description of the radio interface follows, the main features introduced in earlier LTE releases, as well as improvements from Release 10 and beyond, focusing on higher order MIMO and CA. Performance aspects are discussed in the third section, concerning capacity, QoS and interference, to establish association with common metrics, such as throughput. The following section is dedicated to describe the different types of traffic in LTE-A networks, including an analysis on how LTE-A improvements address the new demands for services and applications. Finally, this chapter ends with an overview of other authors' work, presenting the state of the art in what concerns MIMO and CA. The focus here is to describe some of the approaches already being used to study and dimension the new LTE-A features, as well as performance expectations that arise from these works.

Chapter 3 presents the model that enables to study LTE-A performance in multi-user scenarios. The first section outlines the model, explaining its main assumptions, which include some of the fundamental equations that were used to address the calculations of performance metrics, introduced in Chapter 2. Signal power and interference, throughput metrics, aggregated cell-capacity, coverage and load distribution are some of the many analysis vectors considered in this section. A description of the algorithms used throughout in simulation follows, including the ones that are dedicated to RB allocation and spectrum distribution, with particular emphasis on the latter, due to its closer relation to CA and load balancing between CCs. Then, one offers a description of the simulator, covering its structure, implementation and workflow. Finally, an assessment of the simulator is presented, determining the minimum number of simulation runs and number of users to be considered, as well as validating some key aspects, to support the obtained results.

Chapter 4 is dedicated to present and to analyse the results from the multi-user simulations. These simulations were performed for the city of Lisbon, using information provided by Optimus on the location of the deployed LTE BSs. Moreover, they were done for both low- and high-load scenarios, in order to extract relevant conclusions on peak performances, with no capacity limitations, and normalised gains over a fully matured network. Starting with the definition of the default conditions and parameters used for any simulation, including a reference scenario, one first presents results for low-load simulations and field measurements, and then proceeds to the analysis of the simulations with significant number of users distributed over the network.

Simulation results, with approximately 80 users in the whole city (*i.e.*, low-load simulation scenarios), all requesting for the maximum device category throughput, are compared with the single-user field measurements that, in turn, were performed on a live LTE-A cell site. These included results for three different situations: one using 20 MHz of inter-band CA, in the 1800 MHz and 2600 MHz bands, and

the other two using each of the previous CCs alone. Field results confirm that CA actually allows one to double the performance of a single user, using two CCs instead of just one. They also show that performance distribution over different received power values do not differ much between the 1800 MHz and 2600 MHz bands, despite a slight shift in the RSRP ranges, due to the differences in cell coverage. Compared with the multi-user, low-load, simulation results, field measurements clearly match the throughput distribution obtained for the simulated users that are not limited by cell capacity. The obtained ranges of values are consistent between the two methodologies, apart from some minor differences, which result from some truncations performed by the real system.

CA was the only LTE-A feature that was possible to test during the field measurements, overthrowing the possibility of having a realistic perspective on the performances of higher order MIMO configurations. This can be considered a limitation in this work, due to the importance of providing realistic validation of the extrapolated MIMO model. Only simulated results were included, showing average network capacity gains of 36% and 73%, using MIMO 4×4 and MIMO 8×8, respectively.

The following section in Chapter 4 is exclusively dedicated to the results of high-load simulations, considering a total of nearly 8000 users. Different sets of configurations were, progressively, tested by keeping the remaining of the default parameters constant. Results obtained for the reference scenario, with 20 MHz bandwidth and MIMO 2×2, are carefully analysed and used afterwards as a baseline for the capacity and performance gains intended in this study.

The first analysis is conducted by simulating different CA configurations, keeping the same aggregated bandwidth, which means using different combinations of frequency bands, in two or more CCs, testing both intra- and inter-bands aggregation. Results show different types of variation in the number of users and respective performances, translating the effect of the balance that exists between coverage and interference. When using low frequency bands, such as the 800 MHz band, the network is able to cover more users, though it carries much more interference. By combining high with low frequency bands, using the same aggregated bandwidth, the total contribution of interference is less, still ensuring the same basic coverage. These effects translate into marginal changes in the number of covered users and improved average and peak users' performances, increasing overall network capacity.

The next analysis is to vary the aggregated bandwidth within [20, 100] MHz, using multiple component carriers from the 1800 MHz and 2600 MHz bands. The results show that the number of served users grows linearly with bandwidth, despite almost no variation is observed in the number of covered users. This can be explained by the use of the same combination of frequency bands, delivering the same coverage basis. The increase in the number of served users follows the increase in cell capacity, with more RBs available per sector. Users also show improved performance results, measured by average and top 5% throughputs. As in previous analysis, variations in top-performing users' performances are more "aggressive" than variations in average throughputs. The combination of the user throughput gains with increases in number of served users reflects on average cell-capacity, according to the numbers of users served per BS and average BS throughputs. Network aggregated capacity increases with bandwidth, reflecting approximate gains to the ones observed in average BS throughputs. These

correspond to double the capacity with 40 MHz of aggregated bandwidth and quadruple it with 100 MHz, comparing to the 20 MHz bandwidth in the reference scenario. Obtained capacity gains reflect the expected impact of bandwidth aggregation on cell capacity, as well as introducing some clues on the relationship between user performance and different capacity vectors, such as number of served users and number of RBs per user. In short, results indicate a slight slowdown in aggregated capacity increase, after 60 MHz bandwidth. This is then reflected on the non-directly proportional increase in capacity, for 100 MHz bandwidth, which is below the theoretical 5 times increase in capacity.

MIMO 4×4 and MIMO 8×8 are also analysed for scenarios with nearly 8000 users, in order to extract the overall performance and capacity gains of using these improved schemes in relatively loaded network conditions. Results show almost no gains in terms of numbers of served users, when using each of the two schemes. On the other hand, average user performance is significantly improved evidencing gains of 17% and 64%, for MIMO 4×4 and MIMO 8×8, respectively. The overall network capacity is consequently increased, with gains of 24% and 74%, for the two tested configurations. These results are in line with expectations.

Finally, the last simulations are concentrated on evaluating the different RB distribution algorithms. These represent three distinct ways of assigning carrier frequencies to the already allocated RBs. The first algorithm, which was initially defined, implemented, and used as default, distributes RBs randomly across all aggregated CCs. The second, defined as an extreme situation, distributing RBs sequentially over the spectrum, starting from higher frequencies, for cell-centre users, and from lower frequencies, for cell-edge users. The third algorithm consists of a mix of the other two and tries to approach what actually happens in a real LTE-A system, defining a prioritised set of CCs, where user's RBs should be allocated.

Despite the existing dissimilarities between the three distribution algorithms, and the fact that percentages of active RBs per CC or frequency band are slightly changed, these are not enough to create a significant impact on performance and overall capacity of the network. The initial idea was to take advantage of the existing frequency diversity that results from inter-band CA, changing the ratios of used RBs between different CCs. This could lead to variations in SNR and SINR levels, which would impact on interference and, consequently, change average user performance in the network. However, results show that SNR and SINR levels are not significantly impacted, and so user performance is kept constant. In high-load conditions, where nearly 80% of the total available RBs in the network are being used, the average concentration of used RBs per sector is also very high. This means that a change in the distribution algorithm does not cause a significant impact on the distributions of RBs per sector available bandwidth, causing only an insignificant number of permutations of RBs' positions, within each sector. Also, the fact that these simulations consider a reference service throughput, in order to compute the reference cell radius for each available frequency band, implies that one has to take into account the key importance of correctly tuning this parameter. By changing it, it is possible to introduce more or less impact on the different algorithms, due to their close dependence on the relative positions of users and reference cell radii, for each

frequency band.

The developed simulator proves to be a reasonable tool for evaluating LTE-A improvements, using the information on today's 4G networks. This affirmation is not only supported by the comparison between low-load simulations results and field measurements, which give very satisfactory indications, but also by the fact that the obtained results are easily justifiable by analogous situations, observed in real networks. Nevertheless, it is also important to note the existence of certain limitations, inherent to the development of the model and simulator. Those limitations need to be acknowledged and then considered while validating unexpected results. A number of limitations are shared with previous versions of the simulator, such as the lack of temporal depth (*i.e.*, snapshot based simulations), full randomisation of the radio channel conditions, regardless of some relevant topographic indicators, *a priori* coverage estimation performed by the MapInfo module, *a posteriori* computation of the SINR levels, and adapted RB allocation and reduction algorithms that do not exactly replicate real systems. Besides those, other limitations were added, regarding the implementation of the new LTE-A features in the simulator. Adaptation of the RB scheduling algorithm over multiple CCs, impossibility of simulating a mix of LTE and LTE-A users and extrapolation of MIMO gains without any validation, based on field measurements, are some of the limitations introduced.

Performance results are clearly affected by some of these limitations, showing only marginal variations around the reference value, especially in terms of absolute values. On one hand, cell-edge performance, measured by the bottom 5% user throughput, shows only marginal variations around a reference value, indicating that it is highly conditioned by the truncation of the established minimum user throughputs. On the other hand, average and cell-centre throughputs present generally low values, compared to the maximum expected, and significant disparity between the users. These results indicate lack of capacity in the system, but also some considerable inefficiency when allocating resources to users and distributing the load. The identified limitations and associated impacts are two of the reasons for providing an analysis focused on gains, rather than in scrutinising only absolute figures and numbers. Another critical limitation in this simulator is the time that is needed to process information in high-load scenarios, which is responsible for not including other kinds of results and combined scenarios.

High-load simulations results provide ratios and percentages that can be interpreted as the average gains of using each of the different studied options. An important conclusion is the fact that network aggregated capacity can be positively impacted by a number of different aspects, such as the combination of different frequency bands, total aggregated throughput and adopted MIMO capabilities, increasing numbers of users and overall QoS. These are key aspects that drive operators in order to provide better service to more and more users.

In the end, results from CA seem to be more optimistic that those coming from higher order MIMO configurations. This is not a simple conclusion, as it is supported by many reasons and indicators. Most of them are related to the fact that higher order MIMO would only achieve the theoretical gains if used under extremely good radio channel conditions, a fact that is already reflected on the correction factors, used in the data rate and MIMO models. The gains from using this upgrade are associated

with improvements in spectral efficiency. On the other hand, CA actually extends the available cell capacity of the system, by increasing the number of available RBs that can be allocated to users, in each sector. It is evidenced from the results that MIMO contributes to an increase in network capacity by improving the efficiency of user transmission performance, whereas CA improves capacity by directly increasing the number of RBs that can be allocated to each user, in every sector of the network.

Future work should concentrate on the main limitations of this thesis, in order to validate results and extend the analysis. Focus should be given to shorten the distance between simulations and field measurements results, approximating algorithms to the real schedulers. This is also related to the need of having additional data on the performance of higher order MIMO configurations, in order to validate the models and results, for instance, through field measurements. Moreover, a study of the technological and financial impacts, for operators, of introducing each of these LTE-A features should be continued, as it will certainly become a strategic topic for operators in Portugal and around the world.

More and more, operators are interested in prioritising modifications in the networks. Also, due to the fact that devices still need to evolve and penetrate the market, there will be a period of time where LTE-only and LTE-A users, along with previous generations' users, will coexist in the network. This thesis is limited by the assumption that all users have access to the same system features, lacking of results for mixed environments, closer to reality. However, as seen in results for high-load simulations, there is always a considerably large portion of users with performances limited by the existing cell resources, and not by the available functionalities, such as CA or MIMO. This means that average network capacity can still be incremented from using, alternately, two overlapped carriers, even if not aggregated for each user. On the other hand, higher order MIMO almost exclusively reflects on individual user performances, as seen in results. In this case, having a mixed distribution of LTE Release 8 and LTE-A users, the average network gains will be smaller, due to the portion of users that does not benefit from higher order transmission schemes. These conclusions may indicate a wiser investment on using multiple overlapped carriers per BS, to improve average network capacity, instead of concentrating technological and financial resources on obtaining increased peak performances, with higher order MIMO.

Annex A

LTE-A UE Categories

This annex presents additional information on LTE-A, regarding the device categories.

LTE uses UE categories or classes to define the performance specifications and enable BSs to communicate effectively with them knowing their performance levels. Table A.1 characterises the different device categories that were standardised for LTE-A UEs, including maximum number of transmission layers, maximum supported modulation and maximum data rates, for both DL and UL directions.

Table A.1 – LTE-A device categories (adapted from [AGIL11]).

	UE Category							
	1	**2**	**3**	**4**	**5**	**6**	**7**	**8**
Max. DL MIMO layers supported	2	2	2	2	4	4	4	8
Max. UL MIMO layers supported	1	2	2	2	4	4	4	4
DL support for 64-QAM modulation	✓	✓	✓	✓	✓	✓	✓	✓
UL support for 64-QAM modulation	-	-	-	-	✓	-	-	✓
Max. DL data rate [Mbit/s]	10	50	100	150	300	300	300	1200
Max. UL data rate [Mbit/s]	5	25	50	50	75	50	150	600

Annex B

Radio Link Budget

This annex presents the link budget calculation regarding propagation between the transmitter and receiver, in DL, through the calculation of the losses along the link.

The Radio Link Budget (RLB) is a necessary tool for coverage planning, giving an estimate of the allowed signal attenuation between the BS and the mobile, in DL. The maximum path loss calculation is based on the required SINR at the receiver, taking into account a set of parameters related to the system's gains and losses as well as environment noise and interference. The considered procedure is in accordance with the RLB suggested in [Corr13], including the estimation of the path loss, based on COST-231-Walfisch-Ikegami model, and the computation of the SINR, at RB level.

The signal power at the receiving antenna can be expressed by:

$$P_{r_{[\mathrm{dBm}]}} = P_{t_{[\mathrm{dBm}]}} + G_{t_{[\mathrm{dBi}]}} + G_{r_{[\mathrm{dBi}]}} - L_{p_{[\mathrm{dB}]}} \tag{B.1}$$

where:

- L_p: path loss.

The power fed to the transmitting antenna in the DL is given by:

$$P_t^{DL}{}_{[\mathrm{dBm}]} = P_{Tx_{[\mathrm{dBm}]}} - L_{c_{[\mathrm{dB}]}} \tag{B.2}$$

where:

- P_{Tx}: transmitter output power;
- L_c: losses in the cable between the transmitter and the antenna.

The power at the receiver, in the DL, is then obtained from:

$$P_{Rx_{[\mathrm{dBm}]}} = P_r^{DL}{}_{[\mathrm{dBm}]} - L_{u_{[\mathrm{dB}]}} \tag{B.3}$$

where:

- P_r^{DL}: power at the Rx antenna, in DL;
- L_u: losses in the UE.

The path loss can be expressed by:

$$L_{p_{[\mathrm{dB}]}} = L_p^{COST\ 231\ WI}{}_{[\mathrm{dB}]} + L_p^{environment}{}_{[\mathrm{dB}]} + M_{SF_{[\mathrm{dB}]}} \tag{B.4}$$

where:

- $L_p^{COST\ 231\ WI}$: path loss from the COST 231-Walfish-Ikegami model;
- $L_p^{environment}$: path loss due to the user specific environment;
- M_{SF}: slow fading margin.

The SNR can be computed using the obtained value of the received signal power and the total noise power at the receiver, according to (B.5):

$$\rho_{N_{[\mathrm{dB}]}} = P_{Rx_{[\mathrm{dBm}]}} - N_{[\mathrm{dBm}]} \tag{B.5}$$

where:

- N: noise power at the receiver.

The total noise power can be obtained from:

$$N_{[\mathrm{dBm}]} = -174 + 10\log_{10}\left(\Delta \mathrm{f}_{[\mathrm{Hz}]}\right) + F_{N\,[\mathrm{dB}]} \tag{B.6}$$

where:

- Δf: signal bandwidth, taken as the chip rate, R_c;
- F_N: noise figure.

The SINR calculation is just an extension from (B.5), which adds the interference term:

$$\rho_{IN\,[\mathrm{dB}]} = P_{Rx\,[\mathrm{dBm}]} - (I + N)_{[\mathrm{dBm}]} \tag{B.7}$$

where:

- I: interference power.

For coverage estimation purposes, the LTE receiver sensitivity (*i.e.*, minimum power at the receiver) can be approximately defined by [Zhan10]:

$$P_r^{ref}{}_{[\mathrm{dBm}]} = \rho_N^{ref}{}_{[\mathrm{dB}]} - N_{[\mathrm{dBm}]} + L_{u\,[\mathrm{dB}]} + M_{I\,[\mathrm{dB}]} \tag{B.8}$$

where:

- ρ_N^{ref}: average required SNR associated with the specified reference service throughput;
- M_I: implementation margin.

The average SNR associated to a specific reference service is obtained using the SNR-to-throughput mapping functions in Annex D.

Annex C

COST 231-Walfisch-Ikegami

This annex presents the propagation model used to calculate the path loss in the urban environment.

Path loss is calculated using the COST 231-Walfisch-Ikegami Model, proposed by the COST 231 group for micro and macro cells. It combines the Ikegami and Walfisch-Bertoni models and extends the COST 231-Hata Model by considering additional characteristics of the urban environment. The main parameters are depicted in Figure C.1, representing the default situation.

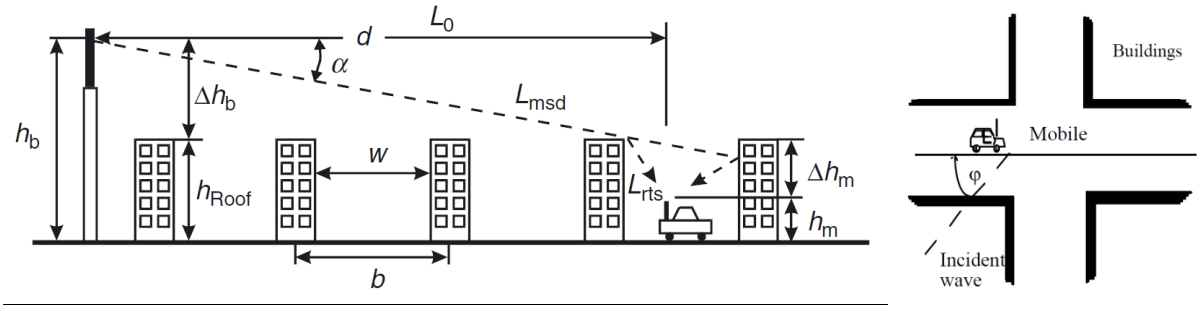

(a) Typical urban propagation scenario (b) Street orientation angle φ

Figure C.1 – COST 231-Walfisch-Ikegami Model diagram and parameters (extracted from [Moli11] and [CiKu96]).

The COST 231-Walfisch-Ikegami Model distinguishes between the LoS and NLoS cases, according to the description provided in [CiKu96]. For LoS propagation, the path loss between BS and MT, with a street orientation angle $\varphi = 0°$, according to Figure C.1.b), is given by:

$$L_p^{LoS}{}_{[\mathrm{dB}]} = 42.6 + 26 \log d_{[\mathrm{km}]} + 20 \log f_{c\,[\mathrm{MHz}]}, \quad \text{for} \quad d \geq 0.02 \text{ km} \tag{C.1}$$

where:

- d: horizontal distance between the BS and the MT;
- f_c: frequency carrier of the signal.

For NLoS propagation along a street (also for $\varphi = 0°$), path loss is given by:

$$L_p^{NLoS}{}_{[\mathrm{dB}]} = \begin{cases} L_{0\,[\mathrm{dB}]} + L_{rts\,[\mathrm{dB}]} + L_{msd\,[\mathrm{dB}]}, & \text{for} \quad L_{rts} + L_{msd} > 0 \\ L_{0\,[\mathrm{dB}]}, & \text{for} \quad L_{rts} + L_{msd} \leq 0 \end{cases} \tag{C.2}$$

where:

- L_0: free-space propagation path loss;
- L_{rts}: loss between the last rooftop and the MT (rooftop-to-street diffraction and scatter loss);
- L_{msd}: loss between the BS and the last rooftop (multi-screen loss).

The free-space path loss is given by:

$$L_{0\,[\mathrm{dB}]} = 32.45 + 20 \log d_{[\mathrm{km}]} + 20 \log f_{c\,[\mathrm{MHz}]} \tag{C.3}$$

The loss between the last rooftop and the MT is given by:

$$L_{rts_{[\mathrm{dB}]}} = -16.9 - 10\log w_{[\mathrm{m}]} + 10\log f_{c_{[\mathrm{MHz}]}} + 20\log \Delta h_{m_{[\mathrm{m}]}} + L_{ori_{[\mathrm{dB}]}} \quad \text{(C.4)}$$

where:

- w: width of the streets;
- Δh_m: difference between the buildings height, h_{Roof}, and the height of the MT, h_m;
- L_{ori}: street orientation correction factor.

The orientation of the street is taken into account by the empirical correction factor given by:

$$L_{ori_{[\mathrm{dB}]}} = \begin{cases} -10.0 + 0.354\varphi_{[°]} \quad , & \text{for } 0° \leq \varphi \leq 35° \\ 2.5 + 0.075(\varphi_{[°]} - 35), & \text{for } 35° \leq \varphi \leq 55° \\ 4.0 - 0.114(\varphi_{[°]} - 55), & \text{for } 55° \leq \varphi \leq 90° \end{cases} \quad \text{(C.5)}$$

where:

- φ: angle between the street orientation and the direction of incidence of the signal, according to Figure C.1.b).

The loss between the BS and the last rooftop, or multi-screen loss, is obtained by modelling building edges as screens, as given by:

$$L_{msd_{[\mathrm{dB}]}} = L_{bsh_{[\mathrm{dB}]}} + k_a + k_d \log d_{[\mathrm{km}]} + k_f \log f_{c_{[\mathrm{MHz}]}} - 9\log b_{[\mathrm{m}]} \quad \text{(C.6)}$$

where:

- L_{bsh}: loss due to the height difference between the rooftop and the antennas;
- k_a: increase of path loss for the BS antennas below the roof tops of the adjacent buildings;
- k_d: dependence of the multi-screen diffraction loss versus distance;
- k_f: dependence of the multi-screen diffraction loss versus frequency;
- b: buildings separation distance.

The loss due to the height difference between the rooftop and the antennas is given by:

$$L_{bsh_{[\mathrm{dB}]}} = \begin{cases} -18\log\left(1 + \Delta h_{b_{[\mathrm{m}]}}\right), & \text{for } h_b > h_{Roof} \\ 0 \quad , & \text{for } h_b \leq h_{Roof} \end{cases} \quad \text{(C.7)}$$

where:

- Δh_b: difference between the height of the BS, h_b, and the height of the buildings, h_{Roof};

The remaining parameters in (C.6) are given by:

$$k_a = \begin{cases} 54 \quad , & \text{for } h_b > h_{Roof} \\ 54 - 0.8\Delta h_{b_{[\mathrm{m}]}}, & \text{for } d \geq 0.5\mathrm{km} \text{ and } h_b \leq h_{Roof} \\ 54 - 1.6\Delta h_{b_{[\mathrm{m}]}}, & \text{for } d < 0.5\mathrm{km} \text{ and } h_b \leq h_{Roof} \end{cases} \quad \text{(C.8)}$$

$$k_d = \begin{cases} 18 & , \quad \text{for} \quad h_b > h_{Roof} \\ 18 - 15\dfrac{\Delta h_{b_{[\mathrm{m}]}}}{h_{Roof_{[\mathrm{m}]}}}, & \quad \text{for} \quad h_b \leq h_{Roof} \end{cases} \tag{C.9}$$

$$k_f = -4 + \begin{cases} 0.7\left(\dfrac{f_{c_{[\mathrm{MHz}]}}}{925} - 1\right), & \text{for urban and suburban scenarios} \\ 1.5\left(\dfrac{f_{c_{[\mathrm{MHz}]}}}{925} - 1\right), & \text{for dense urban scenarios} \end{cases} \tag{C.10}$$

This model assumes a Manhattan street grid (streets intersecting at right angles), constant building height, and flat terrain. The model does not include the effect of wave guiding through street canyons, which can lead to an underestimation of the received field strength [Jain07]. Moreover, it incorporates measure assessments in several European cities and provides a list of restricted ranges of parameters, where the measurement validation is guaranteed:

- $f_c \in [800,\ 2000]$ MHz;
- $d \in [0.02,\ 5]$ km;
- $h_b \in [4,\ 50]$ m;
- $h_m \in [1,\ 3]$

Although some of the frequency bands used by LTE are out of the model validation interval (*e.g.,* 2100 MHz and 2600 MHz bands), the COST 231-W-I Model still provides satisfactory results for urban and suburban propagation environments in these conditions. Therefore, it is assumed to be the default propagation (path loss) model for all studied scenarios.

The model takes a mean error in the range of ±3 dB and standard deviation from 4 to 7 dB. The error of the model increases as h_b decreases relatively to h_{Roof}.

In the absence of specific values, the following are recommended in [CiKu96]:

- $h_{Roof_{[m]}} = 3 \times \{\text{no. of floors}\} + \text{roof-height}$;
- $\text{roof-height} = \begin{cases} 3\ \mathrm{m}, & \text{pitched} \\ 0\ \mathrm{m}, & \text{flat} \end{cases}$;
- $b = 20 \ldots 50\ \mathrm{m}$;
- $w = b/2$;
- $\varphi = 90°$.

Annex D

SINR and Data Rate Models

This annex describes the adopted LTE-A link performance model and corresponding SINR-to-throughput mapping functions.

This annex presents the adopted LTE-A link performance model and corresponding expressions, used to model the relation between SNR/SINR and throughput, over the existing links in the system. The obtained expressions were adapted from a semi-empirical LTE Link Performance Model [OPT13] and updated DL performance results, issued by the 3GPP. These results refer to periodic trial measurements collected from several 'players' in the Telecommunications Industry, such as operators, manufacturers and hardware suppliers, being supervised by the 3GPP.

Both Optimus' semi-empirical model and the measurements from 3GPP are referenced to the ITU-R defined channel models [ITUR97]. These are responsible for the association of extended wideband models with low, medium, and large delay spread values. Moreover, the key parameters used to describe each ITU channel model include time delay spread and its statistical variability; path loss and shadow fading characteristics; multipath fading characteristics; and operating radio frequency. The mentioned parameters provide tapped delay line propagation conditions and Power Delay Profile (PDP), required for a complete characterisation of the different channel models. Low delay spread scenarios mostly relate to the Extended Pedestrian A (EPA) model, which can be used to represent small cell and indoor cases, while medium and large delay spreads are generally associated with the Extended Vehicular A (EVA) and Extended Typical Urban (ETU) models [SeTB11]. The extended channel models are only fully characterised when associated with a Doppler shift, being 5 Hz, 70 Hz and 300 Hz the most common cases.

The obtained LTE-A link performance model is primarily based on the semi-empirical parameterised expressions, provided in [Opti13] for LTE systems, which consider the relationship between throughput per resource block, R_{RB}, and SNR/SINR, ρ_{SNR} or ρ_{SINR}. Then, some of the semi-empirical coefficients in these expressions were adapted to fit the updated measurement results issued by the 3GPP [3GPP11]. These refer to data rate performance results, obtained at the physical layer, for three different test cases, all using the recent LTE-A Transmission Mode 9 (TM9) with a 2×2 MIMO scheme:

- Case 1: SU-MIMO 2×2 Rank-1, QPSK 1/3;
- Case 2: SU-MIMO 2×2 Rank-1, 16-QAM 1/2 ;
- Case 3: MU-MIMO 2×2 Rank-2, 64-QAM 1/2.

The 3GPP results were used to obtain fitted expressions for the maximum achievable bitrate per RB, at the physical layer, considering the three available cases of transmission. For each entered value of SNR/SINR, one obtains the maximum achievable throughput by taking the maximum value among the three case expressions. Figure D.1 shows a sweeping of the throughput per RB results for a range of SINR values between -12 dB and 50 dB, which are taken as the minimum and maximum limits of the receiver's sensitivity. A maximum bitrate of 1.48 Mbit/s per RB can be obtained under extremely good radio conditions (SINR ≥ 50 dB). The presented bitrate values report to the physical layer throughput that can be achieved, considering typical control and signalling overhead, as described in Section 3.1.3. Comparing to the theoretical maximum of 2.016 Mbit/s per RB for a MIMO 2×2 configuration, according to Table 2.2, one can see that only about 75% is achieved, matching the predicted overhead losses.

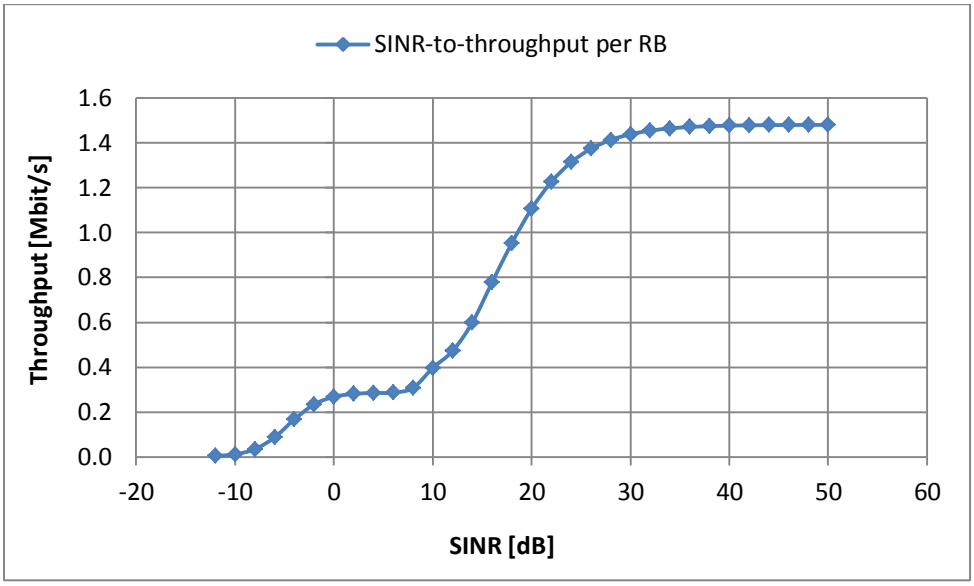

Figure D.1 – SINR-to-throughput per RB results obtained from the LTE-A eDL-MIMO performance tests in [3GPP11].

The semi-empirical expressions recommended in [Opti13] include simulated results for the following LTE DL cases:

- Transmission modes: TM1, TM2, TM3, TM4.
- Modulation schemes: QPSK, 16-QAM, 64-QAM.
- Channel models: EPA 5 Hz, EVA 70 Hz and ETU 300 Hz.
- Bandwidth: 1.4 MHz and 10 MHz (representing all bandwidths except 1.4 MHz).

Table D.1 characterises the three adopted channel models in terms of the maximum Doppler frequency shift and maximum delay spread. It is important to note that only the first two will be considered relevant in this thesis, given the non-presence of users in high-speed scenarios, such as in highways or trains.

Table D.1 – Channel models characterisation in terms of the Doppler frequency shift and delay spread (adapted from [SeTB11]).

Channel Model	Doppler frequency [Hz]	Delay Spread [ns]
EPA 5Hz	5 (low)	43 (low)
EVA 70Hz	70 (medium)	357 (medium)
ETU 300Hz	300 (high)	991 (high)

Optimus' proposed model also includes link curve parameters associated with different antenna configurations, in particular, 2×2 and 4×4 schemes. A number of coefficients and correction factors are available and should be used accordingly by the model, in order to introduce the correct gains related to each configuration.

The bitrate calculation is done using (D.1):

$$\begin{cases} R_{RB\,[\mathrm{Kbit/s}]} = max\left[0, a_3 + (a_0 - a_3)\cdot e^{-\ln(2)\cdot\left[\left(\rho_{[\mathrm{dB}]}-a_1\right)/a_2\right]^{a_4}}\right], & \rho < a_1 \\ R_{RB\,[\mathrm{Kbit/s}]} = a_0 & , \quad \rho \geq a_1 \end{cases} \tag{D.1}$$

where a_0, a_1, a_2, a_3 and a_4 are fitted coefficients and the SNR/SINR, ρ, is expressed in dB. In particular, the semi-empirical coefficient a_0 represents the maximum achievable bitrate in one resource block, considering control and signalling overhead.

The inverse relationship is used to obtain the SINR for a given throughput:

$$\rho_{[\mathrm{dB}]} = a_1 - a_2\left[\log_2\left(\frac{a_0 - a_3}{R_{RB\,[\mathrm{Kbit/s}]} - a_3}\right)\right]^{1/a_4} \tag{D.2}$$

Both the a_0 and a_3 coefficients have to be adjusted with respect to the control channel configuration, according to

$$a_0 = a_{0,max}\cdot\left[1 - \frac{n_{PDCCH}}{14} - \frac{n_{CRS}}{168} - \frac{48 - n_{ant,DL}}{140 n_{RB}}\right] \tag{D.3}$$

$$a_3 = a_{3,max}\cdot\left[1 - \frac{n_{PDCCH}}{14} - \frac{n_{CRS}}{168} - \frac{48 - n_{ant,DL}}{140 n_{RB}}\right] \tag{D.4}$$

where:

- $a_{0,max}, a_{3,max}$: maximum theoretical bitrates, without considering control and signalling overhead;
- n_{PDCCH}: number of allocated symbols for PDCCH, 1 to 3 for bandwidths larger than 1.4 MHz and 2 to 4 for 1.4 MHz.
- n_{CRS}: number of cell-specific Reference Signals multiplexed with PDSCH per RB. It takes values according to Table D.2.
- $n_{ant,DL}$: number of configured antenna ports.
- n_{RB}: total number of RBs for the deployed bandwidth.

Table D.2 shows the values adopted for the n_{CRS} parameter when using different antennas configurations. Table D.3 shows the values for the different semi-empirical parameters considered in the previous equations. These values were extracted from the tables recommended in [Opti13], with the exception of the $a_{0,max}$ coefficient, which was adapted to fit the maximum bitrates to the updated results from 3GPP.

In order to obtain the link performance for higher order MIMO schemes, the coefficients for the corresponding 2×2 configuration are selected from Table D.3 and corrected accordingly. When using MIMO 4×4, the a_1 coefficient is reduced by 2.9 dB and a correction factor is added to the obtained 2×2 bitrate, according to [Opti13]. This compensation factor depends on the transmission mode and can be

consulted in Table D.4.

Table D.2 – Number of Cell Reference signals multiplexed with PDSCH per RB.

Configuration	n_{CRS}
$n_{ant,DL} = 1$	6
$n_{ant,DL} = 2$	12
$n_{ant,DL} = 4$ and $n_{PDCCH} = 1$	20
$n_{ant,DL} = 4$ and $n_{PDCCH} = 1$	16
$n_{ant,DL} = 8$	16

Table D.3 – Semi-empirical parameters for DL.

Transmission mode	TM1		TM2		TM3		TM4	
Channel model	**EPA 5**	**EVA 70**	**EPA 5**	**EVA 70**	**EPA 5**	**EVA 70**	**EPA 5**	**EVA 70**
$a_{0,max}$ **[kbit/s]**	1004.3	1003.4	1047.7	1047.1	1846.6	1677.2	1866.8	1627.4
a_1 **[dB]**	44.3	49.0	43.7	46.6	56.8	59.4	58.6	62.9
a_2 **[dB]**	34.2	36.5	33.9	35.2	41.0	42.4	43.1	44.5
$a_{3,max}$ **[kbit/s]**	0	0	0	0	0	0	0	0
a_4	4	4	4	4	4	4	4	4

Table D.4 – 2×2 to 4×4 capacity correction factors, averaged over channel model and bandwidth.

Transmission mode	Correction factor
TM2	54%
TM3, TM4	35%

When using MIMO 8×8, the a_1 coefficient is also reduced by 2.9 dB, whereas the capacity correction factor is obtained from the Relative MIMO Gain Model, described in Annex E. This model defines a way for computing distance-dependent capacity gains for MIMO schemes. Since MIMO 8×8 is the only arrangement that is not contemplated in Optimus' model, the RMG will only be used for this particular case. Thus, the throughput is calculated using Optimus' model, for the corresponding 4×4 configuration, and then a compensation factor is added based on the relative gain between a MIMO 8×8 scheme and a 4×4 scheme. The former is divided by the latter, providing an approximate capacity compensation factor between both schemes.

Annex E

Considerations on MIMO

This annex describes MIMO related aspects that were considered in this thesis, as well as the Relative MIMO Gain Model used in the calculations for the throughputs.

In terms of antenna configuration in an LTE system, there are four different types of transmission schemes: SISO, MISO, SIMO and MIMO. SIMO configurations are used for transmit diversity, whereas MIMO schemes are mostly intended for spatial multiplexing gains over transmission.

The performance of MIMO depends on a number of factors, such as the radio channel conditions (*e.g.* low versus high scattering), signal quality (measured by the SINR), the speed of the MT, and the correlation between received signals. Therefore, different MIMO modes will be more effective than others, depending on these critical factors [Carr11].

The number of spatial layers used in the wireless channel is a key aspect of MIMO, allowing one to improve spectral efficiency. Spatial layers take advantage of the multipath and scattering environment between transmitters and receivers. Simultaneously, the increase in data rate of a MIMO system is linearly proportional to the minimum number of transmit and receive antennas, subject to the rank limit, *i.e.*, number of independent spatial layers. For instance, in plain LoS conditions the channel matrix rank is one and hence, even with 4 antennas, the spectral efficiency of the channel does not increase. Therefore, the model should be able to account for the possibility of spatial multiplexing scenarios with limited increase in data rates, thus limiting the overall gain of the corresponding MIMO scheme.

The difference between using rank-1 and rank-2 transmission, in a system with two receiving antennas, can be seen by comparing the SINR levels with a reference SINR, measured at one single antenna. The rank-1 SINR corresponds to the one measured after combining the signals received by the two antennas, whereas the rank-2 SINR is the one measured separately for each MIMO stream (layer). On one hand, when using rank-1 transmission one is generally using a receive (or transmit) diversity scheme, adequate for poor radio channel conditions, due to the fact that it allows obtaining higher combined SINRs. On the other hand, when using rank-2 transmission two streams are employed and thus, being the transmit signal power divided in two, the measured rank-2 SINR will be lower than the average SINR. This case is only adequate for good channel conditions, providing for higher transmission rates, due to the use of two data streams.

The 9 transmission modes defined for LTE-A, in DL, allow to take advantage of the different types of diversity gain and MIMO techniques. Table E.1 offers a brief description for each transmission mode.

The link performance model used in this thesis only considers results from the first 4 LTE modes, TM1, TM2, TM2 and TM4, modes, plus the TM9, introduced in Release 10. The first mode corresponds to transmitting a single data stream by one antenna and receiving it either by one or multiple antennas (*i.e.*, SISO and SIMO, respectively). The second mode corresponds to transmitting the same information over multiple antennas (2 or 4), being the information coded differently on each antenna, using Space-Frequency Block Codes (SFBCs). Although it does not offer improved peak data rates, being a single-layer transmission mode, it implies better signal quality due to higher robustness and lower SINR is required to decode the signal. Both modes 3 and 4 correspond to SU-MIMO schemes, with two or four antennas in the DL, and supporting up to four transmission layers. Transmission mode 9 (TM9) extends the concept of MIMO to 8 layers transmission, supporting both SU-MIMO and MU-MIMO and the possibility of switching between the two, dynamically.

Table E.1 – DL transmission modes (extracted from [Cox12]).

TM	Description
1	Single antenna transmission
2	Open loop transmit diversity
3	Open loop spatial multiplexing
4	Closed loop spatial multiplexing
5	Multi-User MIMO
6	Closed loop transmit diversity
7	Beamforming
8	Dual layer beamforming
9	Eight layer spatial multiplexing (LTE-A)

Since MIMO 8×8 is still a recent development in LTE systems, the resulting improvements in capacity are not yet well-established and can only be estimated resorting to approximate models, using relative gains. The Relative MIMO Gain (RMG) Model is used in this thesis and relates the capacity from different antenna schemes, such as 2×2, 4×4 and 8×8, with that of a SISO scheme, according to (E.1). The description of this model is presented below, based in [KuCo07], and relies on simulation results for different multi-antenna configurations, using a MIMO radio channel simulator based on the Geometrically Based Single Bounce (GBSB) channel model [Pire12]:

$$G_{M/S} = \frac{C_{MIMO}}{C_{SISO}} \tag{E.1}$$

where:

- C_{MIMO}: capacity (bit rate) of a MIMO scheme;
- C_{SISO}: capacity (bit rate) of a SISO scheme.

According to [KuCo08], the distribution of the MIMO capacity gain can be modelled by sigmoid functions, which are completely defined by their mean and variance. Both these parameters depend on the number of transmitting and receiving antennas and on the distance between them, and can be consulted in Table E.2 and Table E.3 for different antenna configurations. These are mostly based on the information provided in [KuCo08] and completed with the results obtained in [WAFJ12], regarding the average gains of MIMO 8×8 transmission.

Table E.2 – Mean values (μ_{RMG}) for 4×4 and 8×8 antenna configurations and for different cell types (adapted from [KuCo08]).

$N_T \times N_R$	Range [m]	μ_{RMG}	$\overline{\varepsilon_r}$ [%]	$\overline{\varepsilon_r{}^2}$ [%]
$\mathbf{4 \times 4}$	< 10	2.27	-0.1	0.1
	$10 - 31$	$50.32 d_{[km]} + 1.77$		
	$31 - 57$	3.36		
	$57 - 686$	$-2.00 d_{[km]} + 3.47$	-0.1	0.4
	> 686	2.10		
$\mathbf{8 \times 8}$	< 10	4.46	-0.1	0.1
	$10 - 29$	$117.59 d_{[km]} + 2.11$		
	$29 - 59$	3.36		
	$59 - 703$	$-4.88 d_{[km]} + 5.86$	3.0	2.6
	> 703	2.42		

Table E.3 – Variance values for 4×4 and 8×8 antenna configurations and for different cell types (adapted from [KuCo08]).

$N_T \times N_R$	Cell Type	σ^2_{RMG} (10^{-3})
$\mathbf{4 \times 4}$	pico-cell	45.4
	micro-cell	71.4
	macro-cell	1.1
$\mathbf{8 \times 8}$	pico-cell	112.6
	micro-cell	137.4
	macro-cell	0.0

The realistic (statistical) RMG is obtained using (E.2):

$$g(u, \mu_{RMG}, \sigma_{RMG}) = \mu_{RMG}(d, N_T, N_R) - \frac{\sqrt{3\sigma_{RMG}{}^2(d, N_T, N_R)}}{\pi} \cdot \ln\left(\frac{1-u}{u}\right) \tag{E.2}$$

where:

- u: random value with uniform distribution, *i.e.*, $u = U[0,1]$;
- d: distance between MT and BS;
- μ_{RMG}: average RMG depending on the cell type (d) and antenna configuration (N_T, N_R);
- σ_{RMG}: Standard deviation depending on the cell type (d) and antenna configuration (N_T, N_R);

- N_T: number of transmitting antennas;
- N_R: number of receiving antennas.

Then, using the same “relative gain” rationale, one can apply the ratio between the MIMO 8×8 and MIMO 4×4 gains to the throughputs obtained from the data rate model defined in Annex D. This allows to extrapolate the results of MIMO 8×8 transmission from those of MIMO 4×4, which is the highest order that can be obtained with the adopted data rate model:

$$R_b^{8\times8}{}_{[\mathrm{Mbit/s}]} = R_b^{4\times4}{}_{[\mathrm{Mbit/s}]} \cdot \frac{G_{RMG}^{8\times8}}{G_{RMG}^{4\times4}} \tag{E.3}$$

where:

- $R_b^{8\times8}$: throughput of a MIMO 8×8 scheme;
- $R_b^{4\times4}$: throughput of a MIMO 4×4 scheme (obtained from the Data Rate model);
- $G_{RMG}^{8\times8}$: RMG for a MIMO 8×8 scheme;
- $G_{RMG}^{4\times4}$: RMG for a MIMO 4×4 scheme.

Annex F

User’s Manual

This annex explains how to configure the simulator parameters and run a simulation.

To start the Network Deployment module, one must run the “LTE_A_Simulator.mbx” file and then select, when prompted, the following three input files, as Figure F.1 shows for the first selection:

- “Ant65deg.tab”, with information regarding BS antennas’ gain pattern;
- “DADOS_Lisboa.tab”, with the information regarding the city of Lisbon and its districts;
- “ZONAS_Lisboa.tab”, with some topographic information regarding the districts.

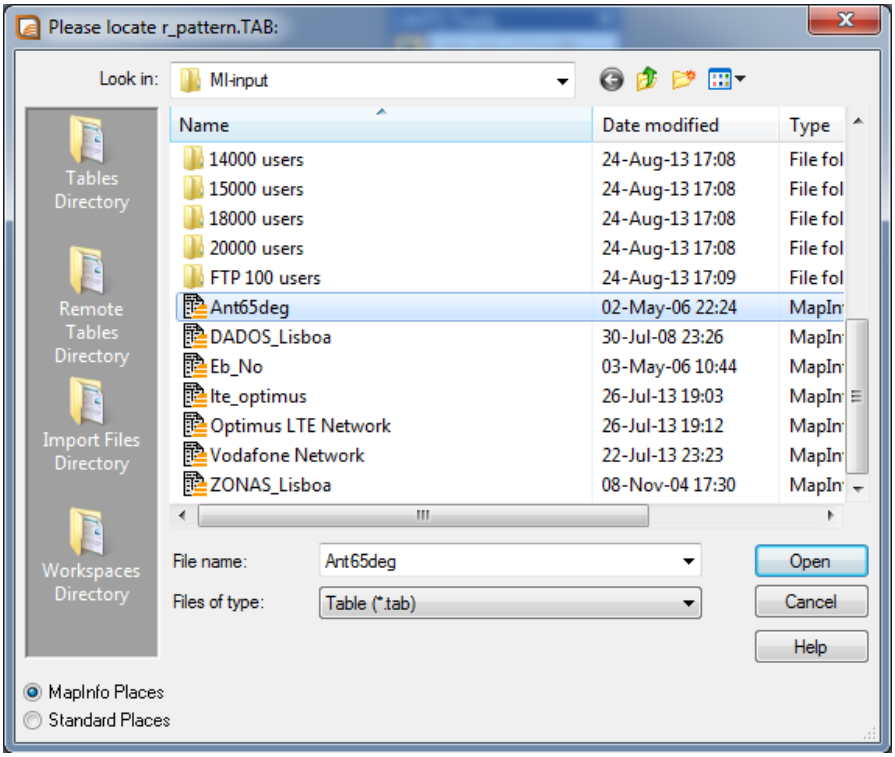

Figure F.1 – Window for the selection of the BS antennas’ pattern file.

After introducing the input files in the program, a map of Lisbon will appear in the centre and a tab named “System” will become available on top of the window. In that tab, one should access “LTE-DL”, as shown in Figure F.2, and then choose one of the options that will appear. These will open different windows, where it is possible to configure several parameters for the simulation. These will correspond to the ones established for the reference scenario.

The first window, shown in Figure F.3, corresponds to the configuration of the propagation model. Here, one can define the average dimensions and angles for the characterisation of the urban environment, according to the parameters of the propagation model, described in Annex C. The next window, “Traffic Properties”, allows one to define the priorities for the different data services, from a scale of 2 to 7.

The “Network Settings” option opens a window where the majority of the radio interface and algorithms parameters can be configured, as shown in Figure F.4. Most of the changes that had to be introduced in the Network Deployment module were done here, including the possibility of configuring CA, with up to three combinations of one frequency band, a certain number of CCs and a common bandwidth. There is also the possibility of selecting between MIMO 2×2, MIMO 4×4 or MIMO 8×8, as well as choosing the RB distribution algorithm, “Random”, “Sequential Selective” or “Random Selective”.

Besides these parameters, there are a number of others most of them were inherited from the previous works that started the development of this simulator.

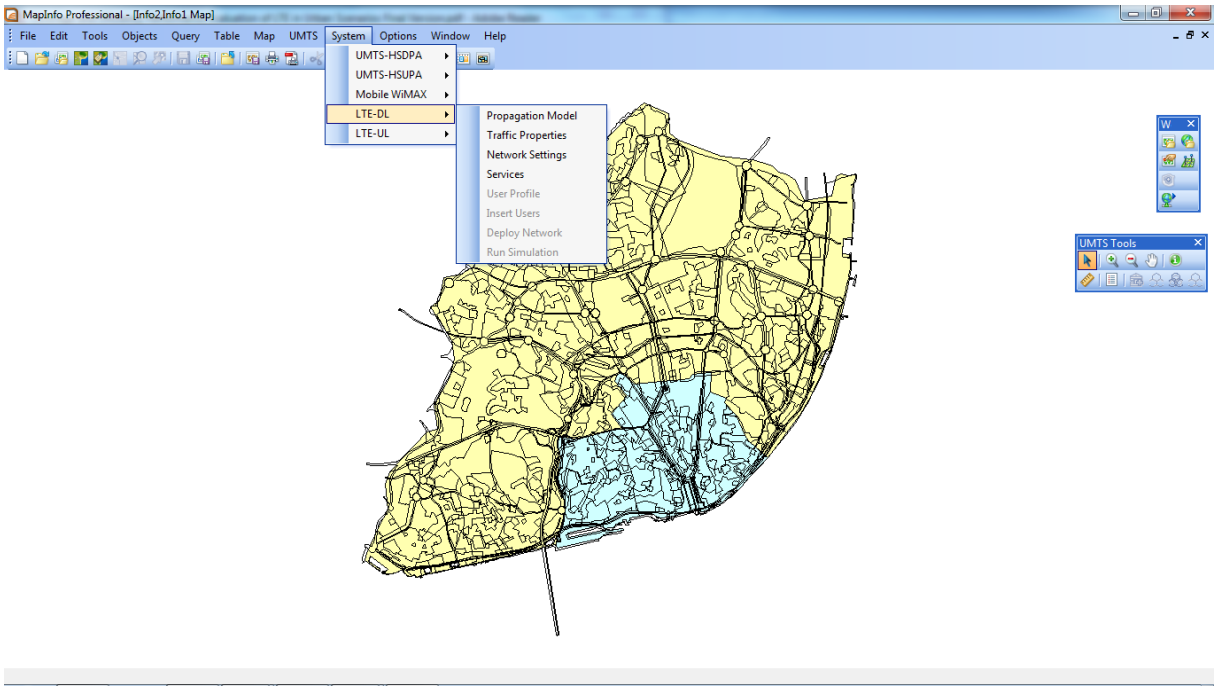

Figure F.2 – “LTE-DL” option in System tab.

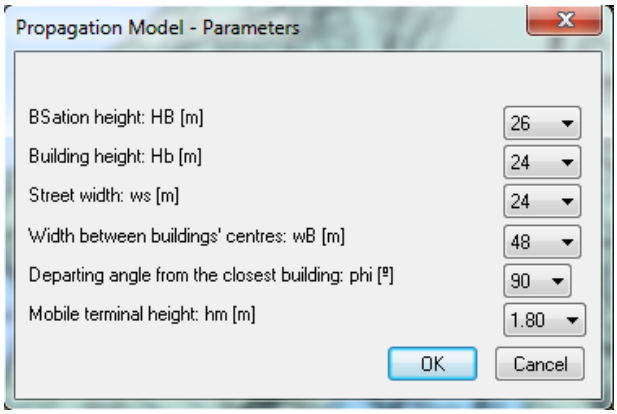

Figure F.3 – Propagation model parameters.

In the “User Profile” window, one can choose the minimum and maximum throughputs associated with each service, according to Figure F.5. Afterwards, the “Insert Users” tab becomes available, allowing one to select the input file that contains information on the mix of users. Multiple user files were generated using the Users Generator (SIM) program, going from mixes of less than 100 users up to 10000 users. Once this file is loaded into the program, users are represented by flags in the map, according to Figure F.6, each one with a colour associated to the service required.

The “Deploy Network” option becomes available after the users are loaded into the program, allowing one to select the file that contains the positions of the BSs. These coordinates have to be consistent with map files, previously introduced, in order to overlap the network with the map of the ROA and users loaded. A similar image to the one in Figure F.7 should be obtained, showing all these elements

overlaid together, as well as some red marks representing users that cannot be covered by the network. Furthermore, the “Run Simulation” option becomes available allowing one to call the Performance Analysis module, which will be responsible for generating the final results. At the end, three windows will appear, presenting some general statistics regarding the results of the simulation.

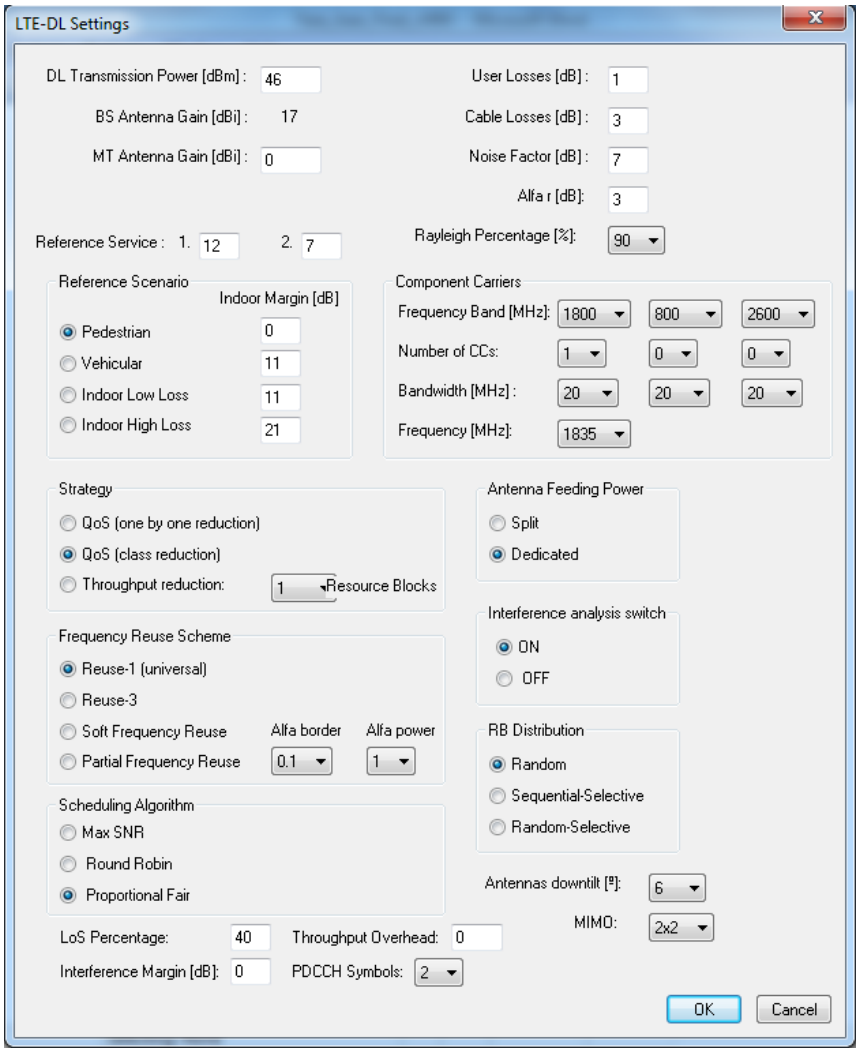

Figure F.4 – Network configuration parameters.

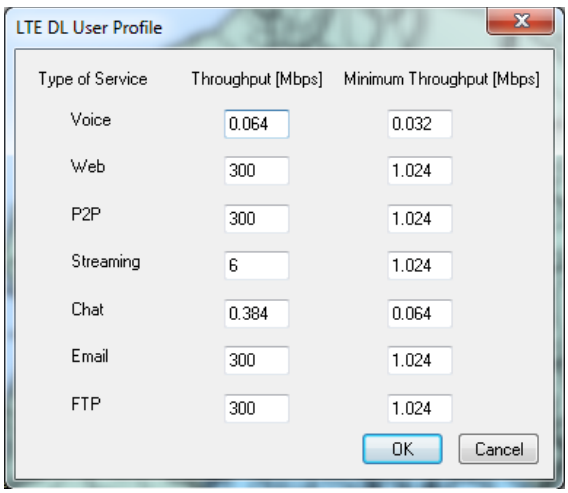

Figure F.5 – User profile parameters.

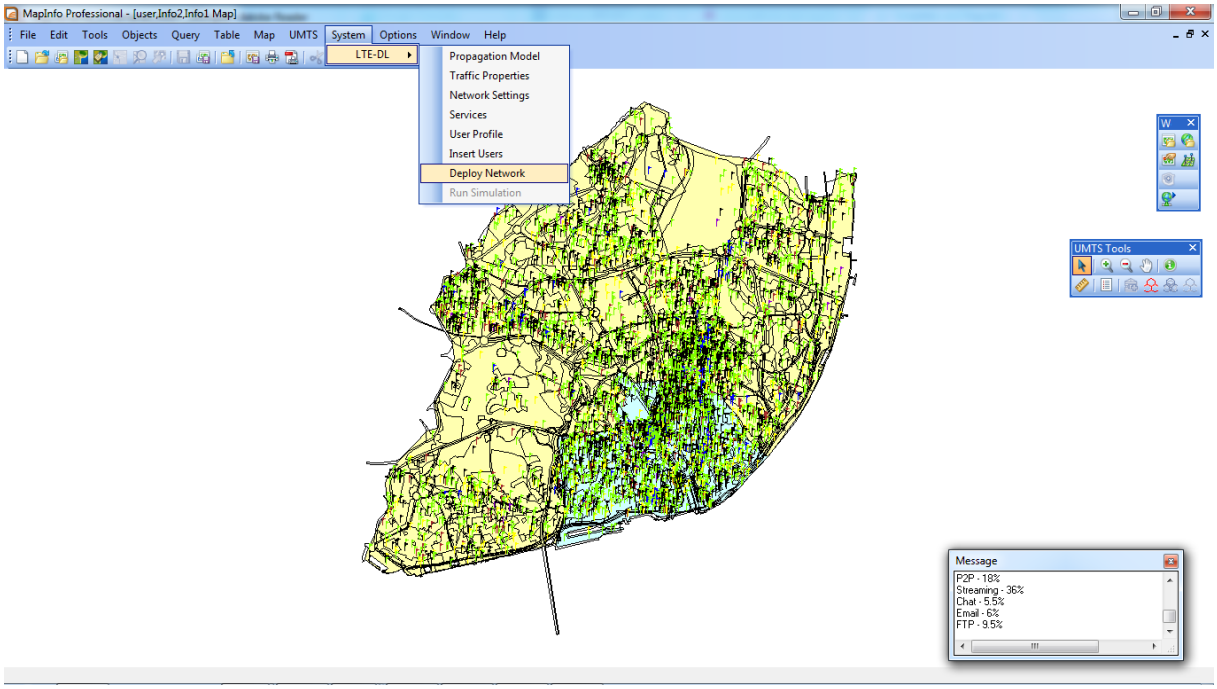

Figure F.6 – Users distribution over the city of Lisbon.

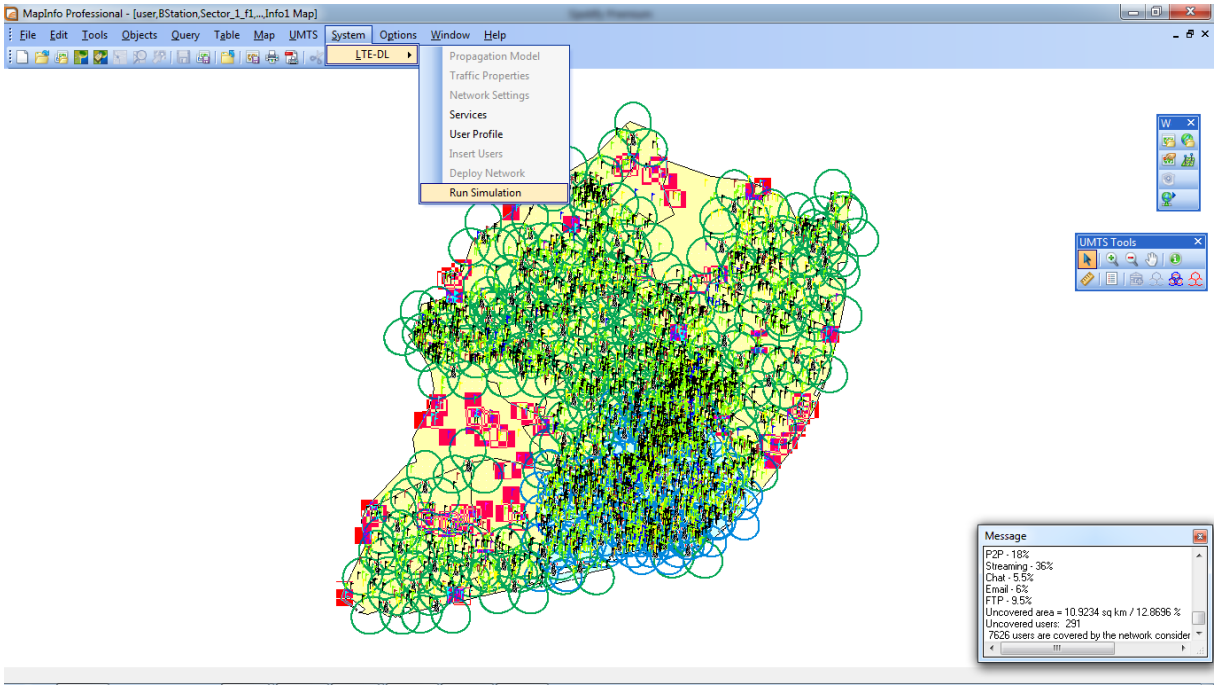

Figure F.7 – Run simulation command, after network being deployed.

Annex G

Additional Results

This annex contains additional results that were obtained the same way as those presented in Chapter 4, but are not presented there due to being less relevant or conclusive.

Concerning the use of different MIMO schemes, low-load simulated results show almost no difference in terms of the numbers of users, according to Figure G.1. Despite a slightly increase in the numbers of covered users, which is due to the coverage estimation algorithm, performed by the MapInfo module, the amount of served users remains practically the same as the reference, in both scenarios. This means that capacity is compensated in some other aspect of the network, as evidenced by the results of user throughput performance, presented in Figure 4.10.

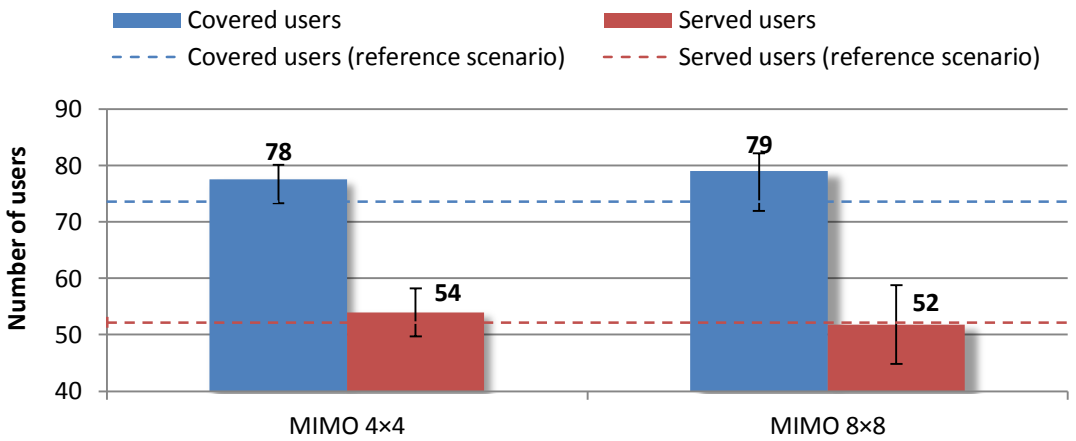

Figure G.1 – Number of covered and served users obtained for different MIMO configurations, in low-load conditions.

High-load simulation results are also presented for average number of users per BS and per sector, which showed almost no variation from the reference scenario, for both tested situations, according to Figure G.2. These results point for increases in average user performance, which were confirmed by the results presented in Chapter 4.

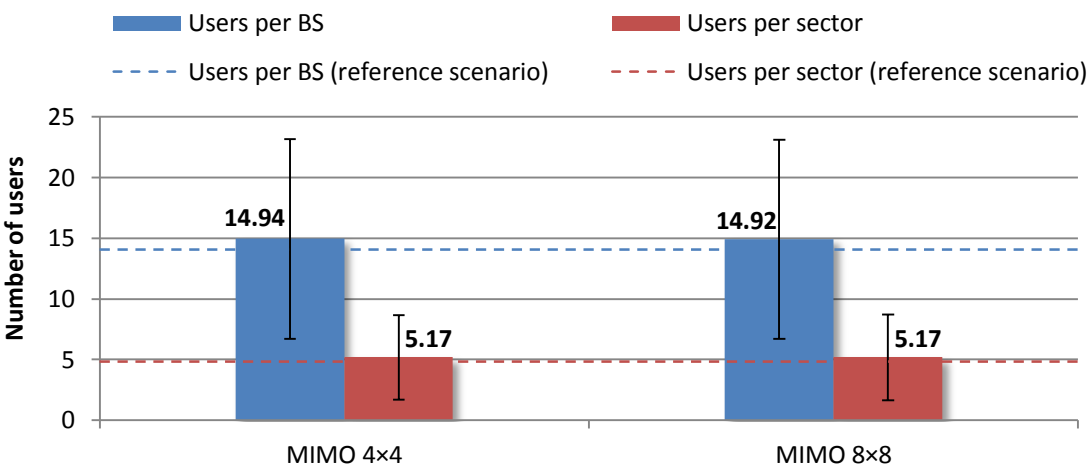

Figure G.2 – Average number of users per BS and per sector for different MIMO configurations, under heavy load conditions.

Regarding the results on average SNR and SINR levels for different MIMO configurations, it is important to understand that these reflect the impact of the coverage estimation algorithm, performed by the Network Deployment module. Since coverage is estimated based on the maximum distance

that a user can have in order to accomplish the reference throughput, performance efficiency due to higher order MIMO will have a direct impact on reference radii. In other words, by using higher order MIMO, users will be able to achieve the same throughputs at larger distances from the serving BSs. This will increase the reference coverage radii considered by the simulator, thus decreasing average user SNR and SINR levels. In general, users will be able to achieve the same performances with lower SINR levels, as shown in Figure G.3.

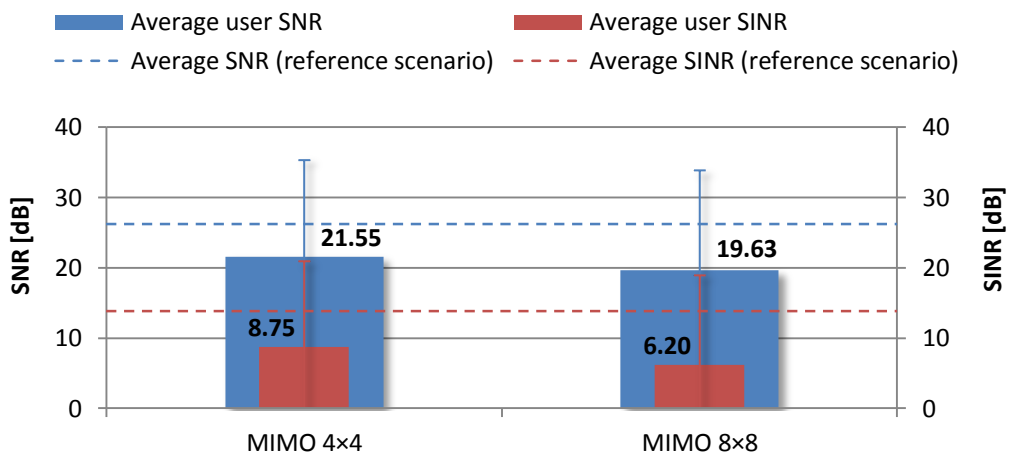

Figure G.3 – Average user SNR and SINR levels for different MIMO configurations, under heavy load conditions.

Figure G.4 shows that the choice of the RB distribution algorithm does not significantly impact average user performance. However, as stated in Chapter 4, these results can be influenced by an inadequate parameterisation of the algorithms, meaning that in order to produce significant results, one may have to explore variations in the reference coverage radii, using more restrictive conditions for the selective distribution of RBs along the spectrum.

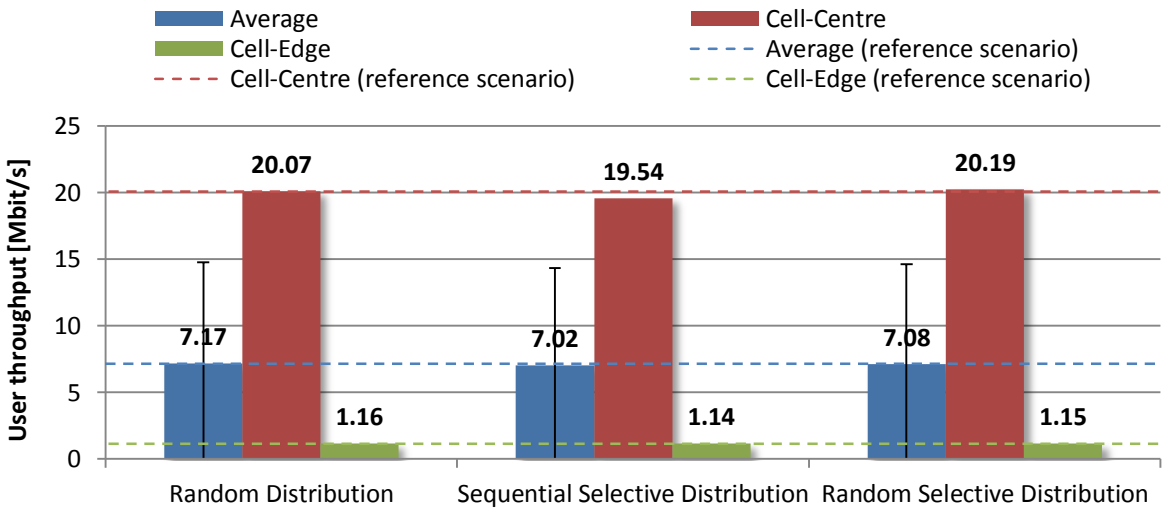

Figure G.4 – User throughput metrics for different RB distribution algorithms.

Despite what one could expect, average SNR and SINR levels do not vary much between the different RB distribution algorithms, according to Figure G.5. This can mean that there is not a sufficient number

of RBs being affected by the different use of the available frequency bands, which ends up resulting in the same average levels of interference and noise.

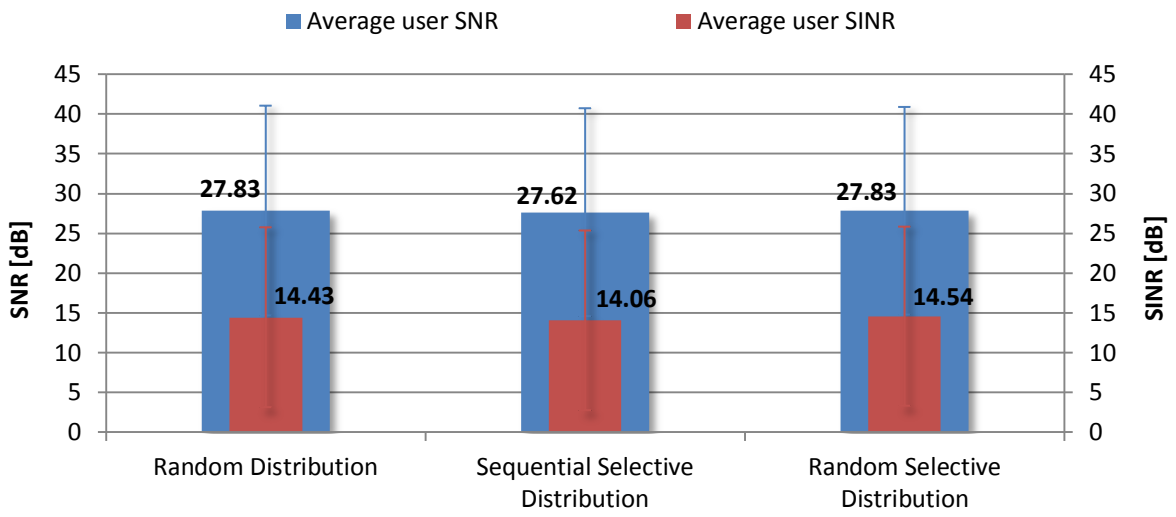

Figure G.5 – Average user SNR and SINR levels for different RB distribution algorithms.

The same inexpressive results were obtained for the average BS throughput capacity, as shown in Figure G.6, confirming that overall network capacity is not much affected by this aspect.

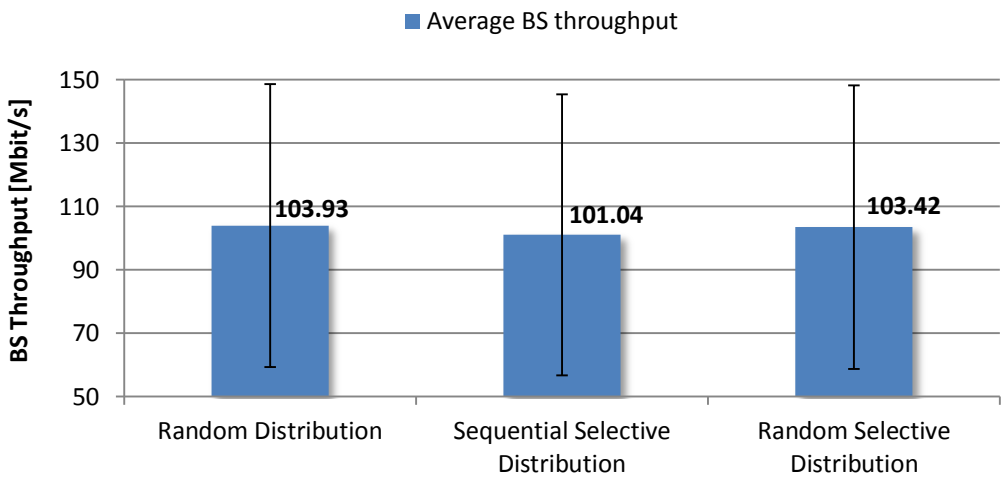

Figure G.6 – Average BS throughput for different RB distribution algorithms.

References

[3GPP10] 3GPP, *Universal Mobile Telecommunications System (UMTS); LTE; Requirements for Evolved UTRA (E-UTRA) and Evolved UTRAN (E-UTRAN) (Release 9)*, ETSI Technical Report, No. 25.913, Ver. 9.0.0, Feb. 2010 (http://www.3gpp.org/ftp/Specs/html-info/25913.htm).

[3GPP11] 3GPP, Technical Specification Group – Radio Access Network Working Group, *Simulation results for eDL-MIMO demodulation requirements*, Report R4-114209, Athens, Greece, Aug. 2011.

[3GPP12a] 3GPP, *LTE; Requirements for further advancements for Evolved Universal Terrestrial Radio Access; E-UTRA; LTE-Advanced (Release 11)*, ETSI Technical Report, No. 36.913, Ver. 11.0.0, Nov. 2012 (http://www.3gpp.org/ftp/Specs/html-info/36913.htm).

[3GPP12b] 3GPP, *Digital cellular telecommunications system (Phase 2+); Universal Mobile Telecommunications System (UMTS); LTE; Quality of Service (QoS) concept and architecture (Release 11)*, ETSI Technical Specification, No. 23.107, Ver. 11.0.0, Nov. 2012 (http://www.3gpp.org/ftp/Specs/html-info/23107.htm).

[3GPP12c] 3GPP, *LTE; Feasibility study for Further Advancements for E-UTRA; LTE-Advanced (Release 11)*, ETSI Technical Report, No. 36.912, Ver. 11.0.0, Oct. 2012 (http://www.3gpp.org/ftp/Specs/html-info/36912.htm).

[3GPP13a] 3GPP, *Digital cellular telecommunications system (Phase 2+); Universal Mobile Telecommunications System (UMTS); LTE; Policy and charging control architecture (Release 11)*, ETSI Technical Specification, No. 23.203, Ver. 11.8.0, Jan. 2013 (http://www.3gpp.org/ftp/Specs/html-info/23203.htm).

[3GPP13b] 3GPP, *LTE; Evolved Universal Terrestrial Radio Access (E-UTRA) and Evolved Universal Terrestrial Radio Access Network (E-UTRAN); Overall description; Stage 2 (Release 11)*, ETSI Technical Specification, No. 36.300, Ver. 11.5.0, Apr. 2013 (http://www.3gpp.org/ftp/Specs/html-info/36300.htm).

[3GPP13c] 3GPP, *LTE; Evolved Universal Terrestrial Radio Access (E-UTRA);Requirements for support of radio resource management (Release 11),* ETSI Technical Specification, No. 36.133, Ver. 11.5.0, Jul. 2013 (http://www.3gpp.org/ftp/Specs/html-info/36133.htm).

[3GPP13d] 3GPP, *LTE; Evolved Universal Terrestrial Radio Access (E-UTRA); User Equipment (UE) radio transmission and reception (Release 11)*, ETSI Technical Specification, No. 36.101, Ver. 11.5.0, Jul. 2013 (http://www.3gpp.org/ftp/Specs/html-info/36101.htm).

[AGIL11] Agilent Technologies, *Introducing LTE-Advanced*, Application Note, Mar. 2011 (http://cp.literature.agilent.com/litweb/pdf/5990-6706EN.pdf).

[AlLu08] Alcatel-Lucent, *Long Term Evolution (LTE) Overview*, White Paper, Oct. 2008 (http://www3.alcatel-lucent.com).

[BCDD13] Badic, B., Cattoni, A. F., Dieudonne, M., Duplicy, J., Fazekas, P., Kaltenberger, F., Kovács, I. Z., Vivier, G, *Advances in Carrier Aggregation and Multi- User MIMO for LTE-Advanced: Outcomes from SAMURAI project*, White Paper, Feb. 2013 (http://www.eurecom.fr/en/publication/3900/download/cm-publi-3900.pdf).

[BNCB12] Bhat, P., Nagata, S., Campoy, L., Berberana, Derham, T., Lui, G., Shen, X., Zong, P., Yang, J., "LTE-Advanced: An Operator Perspective", *IEEE Communications Magazine*, Vol. 50, No. 2, Feb. 2012, pp. 104-114.

[Card06] Cardeiro,J., *Optimisation of Base Station Location in UMTS-FDD for Realistic Traffic Distribution*, M.Sc. Thesis, Instituto Superior Técnico, Lisbon, Portugal, Mar. 2006..

[Carr11] Carreira, P., *Data Rate Performance Gains in UMTS Evolution to LTE at the Cellular Level*, M.Sc. Thesis, Instituto Superior Técnico, Lisbon, Portugal, Oct. 2011.

[CiKu96] Cichon, D. J., Kürner, T., "Propagation Prediction Models", in Damosso, E., COST 231 Action, *Digital Mobile Radio Towards Future Generation Systems*, COST 231 Final Report, Brussels, Belgium, 1996.

[Cisc13] Cisco, *Long-Term Evolution: Simplify the Migration to 4G Networks*, White Paper, Feb. 2013 (http://www.cisco.com).

[Corr13] Correia, L., *Mobile Communications Systems, Lecture Notes*, Instituto Superior Técnico, Lisbon, Portugal, 2013.

[Cox12] Cox, C., *An Introduction to LTE – LTE, LTE-Advanced, SAE and 4G Mobile Communications*, Wiley, Chichester, United Kingdom, 2012.

[DaPS11] Dahlman, E., Parkvall, S., Sköld, J., *4G LTE/LTE-Advanced for Mobile Broadband*, Academic Press, Oxford, United Kingdom, 2011.

[Duar08] Duarte, S., *Analysis of Technologies for Long Term Evolution in UMTS*, M.Sc. Thesis, Instituto Superior Técnico, Lisbon, Portugal, Sep. 2008.

[Eric11] Ericsson, *LTE: an introduction*, Lite Paper, Stockholm, Sweden, 2011 (http://www.ericsson.com/res/docs/2011/lte_an_introduction.pdf).

[Eric13a] Ericsson, *LTE Release 12 – Taking Another Step Toward The Networked Society*, White Paper, Jan. 2013 (http://www.ericsson.com/res/docs/whitepapers/wp-lte-release-12.pdf).

[Eric13b] Ericsson, *Ericsson Mobility Report – On The Pulse Of The Networked Society*, Report, June. 2013 (http://www.ericsson.com/res/docs/2013/ericsson-mobility-report-june-2013.pdf).

[Eric13c] Blennerud, G., "Mobile broadband – busting the myth of the scissor effect", *Ericsson Business Review*, No. 2, Jun. 2010, pp. 50-55.

[FCDY09] Farajidana, A., Chen, W., Damnjanovic, A., Yoo, T., Malladi, D., Lott, C., "3GPP LTE Downlink System Performance", in *Proc. of GLOBECOM'09 – IEEE Global Telecommunications Conference*, Honolulu, USA, Nov. 2009.

[HNHI10] Hiramatsu, K., Nakao, S., Hoshino, M., Imamura, D., "Technology Evolutions in LTE/LTE-Advanced and Its Applications", in *Proc. of ICCS'10 – IEEE International Conference on Communication Systems*, Singapore, Nov. 2010.

[HoTo11] Holma, H., Toskala,A., *LTE for UMTS – Evolution to LTE-Advanced Second Edition*, Wiley, Chichester, United Kingdom, 2011.

[IkWR10] Ikuno, J.C., Wrulich, M., Rupp, M., "System Level Simulation of LTE Networks", in *Proc. of VTC'10 – 71st IEEE Vehicular Technology Conference*, Taipei, Taiwan, May 2010.

[ITUR08a] ITU-R, *Requirements related to technical performance for IMT-Advanced radio interface(s)*, ITU-R Report, No. M.2134, Nov. 2008 (http://www.itu.int/pub/R-REP-M.2134-2008/en).

[ITUR08b] ITU-R, *Guidelines for evaluation of radio interface technologies for IMT-Advanced*, ITU-R Report, No. M.2135-1, Dec. 2008 (http://www.itu.int/pub/R-REP-M.2135-2008/en).

[ITUR97] ITU-R, *Guidelines for evaluation of radio transmission technologies for IMT-2000*, ITU-R Report, No. M.1225, Feb. 1997 (http://www.itu.int/rec/R-REC-M.1225/en).

[Jaci09] Jacinto, N., *Performance Gains Evaluation from UMTS/HSPA+ to LTE at the Radio Network Level*, M.Sc. Thesis, Instituto Superior Técnico, Lisbon, Portugal, Nov. 2009.

[Jain07] Jain, R., "Channel Models: A Tutorial", WiMAX Forum AATG, Feb. 2007 (http://www.cse.wustl.edu/~jain/wimax/channel_model_tutorial.htm).

[Kath13] Kathrein 80010675 catalogue (http://www.kathrein.de/svg/download/9363879b.pdf).

[KDAT10] Kusume, K., Dietl, G., Abe, T., Taoka, H., Nagata, S., "System Level Performance of Downlink MU-MIMO Transmission for 3GPP LTE-Advanced", in *Proc. of VTC Spring'10 – 71st IEEE Vehicular Technology Conference*, Taipei, Taiwan, May. 2010.

[KuCo08] Kuipers,M., Correia, L.M., "Modelling the Relative MIMO Gain", in *Proc. of PIMRC'08 – IEEE Personal, Indoor and Mobile Radio Communications*, Cannes, France, Sep. 2008.

[LaCo06] Ladeira, D., Costa, P., *Optimal planning of UMTS cellular networks for HSDPA data-based services* (in Portuguese), M.Sc. Thesis, Instituto Superior Técnico, Lisbon, Portugal, Mar. 2006.

[LCGS12] Liu, L., Chen, R., Geirhofer, S., Sayana, K., Shi, Z., Zhou, Y., "Downlink MIMO in LTE-Advanced: SU-MIMO vs. MU-MIMO", *IEEE Communications Magazine*, Vol. 50, No. 2, Feb. 2012, pp. 140-147.

[LEVB12] Landre, J.-B., El Rawas, Z., Visoz, R., Bouguermouh, S., "Realistic Performance of LTE: In a Macro-Cell Environment", in *Proc. of VTC Spring'12 – 75th IEEE Vehicular Technology Conference*, Yokohama, Japan, May. 2012.

[Lope08] Lopes,J., *Performance of UMTS/HSDPA/HSUPA at the Cellular Level,* M.Sc. Thesis, Instituto Superior Técnico, Lisbon, Portugal, Mar. 2008.

[Moli11] Molisch, A. F., *Wireless Communications*, Wiley, Chichester, United Kingdom, 2011.

[Mora10] Morais, M., *Probability and Statistics – Course Notes (In Portuguese)*, Technical University of Lisbon, Lisbon, Portugal, 2010 (http://www.math.ist.utl.pt/~mjmorais/2010-09-12-NotasApoioPE-EdRevista-SeccaoFolhas.pdf).

[NoSN11] Nokia Siemens Networks, *LTE-Advanced: The advanced LTE toolbox for more efficient delivery of better user experience*, Technical White Paper, Mar. 2011 (http://www.nokiasiemensnetworks.com).

[Ofco12] Ofcom, *Assessment of future mobile competition and award of 800 MHz and 2.6 GHz*, Annexes 7-12, Jul. 2012 (http://stakeholders.ofcom.org.uk/binaries/consultations/award-800mhz/statement/Annexes7-12.pdf).

[Opti13] Private Communication, Optimus, 2013.

[Perg08] Preguiça,R., *Comparison between UMTS/HSPA+ and WiMAX/IEEE 802.16e in Mobility Scenarios*, M.Sc. Thesis, Instituto Superior Técnico, Lisbon, Portugal, Sep. 2008.

[Pire12] Pires, R. A., *Coverage and Efficiency Performance Evaluation of LTE in Urban Scenarios*, M.Sc. Thesis, Instituto Superior Técnico, Lisbon, Portugal, Oct. 2012.

[Salv08] Salvado, L., *UMTS/HSDPA comparison with WiMAX/IEEE 802.16e in mobility scenarios*, M.Sc. Thesis, Instituto Superior Técnico, Lisbon, Portugal, Fev. 2008.

[SeCa04] Sebastião, D., Cardeiro, J., *Modelation and Traffic Dimensioning in the UMTS Radio Interface* (in Portuguese), Graduation Thesis, Instituto Superior Técnico, Lisbon, Portugal, Oct. 2004.

[SeTB11] Sesia, S., Toufik, I., Baker, M., *LTE – The UMTS Long Term Evolution: From Theory to Practice*, Wiley, Chichester, United Kingdom, 2011.

[ShIN12] Shayea, I., Ismail, M.; Nordin, R., "Capacity Evaluation of Carrier Aggregation Techniques in LTE-Advanced System", in *Proc. of ICCCE'12 – International Conference on Computer and Communication Engineering*, Kuala Lumpur, Malaysia, Jul. 2012.

[SPZG12] Sivaraj, R., Pande, A., Zeng, K., Govindan, K., Mohapatra, P., "Edge-prioritized Channel- and Traffic-aware Uplink Carrier Aggregation in LTE-Advanced Systems", in *Proc. of WoWMoM'12 – IEEE International Symposium on World of Wireless, Mobile and Multimedia Networks*, San Francisco, USA, Oct. 2012.

[TGBA11] Tabia, N., Gondran, A., Baala, O., Caminada, A., "Interference Model and Evaluation in LTE Networks", in *Proc. of WMNC'11 – 4th Joint IFIP Wireless and Mobile Networking Conference*, Toulouse, France, Oct. 2011.

[WAFJ12] Werner, K., Asplund, H., Figueiredo, D.V.P., Jalden, N., Halvarsson, B., "LTE-Advanced 8×8 MIMO Measurements in an Indoor Scenario", in *Proc. of ISAP'12 – International Symposium on Antennas and Propagation,* Nagoya, Japan, Oct. 2012.

[Wang10] Wang Y., *System Level Analysis of LTE-Advanced: with Emphasis on Multi-Component Carrier Management*, Ph. D. Thesis, Aalborg University, Aalborg, Denmark, Sep. 2010.

[WaRP10] Wang, H., Rosa, C., Pedersen, K., "Performance of Uplink Carrier Aggregation in LTE-Advanced Systems", in *Proc. of VTC Fall'10 – 72nd IEEE Vehicular Technology Conference*, Ottawa, Canada, Sep. 2010.

[WaRP11] Wang, H., Rosa, C., Pedersen, K., "Performance Analysis of Downlink Inter-Band Carrier Aggregation in LTE-Advanced", in *Proc. of VTC Fall'11 – 74th IEEE Vehicular Technology Conference*, San Francisco, USA, Sep. 2011.

[WPMS09] Wang, Y., Pedersen, K.I., Mogensen, P.E., Sørensen, T.B., "Carrier Load Balancing Methods with Bursty Traffic for LTE-Advanced Systems", in *Proc. of PIMRC'09 – 20th IEEE International Symposium on Personal, Indoor and Mobile Radio Communications*, Tokyo, Japan, Sep. 2009.

[WPSM10] Wang, Y., Pedersen, K.I., Sorensen, T.B., Mogensen, P.E., "Carrier Load Balancing and Packet Scheduling for Multi-Carrier Systems", *IEEE Transactions On Wireless Communications*, Vol. 9, No. 4, May 2010, pp. 1780-1789.

[YKKT12] Yasukawa, S., Kawamura, T., Kishiyama, Y., Taoka, H., Andoh, H., "Field Experiments on Closed-Loop SU-MIMO Transmission Considering Effect of Antenna Configurations in LTE-Advanced Uplink", in *Proc. of VTC Spring'12 – 75th IEEE Vehicular Technology Conference,* Yokohama, Japan, May 2012.

[Zhan10] Zhang, L., *Network Capacity, Coverage Estimation and Frequency Planning of 3GPP Long Term Evolution*, M.Sc. Thesis, Linköping Institute of Technology, Linköping, Sweden, Sep. 2010.